3D Numerical Modelling of Sediment Transport under Current and Waves

Mohammad Saud Afzal

Coastal and Marine Civil Engineering
Submission date: June 2013
Supervisor: Øivind Asgeir Arntsen, BAT
Co-supervisor: Hans Sebastian Bihs, BAT

Norwegian University of Science and Technology
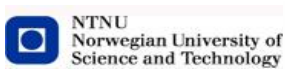Department of Civil and Transport Engineering

ERASMUS MUNDUS MSc PROGRAMME

COASTAL AND MARINE ENGINEERING AND MANAGEMENT
CoMEM

3D NUMERICAL MODELLING OF SEDIMENT TRANSPORT UNDER CURRENT AND WAVES

Norwegian University of Science and Technology
28 June 2013

Mohammad Saud Afzal
4192052

The Erasmus Mundus MSc Coastal and Marine Engineering and Management
is an integrated programme organized by five European partner institutions,
coordinated by Delft University of Technology (TU Delft).
The joint study programme of 120 ECTS credits (two years full-time) has been
obtained at three of the five CoMEM partner institutions:

- Norges Teknisk- Naturvitenskapelige Universitet (NTNU) Trondheim, Norway
- Technische Universiteit (TU) Delft, The Netherlands
- City University London, Great Britain
- Universitat Politècnica de Catalunya (UPC), Barcelona, Spain
- University of Southampton, Southampton, Great Britain

The first year consists of the first and second semesters of 30 ECTS each, spent at
NTNU, Trondheim and Delft University of Technology respectively.
The second year allows for specialization in three subjects and during the third semester
courses are taken with a focus on advanced topics in the selected area of specialization:
- Engineering
- Management
- Environment
In the fourth and final semester an MSc project and thesis have to be completed.
The two year CoMEM programme leads to three officially recognized MSc diploma
certificates. These will be issued by the three universities which have been attended by
the student. The transcripts issued with the MSc Diploma Certificate of each university
include grades/marks for each subject. A complete overview of subjects and ECTS
credits is included in the Diploma Supplement, as received from the CoMEM coordinating
university, Delft University of Technology (TU Delft).

Information regarding the CoMEM programme can be obtained from the programme
coordinator and director

Prof. Dr. Ir. Marcel J.F. Stive
Delft University of Technology
Faculty of Civil Engineering and geosciences
P.O. Box 5048
2600 GA Delft
The Netherlands

NORWEGIAN UNIVERSITY OF SCIENCE AND TECHNOLOGY
DEPARTMENT OF CIVIL AND TRANSPORT ENGINEERING

Report Title:	Date: 28 June 2013		
3D Numerical Modelling of Sediment Transport under Current and Waves	Number of pages (incl. appendices): 94		
	Master Thesis	x	Project Work	

Name:
Mohammad Saud Afzal

Professor in charge/supervisor:
Øivind A. Arntsen

Other external professional contacts/supervisors:
Hans Bihs

Abstract:

The sediment transport module of REEF3D is used to calculate the scour and the deposition pattern for abutment, pier and contraction under constant discharge and for pier under waves. The time development of scour for all these cases is also observed. To this effect, the Reynolds-Averaged Navier Stokes (RANS) equations are solved in all three dimensions, making it fully three dimensional. The location of the free surface is represented using level set method. The eddy viscosity in the RANS equation is determined by the use of the two-equation k-ω model and k-ε model. Using the conservative finite-difference framework on a structured-staggered grid, convective terms of RANS equation is discretized with the fifth-order WENO scheme. The pressure gradient term in the RANS equation is modelled using Chorin´s projection method on a staggered grid. For the implementation of waves, the CFD code is used as a numerical wave tank. For the representation of the moveable sediment bed, the level set method is used. Kovacs and Parker and Dey formulations of bed shear stress reduction due to the sloping bed is implemented along with the sand slide algorithm to take care of erosion of individual bed cells.

In the first case, the numerical model results are validated against the experimental findings of the abutment scour study done at Politecnico di Milano, Dept. I.I.A.R., Milan, Italy.. This test case is used as a benchmark for validation of the sediment transport module of REEF3D. The effect of the grid size, the turbulence model, the time discretization scheme, the formulations of critical shear stress for the sloping bed and porosity was observed and compared against the experimental results.. In the second configuration, the numerical model is used to predict the scour pattern around a circular pier. The scour pattern around the pier is compared against the experimental data of the hydraulic laboratory of the Technical University Darmstadt. The performance of the turbulence model and the formulations of critical shear stress for the sloping bed was observed. The numerical model is then tested for predicting a general contraction scour. The result is compared against the physical experiments of the contraction case conducted at the laboratories of the BAW (Federal Waterways Engineering and Research Institute), Karlsruhe, Germany. For the above mentioned three cases, a constant discharge at the boundary is used. The numerical model in the above configurations predict the general evolution (geometry, location and maximum scour depth) and time development of the scour hole accurately.

In the final configuration, 3D local scour around a vertical pile under waves is modelled. The numerical result is first compared with theoretical observations and then validated against the pier scour experiments conducted in the Department of Hydrodynamics and Water Resources (ISVA), Technical University of Denmark by Sumer and Fredsoe. The effect of the variation of the sediment time stepping with the decoupling of the hydrodynamic and the morphodynamic time step is tested. The numerical model shows good agreement with the experiment and theoretical erosion and deposition pattern. The de-coupled approach for the simulation of hydrodynamic and sediment transport processes is found to be a reasonable assumption.

Keywords:

1. Sediment Transport
2. REEF3D
3. Numerical Wave Tank
4. Abutment, Contraction, Pier

NTNU

Faculty of Engineering Science and Technology
Department of Civil and Transport Engineering

MASTER THESIS
(TBA4920 marine Civil Engineering, master thesis)

Spring 2013
For

Mohammad Saud Afzal

3D Numerical Modelling of Sediment Transport under Current and Waves

BACKGROUND

This thesis work is set out to numerically model the complex phenomena of sediment transport using Computational Fluid Dynamics (CFD). The aim therefore is to validate the sediment transport module of the open-source CFD program REEF3D (www.reef3d.com).

The correct prediction of local sediment transport in the vicinity of structures is an important research field due to its significant practical value as prediction is necessary for calculation of the scouring risk of the structures and the changes in bed form. Several examples of failure of the structures exist where correct prediction of local scour was not done. An accurate prediction of scour depth and its evolution in time is crucial. The need of extensive experience and physical insight into the hydrodynamics, sediment transport and morphological processes are hence necessary to tackle these issues of high importance.

Three methods exist in practice for prediction of sediment transport. These are analytical solutions, building a physical model (experiment) or a numerical simulation. Analytical solutions work for very simplified cases and thus cannot be applied for problems in practice. Compared to experimental results numerical models have the advantage that they are less expensive and do not have similarity problems of the scaled model as they can simulate real dimensions. However, in order to get good numerical results they have to be validated with physical experiments.

TASK DESCRIPTION

In the first part of the thesis, the sediment transport module of the CFD code is to be validated with sediment transport cases of abutment, single pier and contraction scour. The numerical results will be compared with experimental data. For these cases current only with a constant discharge will be used as inlet boundary condition. This simplifies the numerical setup and significantly speed up the solution process, as this results in quasi steady flow conditions. In order to calculate sediment transport under wave conditions, 3D local scour around a vertical pile will be modelled with waves. The numerically resolved time scale needs to be very fine, in order to capture the effect of each wave period on the sediment transport dynamics, which makes this simulation computationally very demanding.

General about content, work and presentation

The text for the master thesis is meant as a framework for the work of the candidate. Adjustments might be done as the work progresses. Tentative changes must be done in cooperation and agreement with the professor in charge at the Department.

The reporting of the work should be academic anchored and well described with respect to the theoretical and scientific basis so that the work could be implemented in the field of international research.

In the evaluation thoroughness in the work will be emphasized, as will be documentation of independence in assessments and conclusions. Furthermore the presentation (report) should be well organized and edited; providing clear, precise and orderly descriptions without being unnecessary voluminous.

The report shall include:

- Standard report front page (from DAIM, http://daim.idi.ntnu.no/)
- Title page with abstract and keywords.(template on: http://www.ntnu.no/bat/skjemabank)
- Preface
- Summary and acknowledgement. The summary shall include the objectives of the work, explain how the work has been conducted, present the main results achieved and give the main conclusions of the work.
- Table of content including list of figures, tables, enclosures and appendices.
- If useful and applicable a list explaining important terms and abbreviations should be included.
- The main text.
- Clear and complete references to material used, both in text and figures/tables. This also applies for personal and/or oral communication and information.
- Text of the Thesis (these pages) signed by professor in charge as Attachment 1..
- The report musts have a complete page numbering.

Advice and guidelines for writing of the report is given in: "Writing Reports" by Øivind Arntsen. Additional information on report writing is found in "Råd og retningslinjer for rapportskriving ved prosjekt og masteroppgave ved Institutt for bygg, anlegg og transport" (In Norwegian). Both are posted on http://www.ntnu.no/bat/skjemabank

Submission procedure

Procedures relating to the submission of the thesis are described in DAIM (http://daim.idi.ntnu.no/). Printing of the thesis is ordered through DAIM directly to Skipnes Printing delivering the printed paper to the department office 2-4 days later. The department will pay for 3 copies, of which the institute retains two copies. Additional copies must be paid for by the candidate.

On submission of the thesis the candidate shall submit a CD with the paper in digital form in pdf and Word version, the underlying material (such as data collection) in digital form. Students must submit the submission form (from DAIM) where both the Ark-Bibl in SBI and Public Services (Building Safety) of SB II has signed the form. The submission form including the appropriate signatures must be signed by the department office before the form is delivered Faculty Office.

Documentation collected during the work, with support from the Department, shall be handed in to the Department together with the report.

According to the current laws and regulations at NTNU, the report is the property of NTNU. The report and associated results can only be used following approval from NTNU (and external cooperation

partner if applicable). The Department has the right to make use of the results from the work as if conducted by a Department employee, as long as other arrangements are not agreed upon beforehand.

Tentative agreement on external supervision, work outside NTNU, economic support etc.
Separate description to be developed, if and when applicable. See http://www.ntnu.no/bat/skjemabank
for agreement forms.

Health, environment and safety (HSE) http://www.ntnu.edu/hse
NTNU emphasizes the safety for the individual employee and student. The individual safety shall be in the forefront and no one shall take unnecessary chances in carrying out the work. In particular, if the student is to participate in field work, visits, field courses, excursions etc. during the Master Thesis work, he/she shall make himself/herself familiar with " Fieldwork HSE Guidelines". The document is found on the NTNU HMS-pages at http://www.ntnu.no/hms/retningslinjer/HMSR07E.pdf

The students do not have a full insurance coverage as a student at NTNU. If you as a student want the same insurance coverage as the employees at the university, you must take out individual travel and personal injury insurance.

Start and submission deadlines
The work on the Master Thesis starts on 11th February 2013

The thesis report as described above shall be submitted digitally in DAIM at the latest
8th July 2013 at 3pm.

Professor in charge: Øivind A. Arntsen

Other supervisors: Hans Bihs

Trondheim, June 28th, 2013

_____
Professor in charge (sign)

Abstract

The sediment transport module of REEF3D is used to calculate the scour and the deposition pattern for abutment, pier and contraction under constant discharge and for pier under waves. The time development of scour for all these cases is also observed. To this effect, the Reynolds-Averaged Navier Stokes (RANS) equations are solved in all three dimensions, making it fully three dimensional. The location of the free surface is represented using level set method. With this method, it is possible to calculate the complex motion of the free surface in a very realistic manner. The flow problem is solved as a two phase flow of water and air, with the free surface represented by the interface between the two phases. The eddy viscosity ν_t in the RANS equation is determined by the use of the two-equation k-ω model and k-ϵ model. Using the conservative finite-difference framework on a structured-staggered grid, convective terms of RANS equation is discretized with the fifth-order WENO (weighted essentially non-oscillatory) scheme. This ensures a smooth and oscillation free solution under large gradients and shocks while maintaining a high order of accuracy. The pressure gradient term in the RANS equation is modelled using ChorinÂťs projection method on a staggered grid, which prevents velocity-pressure decoupling. A preconditioned BiCGStab algorithm is employed for the iterative solution of the Poisson equation. For time treatment Adam Bashforth, a third-order accurate TVD Runge-Kutta scheme and a fourth order accurate TVD Runge-Kutta scheme are employed . Domain decomposition coupled with the MPI library is used to achieve the parallelization of the numerical model. The complex geometries in the numerical models are treated with an immersed boundary method based on ghost cell extrapolation on a cartesian grid. For the implementation of waves, the CFD code is used as a numerical wave tank. Wave generation is modelled through a transient velocity and water elevation profile obtained from wave theory and is implemented through a relaxation zone. Wave reflections of the downstream boundary are prevented by the implementation of a numerical beach. For the representation of the moveable sediment bed, the level set method is used. The sediment transport rates in the bed cells are calculated with standard bed load formulas, with the bed shear stress as the major factor for coupling between the hydrodynamics part and the sediment transport. The resulting sediment continuity defect at the bed is converted into the rate of change

of the vertical bed elevation. This external velocity is used to convect the level set function for the bed topology, resulting in either erosion or deposition. This strategy has two major advantages: At first the topology is a well defined surface when calculating the incipient motion on the sloping bed and the sand avalanche. The second advantage is that the numerically error prone remeshing can be avoided, because the complex boundary surface is accounted for by the immersed boundary method. Van Rijn's formula for the suspended load is used to account for suspended load transport. Bed shear stress formulation based on turbulent viscosity as presented in section is used. Kovacs and Parker and Dey formulations of bed shear stress reduction due to the sloping bed is implemented along with the sand slide algorithm to take care of erosion of individual bed cells.

In the first case, the numerical model results are validated against the experimental findings of the abutment scour study done at Politecnico di Milano, Dept. I.I.A.R., Milan, Italy. This test case is used as a benchmark for validation of the sediment transport module of REEF3D. The effect of the grid size, the turbulence model, the time discretization scheme, the formulations of critical shear stress for the sloping bed and porosity was observed and compared against the experimental results. In the second configuration, the numerical model is used to predict the scour pattern around a circular pier. The scour pattern around the pier is compared against the experimental data of the hydraulic laboratory of the Technical University Darmstadt. The performance of the turbulence model and the formulations of critical shear stress for the sloping bed was observed. The numerical model is then tested for predicting a general contraction scour. The result is compared against the physical experiments of the contraction case conducted at the laboratories of the BAW (Federal Waterways Engineering and Research Institute), Karlsruhe, Germany. For the above mentioned three cases, a constant discharge at the boundary is used. The numerical model in the above configurations predict the general evolution (geometry, location and maximum scour depth) and time development of the scour hole accurately.

In the final configuration, 3D local scour around a vertical pile under waves is modelled. The numerical result is first compared with theoretical observations and then validated against the pier scour experiments conducted in the Department of Hydrodynamics and Water Resources (ISVA), Technical University of Denmark by Sumer and Fredsøe. The effect of the variation of the sediment time stepping with the decoupling of the hydrodynamic and the morphodynamic time step is tested. The numerical model shows good agreement with the experiment and theoretical erosion and deposition pattern. The de-coupled approach for the simulation of hydrodynamic and sediment transport processes is found to be a reasonable assumption.

Acknowledgments

Contents

List of Figures

List of Symbols

λ	Wavelength
D	Diameter
ρ	Density
t	Time
∇	Divergence operator
U	Velocity
$i,\ j,\ k$	Vectors along the x, y and z-axes
μ	Fluid viscosity (dynamic)
P	Pressure
g	Acceleration due to gravity
ϕ	Level set function
$i\ (in\ numerical\ schemes)$	Time step of iteration
$\omega_1,\ \omega_2,\ \omega_3$	WENO stencil weights
$\alpha_1,\ \alpha_2,\ \alpha_3$	WENO stencil weight determiner
$IS_1,\ IS_2,\ IS_3$	WENO stencil smoothness indicators
$L()$	Spatial discretization of the function
C	Courant Number
ν	Fluid viscosity(kinematic)
ν_t	Eddy viscosity
V	Maximum viscosity
S_{max}	Source term contribution from surface and volume forces
U^*	Intermediate velocity
k	Turbulent kinetic energy
ω	Specific turbulent dissipation
$c_\mu,\ c_{\omega 1},\ c_{\omega 2},\ \sigma_k,\ \sigma_\omega$	Closure coefficients
S_{ij}	Strain tensor
U^+	Dimensionless wall velocity
κ	constant = 0.4
d	Water depth
k_s	Equivalent sand roughness

Δy_p	Distance from the wall to cell centre
ϵ_{wall}	Mean wall thickness
τ_ω	Wall shear stress
2ϵ	Transition zone thickness
$S(\phi)$	Smooth signed distance function
Φ	Velocity potential
$\Psi(x)$	Relaxation function
p	Steepness exponent
η	Free surface elevation
ω_f	Wave angular frequency
k_f	Wave number
a	Wave amplitude
H	Wave height
z	Height to the free surface from bed
dx	Grid cell width
KC	Keulegan-Carpenter number
T	Wave period
φ	Angle of Repose
φ'	Modified angle of repose
π	Mathematical constant, $\frac{22}{7}$
θ	Longitudinal bed slope angle
α	Transversal bed slope angle
Re	Reynolds number
x, y, z	Position of structure in the flume
r	Reduction factor for the bed shear stress
Δt	Numerical time step
Γ	Surface vector
$\mathbf{n}$	Surface normal vector
τ	Bed shear stress
d_{50}	Sediment particle diameter

Chapter 1

Introduction

1.1 Sediment Transport Modelling in Marine Civil Engineering

Sediment transport is an important issue within marine civil engineering; it deals with some of the most serious environmental problems, such as soil erosion in rivers and erosion of seabed near ocean shores. Some of the other topics where sediment transport is of importance are the littoral transport near the coastline and coastal erosion in the arctic areas. In particular, river erosion and ocean bed erosion forced due to hydraulic and coastal structures like abutment, pier, weir and breakwaters is of special practical and economical interest in the field of marine civil engineering.

Under uniform flow conditions without the presence of structures, the bed load stays in equilibrium since the same amount of sediment is eroded as is deposited in a river section in a natural river system. Mountains supply the river with bed load (e.g sand or gravel), which is carried further downstream in rivers. Human intervention as natural disasters can interfere with this equilibrium of erosion and deposition. Especially hydraulic structures change the natural flow of water in rivers. The sediment is deposited downstream of the structure and thus leads to sediment starvation upstream. Erosion caused by big obstacles, like bridge piers in rivers have a significant effect on the plant efficiency. The flow pattern change due to such structures can lead to massive erosion in the vicinity of hydraulic structures. Excessive local scour development can threaten the stability of hydraulic structures such as piers, weirs, abutments and can even lead to the collapse of bridges or offshore wind turbines [1][13]. The effect is intensified in case of high discharge in rivers (floods). The climate change has a consequence on environmental parameters and results in extreme weather and therefore floods are expected more frequently with extreme wave conditions in oceans and thus events of massive erosion will increase in the future [36].

The correct prediction of local sediment transport in the vicinity of structures is an important research field due to its significant practical value as prediction is necessary for calculation of the scouring risk of the structures and the changes in bedform. Several examples of failure of the structures exist where correct prediction of local scour was not done [69]. An accurate prediction of scour depth and its evolution in time is crucial. The need of extensive experience and physical insight into the hydrodynamics, sediment transport and morphological processes are hence necessary to tackle these issues of high importance.

Three methods exist in practice for prediction of sediment transport. These are analytical solutions, building a physical model (experiment) or a numerical simulation. Analytical solutions work for very simplified cases and thus cannot be applied for problems in practice. Compared to experimental results numerical models have the advantage that they are less expensive and do not have similarity problems of the scaled model as they can simulate real dimensions. However, in order to get good numerical results they have to be validated with physical experiments.

1.2   Previous Works

Scour problems have been extensively studied numerically by many researchers in the past decades. First investigations on scours due to jets were done by Rouse [89] and Eggenberger and Muller [30].

Several 2D and 3D numerical models with the capability of predicting bedform changes have been developed in recent years. The 2D models developed by Minh Duc et.al. (2004) [27] and Wu and Wang (2004) [117] are some among many of them. Minh proposed a 2D depth-averaged model using a finite volume method with boundary-fitted grids and fixed channel sides. The sediment transport module comprised of semi-empirical models of suspended and non-equilibrium bed load. The secondary flow transport effects were taken into account by adjusting the dimensionless diffusivity coefficient in the depth-averaged k-ω turbulence model. The empirical formulas by van Rijn (1984a) [106] have been used for the calculation of the bed shear driven resultant bed load, . The model has been validated by computing the bed changes of the experiments by Odgaard and Bergs (1988) [76] and Yen and Lee (1995) [118]. Wu and Wang (2004) [117] simulated sediment transport in a channel bend with fixed sides and proposed a 2D depth-averaged model for computing flow and sediment transport in curved channels. A semi-empirical formula was presented to determine the cross-stream distribution of the helical flow intensity in the devel-

oped regions of a channel bend. The formula was used to evaluate the dispersion terms in the depth-averaged 2D momentum equations and suspended load transport equation as well as the bed load transport angle. The experiments done by Yen and Lee (1995) [118] were used for validation in this model. To model the sediment sorting process they considered eight sediment size fraction.

Wu et al. (2000) [116] proposed a 3D model for the calculation of flow and sediment transport. He simulated suspended load transport through the general convection-diffusion equation with an empirical settling velocity term. Simulation of bed load transport was done using a non-equilibrium method and the bed deformation was obtained from an overall mass-balance equation. The empirical formulas by van Rijn (1984a,b) [106] [107] were implemented for the computation of bed and suspended load. The model was tested by calculating the flow and sediment transport of the experiments by Odgaard and Bergs (1988) [76], a 180^0 channel bend with fixed sides. The model was not able to account for the effect of transverse bed slope on the bed load transport. A year later Zeng et al. (2005) [119] presented a fully 3D model to solve the flow, bed load sediment transport and bed morphology changes in open channel flows in non-movable channel banks. The model solved the 3D Reynolds averaged Navier-Stokes equations with integrations up to the wall such that the use of wall functions was avoided. The k-ω model was used together with a non-equilibrium bed load sediment transport model with additional introduction of down-slope gravitational force effects. The empirical formulas proposed by van Rijn (1984a) [106]for the equilibrium bed load transport rate were used in the study. The experiments by Odgaard and Bergs (1988) [76] were employed to validate the model.

The publication by Olsen and Melaaen (1993) [78] on three-dimensional numerical modeling of local pile scour was the earliest of its kind. The initial stage of the pile scour was modelled under the assumption of a stationary flow. For this configuration Olsen and Kjellesvig (1998) [77] later calculated the entire time-dependent scour process. They compared empirical formulas with their results for the maximum scour depth. Both these publications used a finite volume scheme to discretize the Reynolds-Averaged Navier-Stokes (RANS) equations and the equations of the k-ϵ turbulence model. Non-hydrostatic pressure was calculated using the SMIPLE method. The critical bed shear stress was reduced with consideration of the steepest bed slope in the second paper, but the model employed a formula valid only for side slopes. The bed slope was corrected to the angle of repose of the sediment for modelling the sandslide. Roulund et al. (2005) [88] investigated the flow and the scour around a bridge pier both experimentally and numerically. He used a finite volume scheme and calculated the turbulence with the k-ω model. The model used by [88] did not have a free-surface algorithm. Later, Bihs and Olsen (2008) [9] performed numerical

3

simulations of pier scour. Good agreement was found with the physical model studies. They later focussed on the influence of the sloping bed in scour holes on the incipient motion of sediment particles and the corresponding sand avalanche mechanism (Bihs and Olsen, 2011) [6].

The use of large-eddy simulation (LES) for local pile scour studies has also been attempted in the past. Modelling of the flow field around a circular pier with a fixed bed topography, that corresponds to equilibrium scour conditions was done by Kirkil et al. (2008) [56] using LES. So far no paper exists which has used LES to model the entire local scour process. The reason could be that the simulations would be extremely costly in terms of computational resources. The existing sediment transport formulas are defined within the RANS framework. The paper by Escauriaza and Sotiropoulos (2011) [35] used detached-eddy simulation (DES) to capture the coherent structures of the horseshoe vortex together with a Lagrangian sediment particle model where they calculated the evolution of the scour hole for the first 100 seconds. All the studies discussed above for pile scour studies consider steady currents only. To investigate scour process under waves, a three dimensional numerical modelling of local pile scour was done by Liu and Garcia (2008) [66] in which the Volume-of-Fluid method was used for the calculation of the free surface.

Among other configurations, the paper presented by Bihs and Olsen (2007) [8] at IAHR conference deserves mentioning where they focus on the prediction of local scour in a rectangular flume with a contraction. In the study, the Reynolds-averaged Navier-Stokes equations were solved in three directions by the means of the finite volume method. The sediment transport was computed by solving the convection-diffusion equation for suspended sediments together with the bed load. Van Rijn's sediment transport formulas served as boundary conditions. Bed changes were calculated based on sediment continuity. The results from the numerical calculations were compared against data from physical experiments [18]. The numerical model proved to be capable of predicting the location and the magnitude of the scour hole reasonably well, but the correct location of sediment deposition downstream of the scour hole was not very well predicted.

1.3 Objectives of the study

The present master thesis topic builds upon the capabilities of the open-source CFD program REEF3D [10] [54]. The level set method is used for the calculation of the complex free surface. With this method, it is possible to calculate the complex motion of the free surface in a very realistic manner. The flow problem is solved as a two-

phase flow of water and air, with the free surface represented by the interface between the two phases. The physics responsible for the transport and deformation of this interface are accounted for in great detail. The CFD code can be used as a numerical wave tank [10] [55] [54] . Wave generation is modelled through a transient velocity and water elevation profile obtained from wave theory and is implemented through a relaxation zone. Wave reflections of the downstream boundary are prevented by the implementation of a numerical beach.

For the representation of the moveable sediment bed, the level set method is used as well. The sediment transport rates in the bed cells are calculated with standard bed load formulas, with the bed shear stress as the major factor for coupling between the hydrodynamics part and the sediment transport. The resulting sediment continuity defect at the bed is converted into the rate of change of vertical bed elevation, which has the unit of velocity. This external velocity is used to convect the level set function for the bed topology, resulting in either erosion or deposition. This strategy has two major advantages: At first the topology is a well defined surface when calculating the incipient motion on the sloping bed and the sand avalanche. The second advantage is that the numerically error prone re-meshing can be avoided, because the complex boundary surface is accounted for by the immersed boundary method.

In the first part of the thesis, the sediment transport module of the CFD code is to be validated with sediment transport cases of abutment, single pier and contraction scour. The numerical results will be compared with experimental data. For these cases current only with a constant discharge will be used as inlet boundary condition. This simplifies the numerical setup and significantly speed up the solution process, as this results in quasi steady flow conditions. In order to calculate sediment transport under wave conditions, 3D local scour around a vertical pile will be modelled with waves. The numerically resolved time scale needs to be very fine, in order to capture the effect of each wave period on the sediment transport dynamics, which makes this simulation computationally very demanding.

Chapter 2

CFD Model

This chapter describes the basic principles of a computational fluid dynamics (CFD) model in general along with the formulations and schemes employed in REEF3D, the CFD model used for current study.

2.1 Governing Equations

2.1.1 Transport Equation

CFD uses basic equations of fluid mechanics. In order to derive the basic equations of fluid mechanics the balance of a conserved quantity G in an elementary control volume is assumed. G can stand for mass, momentum and energy. A cubic element, fixed in space is chosen with dimensions Δx_1, Δx_2 and Δx_3 coinciding with the orthogonal coordinate axes x_1, x_2 and x_3.

The most simple equation describing the quantity in this volume indicates that the change of G in time interval Δt is caused by net transport of G into the volume.

$$G(t + \Delta t) - G(t) = G_{in}(R - L) + G_{in}(T - Bo) + G_{in}(Ba - F) \qquad (2.1)$$

R stands for right, L for left, T for Top, Bo for bottom, Ba for back and F for front face of the cube.

After dividing the equation 2.1 by volume $\Delta x_1 \Delta x_2 \Delta x_3$ and the time interval Δt the left side of the equation 2.1 becomes the time derivative of concentration c of G in the limit of all increments âĹĘ approaching zero.

$$\lim_{\Delta x_1 \Delta x_2 \Delta x_3 \Delta t \to 0} \frac{G(t + \Delta t) - G(t)}{\Delta x_1 \Delta x_2 \Delta x_3 \Delta t} = \frac{\partial c}{\partial t} \tag{2.2}$$

The right hand side of equation 2.1 describes the transport of G through the faces of the cube. The net amount transported through the right and left side of the cube is then

$$\lim_{\Delta x_1 \to 0} \frac{v_{1R} c_R - v_{1L} c_L}{\Delta x_1} = \frac{\partial (U_1 c)}{\partial x_1} = \nabla_i (U_i c) \tag{2.3}$$

If a diffusion process causes loss or accumulation of material inside the control volume then an extra diffusive transport term is added.

$$\lim_{\Delta x_1 \to 0} \frac{T_{1R} - T_{1L}}{\Delta x_1} = \frac{\partial (T_1)}{\partial x_1} = \nabla_i T_i \tag{2.4}$$

Analogously the source of G becomes a concentration change per unit of time.

$$\lim_{\Delta x_1 \Delta x_2 \Delta x_3 \Delta t \to 0} \frac{G_{source}}{\Delta x_1 \Delta x_2 \Delta x_3 \Delta t} = -D \tag{2.5}$$

The source term is taken negative, so D should be interpreted as a sink term. The above argument leads to a generic transport equation for a property G that can be specified as

$$\frac{\partial c}{\partial t} + \nabla_i (U_i c) + \nabla_i T_i + D = 0 \tag{2.6}$$

2.1.2   Transport of Mass

The transport equation 2.6 is applicable to mass transport with c=ρ. With the knowledge that mass cannot disappear except when accounting for thermo-nuclear processes the sink term D will be zero. Furthermore, mass will not exhibit diffusive transport with respect to itself. The transport equation then simplifies to;

$$\frac{\partial \rho}{\partial t} + \nabla_i (\rho U_i) = 0 \tag{2.7}$$

With the assumption of an incompressible flow, the density of fluid does not change in space or time and thus the velocity field is divergence free. The equation 2.7 hence reduces to

$$\frac{\partial U_i}{\partial x_i} = 0 \tag{2.8}$$

The equation 2.8 in fluid mechanics is called the equation of continuity.

2.1.3 Transport of Momentum

The equations for momentum per unit of volume can be obtained by taking c=ρU in the transport equation 2.6. This is a direct implication of Newton's second law of motion. The equation for the first velocity component results in

$$\frac{\partial(\rho U_1)}{\partial t} + \nabla_i(\rho U_1 U_i) = -\nabla_i p + \mu \nabla_i^2 U_1 + k_1 \tag{2.9}$$

The terms on the left hand side of the momentum equations are called the convection terms of the equations. Convection is a physical process that occurs in a flow of fluid in which some property is transported by the ordered motion of the flow. The terms on the right hand side of the momentum equations consist of a pressure term, diffusive terms and a source term. The diffusive terms contain the normal and viscous shear stresses acting on the elementary volume. A positive acceleration will be achieved proportional to the negative pressure gradient. The differences of the shear stresses between opposite faces of the cube contribute to the viscous diffusion or dissipation. Gravity or coriolis force in a rotating system could be added as source term k_1. The momentum equation can be written as

$$\frac{\partial U_i}{\partial t} + U_j \frac{\partial U_i}{\partial x_j} = -\frac{1}{\rho} \frac{\partial P}{\partial x_i} + \frac{\partial}{\partial x_j} \left[\nu \left(\frac{\partial U_i}{\partial x_j} + \frac{\partial U_j}{\partial x_i} \right) \right] + g_i \tag{2.10}$$

The three components of equation 2.10 form the Navier-Stokes equation and together with the continuity equation makes a complete set to describe a flow.

2.2 Numerical Discretization

It is often complicated to find the analytic or exact solution to many differential equations encountered in fluid flow. Non-linearity and dependency of coefficients on time are major factors that account for this. For constant coefficient linear differential equations, the difficulty is often due to the equation being of high order, or because it must be solved for many inputs and/or initial conditions. There are many methods for finding approximate solutions to differential equations. These methods are referred to by a variety of different names including: numerical methods, numerical integration, or approximate solutions, among others.

Discretization of the governing equations is the first step in numerical evaluation of the equations used in the fluid flow. In practice there are several methods listed in

literature that are used for discretization. The three main methods along with their brief description are;

- Finite Difference Method.
  Historically, it is the oldest of the three methods. Techniques were published as early as 1910 by L. F. Richardson [87]. It is very easy to implement but is generally restricted to simple grids. The computational domain is discretized into a series of grid points which results in âĂIJstructuredâĂİ (ijk) mesh. First and second derivatives are approximated by truncated Taylor series expansions and the resulting set of linear algebraic equations is solved either iteratively or simultaneously.

- Finite Element Method.
  Finite element method (FEM) was first used by Courant (1943) [19] in a lecture presented in 1941 to the American Association for the Advancement of Science. In his work, Courant used the Ritz method and introduced the pivotal concept of spatial discretization for the solution of the classical torsion problem. Courant did not pursue his idea further, since computers were still largely unavailable for his research. Later Ray W. Clough of the University of California, Berkeley and his colleagues essentially reinvented the finite element method as a natural extension of matrix structural analysis and named the method as "Finite Element Method" in 1960 [17]. FEM analysis of fluid flow was developed in the mid to late 1970âĂŹs. The most attractive feature of finite element is its ability to handle complex geometry and boundaries with relative ease. The problem of computational time is strongly influenced by the ability to precondition the problem and is computationally demanding. Some of the other limitations are that it gives an approximate solution and that too at nodes only.

- Finite Volume Method.
  The first use of this discretization technique was done by Evans and Harlow (1957) [45] at Los Alamos Scientific Laboratory. It was attractive because while variables may not be continuously differentiable across shocks and other discontinuities mass, momentum and energy are always conserved. The solution domain is divided into a finite number of control volumes, and conservation equations are applied to each control volume. The computational node is located at centroid of each control volume at which the variable values are to be calculated. The finite volume method is suitable for complex geometries as it can accommodate any type of grid. The disadvantage of this method is that for the higher order techniques, it is difficult to develop as it requires three level of approximation: interpolation, differentiation and integration [84].

The current study uses conservative finite difference method for discretization. Conservative finite difference method has the same conservation properties as finite volume method. As the current study utilizes structured grids, the finite difference method is simple and effective. It is also very easy to obtain higher order schemes on regular grids. It is also very stable.

Numerical solution of the governing equations in fluid flow require definition of numerical grid of nodal points in space and time. The choice of the grid depends strongly on the type of equations to be solved. Depending on the geometry of the basic elements the grid can be rectangular. Depending on the distribution of nodal point the grid can be regular and non-regular. Depending on the character of nodal points the grid can be non-staggered and staggered(half-staggered and fully staggered).

For a non-staggered grid all the variables are defined for the same nodal points (nodes). In case of using finite-differences (FD) with a non-staggered grid, all equations are formulated and discretized at the same nodal points. Half-staggered grid is a combination of a basic non-staggered grid with an additional set of points defined for the centers of cells formed by the basic grid. Part of variables is then defined in this additional points and not in the basic nodal points. Half-staggered grid is more applicable for solving of the combination of Stokes and continuity equations to obtain components of velocity defined in basic nodal points and pressure defined in additional points. Fully staggered grid is applied in two and three dimensions and consist of combination of several types of nodal points having different geometrical positions. Different variables are then defined in different nodal points. Different equations are also formulated and discretized in different nodal points. Fully staggered grid seems to be the most natural choice in numerical problems involving solution of continuity, Stokes and temperature equations using finite-difference. Also, an accuracy of a numerical solution on fully staggered grid is notably (up to four-fold) higher then that on non-staggered grid [67]. A staggered grid configuration leads to a tight velocity-pressure coupling. This is the main reason that the current study utilizes a cartesian staggered grid for spatial discretization.It also serves as a remedy for oscillatory or checkerboard pressure solution while solving Navier Stokes Equation.

There are three quantitative properties of a finite difference scheme which determine the applicability of the particular scheme to a particular scenario:

- Consistency: Finite difference discretization of a differential equation is consistent if the finite difference equations converge to the original differential equation, i.e., the truncation error vanishes as grid spacing and time step tend to zero. The truncation error is the difference between the exact solution and the

numerical approximation.

- Stability: This means that the errors from any source will not grow unbounded with time. This happens when there happens to be an upper and lower bound on the errors.

- Convergence: The solution of the finite difference equations should converge to the true solution of the differential equation as grid spacing and time step tend to zero.

The order and nature of a numerical scheme is strongly dependent on geometrical arrangement of the nodal group which is also called stencil. A stencil relates to the point of interest by using a numerical approximation routine. It indicates the number of points used (e.g. 5 point stencil scheme) and the order of the scheme. A wider stencil has a higher order of accuracy.

2.2.1 Convection Discretization

The governing equations of fluid flow (Section 2.1.1) consist of convective, diffusive and source terms. These terms need to be discretized first before proceeding to the solution. In literature there are several discretization schemes using finite difference method.

- First Order Upwind (FOU) Scheme
  The FOU scheme [21] is a first order scheme which uses an adaptive or solution-sensitive finite difference stencil to numerically simulate the direction of propagation of information in a flow field. The terms are evaluated in the direction of the flow. It assumes that the convected variable at the cell face is the same as the upwind cell centre value. The upwind scheme is stable if the Courant-Friedrichs-Lewy condition (CFL) is satisfied. It is unconditionally bounded and highly stable but is only 1st order accurate in terms of truncation error and may produce severe numerical diffusion. The scheme is, therefore, highly diffusive especially when the flow direction is skewed relative to the grid lines. An example of FOU discretization in forward direction is given;

$$\frac{\partial U_i}{\partial x_j} = \frac{(U_i - U_{i-1})}{\Delta x_j} \qquad for \quad U_i > 0$$

- Central Difference Scheme (CDS)
  Unlike FOU this scheme is of second order and utilizes grid points lying on

11

either side of the point in consideration for calculation of variables.

$$\frac{\partial U}{\partial x} = \frac{U_{i+1} - U_{i-1}}{2\Delta x}$$

For damped situations this scheme is unconditionally unstable. As a result, in a case of large gradients, the performance of CDS would be in question. It is however easy compared to other high order discretization schemes and is independent of the flow direction.

- Quadratic Upstream Interpolation for Convective Kinetics (QUICK)
  This is a higher order differencing scheme which considers a three point upstream weighted quadratic interpolation for the cell phase values. The QUICK scheme was shown by Brian P. Leonard in 1979 [64]. Contrary to CDS and the second order upwind schemes, where the first order derivative is considered and the second order derivative is ignored, QUICK does take the second order derivative into account, but ignores the third order derivative. Hence, this is considered third order accurate. QUICK is most suited for steady flow or quasi steady highly convective elliptic flow. Solutions using QUICK are found to be more accurate than the first order upwind schemes. False diffusion errors also gets minimized when compared with other schemes.

- Sharp and Monotonic Algorithm for Realistic Transport (SMART) Scheme
  The traditional approach in discretization of differential equations is to use a fixed stencil scheme. This means that under all the flow situations the number and the location of neighbouring cells used for the interpolation stays the same. This works well for cases where the modelled data is globally smooth. When discontinuities occur, in case of fixed stencil discretization of higher order than one, discontinuities introduce spurious oscillations, which render the solution useless. SMART [40] was hence developed to derive a new approach to approximate the convection term in equations, such that the solution remains bounded and devoid of the potential to create spurious spatial oscillations in the vicinity of sharp changes in gradient in the dependent variable. SMART is a class of high resolution TVD (total variation diminishing) scheme with smart flux limiter. Flux limiters are generally used in high resolution schemes to avoid spurious oscillations that could occur due to sharp changes in solution domain, shocks and discontinuities. The combination of flux limiter along with high resolution schemes make the solutions TVD. SMART scheme is up to second order accurate. Because of the advantages of this scheme it finds application in solving a three dimensional fluid flow problem.

- Weighted Essentially Non- Oscillatory (WENO) Scheme

The Weighted Essentially Non-Oscillatory (WENO) scheme by Liu et.al. [68] and Jiang and Shu [53] is a modification of ENO scheme which was developed by Harten and Osher [47] . WENO like ENO is an adaptive stencil scheme where each cell has its own stencil of cells. In ENO spurious oscillations are avoided by choosing the stencil which gives the smoothest solution. In WENO, instead of choosing just one âĂİsmoothestâĂİ stencil, multiple stencils are chosen and assigned weights on the basis of the smoothness of the solutions. This convex combinations of stencils leads to a non oscillatory solution. For current study, the fifth-order WENO scheme in conservative finite difference framework is used to discretize the convective terms of the RANS equations. The convection term is approximated in x-direction as follows:

$$U \frac{\partial U}{\partial x} \approx \frac{1}{\Delta x} \left(\tilde{U}_{i+1/2} U_{i+1/2} - \tilde{U}_{i-1/2} U_{i-1/2} \right) \qquad (2.11)$$

Here $\tilde{U}$ is the convection velocity, which is obtained at the cell faces through simple interpolation. For the the cell face $i + 1/2$, $U_{i+1/2}$ is reconstructed with the WENO procedure:

$$U_{i+1/2}^{\pm} = \omega_1^{\pm} U_{i+1/2}^{1\pm} + \omega_2^{\pm} U_{i+1/2}^{2\pm} + \omega_3^{\pm} U_{i+1/2}^{3\pm} \qquad (2.12)$$

The $\pm$ sign indicates the upwind direction. $U_{i+1/2}^1$, $U_{i+1/2}^2$ and $U_{i+1/2}^3$ represent the three possible ENO stencils. For upwind direction in the positive i-direction, they are:

$$
\begin{aligned}
U_{i+1/2}^{1-} &= \frac{1}{3}U_{i-2} - \frac{7}{6}U_{i-1} + \frac{11}{6}U_i, \\
U_{i+1/2}^{2-} &= -\frac{1}{6}U_{i-1} + \frac{5}{6}U_i + \frac{1}{3}U_{i+1}, \\
U_{i+1/2}^{3-} &= \frac{1}{3}U_i + \frac{5}{6}U_{i+1} - \frac{1}{6}U_{i+2}
\end{aligned}
\qquad (2.13)
$$

The smoothness indicators IS is used to determine and calculate the nonlinear weights ω_n for each ENO stencil. A non-smooth solution in the particular ENO stencil is indicated by a large IS . For this stencil, the non linear weights ω_n will be small . The WENO scheme favours stencils with a smooth solution by assigning them the largest weights ω_n. Thus, this scheme can handle large gradients right up to the shock very accurately. The WENO scheme will be third-order of accurate in cases where large gradients are present in all three stencils. In the areas of smooth solution, it will deliver 5th-order accurate results. The WENO

scheme does not smear out the solution unlike other popular high resolution schemes such as MUSCL [105] or TVD [47]. Instead it maintains the sharpness of the extrema. The conservative WENO scheme is used for the treatment of the convective terms for the velocities U_i, while the Jacobi-Hamilton version is used for the variables of the free surface and turbulence algorithms.

2.2.2 Time Discretization

REEF3D has provisions for first and second order Implicit Euler schemes for time discretization. Implicit schemes are stable over a wide range of time steps, sometimes unconditionally, than explicit schemes, but require more effort to compute. These schemes in some cases are less prone to oscillations. The method is difficult to implement and parallelize. The main drawback of implicit time schemes is that convergence of linear solvers deteriorates as Δt increases

Explicit time discretization schemes are easy to implement and parallelize but small time steps are required for stability reasons, especially if the velocity and/or mesh size are varying strongly. Such schemes should have a high order of accuracy. For these reasons REEF3D includes the Adam-Bashforth, third and fourth order TVD Runge-Kutta schemes.

- Adam-Bashforth Scheme
  This is a multi step second order scheme, which requires the values from the previous two time steps for the time integration [44]. The example of application of this scheme to the level set function is presented below in equation 2.14.

$$\phi^{n+1} = \phi^n + \frac{\Delta t_n}{2} \left(\frac{\Delta t_n + 2\Delta t_{n-1}}{\Delta t_{n-1}} L\left(\phi^n\right) - \frac{\Delta t_n}{\Delta t_{n-1}} L\left(\phi^n\right) \right) \tag{2.14}$$

  The term 'L' represents the spatial discretization.

- Total Variance Diminishing (TVD) Runge-Kutta Schemes
  Total variation diminishing (TVD) is a feature of certain discretization schemes used to solve partial differential equations in CFD. The scheme was developed by Harten [47] in 1983. A TVD scheme preserves monotonicity. The 3rd order Runge-Kutta scheme [94] is one such example. An example is shown below;

$$\phi^{(1)} = \phi^n + \Delta t L\left(\phi^n\right)$$
$$\phi^{(2)} = \frac{3}{4}\phi^n + \frac{1}{4}\phi^{(1)} + \frac{1}{4}\Delta t L\left(\phi^{(1)}\right)$$
$$\phi^{n+1} = \frac{1}{3}\phi^n + \frac{2}{3}\phi^{(2)} + \frac{2}{3}\Delta t L\left(\phi^{(2)}\right)$$

$$\tag{2.15}$$

14

Another discretization scheme of a higher order in this category is the 4th order TVD Runge-Kutta scheme. This is a four step scheme. An example is shown below.

$$\begin{aligned}
\phi^{(1)} &= \phi^n + \frac{\Delta t}{2} L\left(\phi^n\right) \\
\phi^{(2)} &= \phi^n + \frac{\Delta t}{2} L\left(\phi^{(1)}\right) \\
\phi^{(3)} &= \phi^n + \Delta t L\left(\phi^{(2)}\right) \\
\phi^{n+1} &= \frac{-1}{3}\phi^n + \frac{1}{3}\phi^{(1)} + \frac{2}{3}\phi^{(2)} + \frac{1}{3}\phi^{(3)} + \frac{\Delta t}{6} L\left(\phi^{(3)}\right)
\end{aligned} \tag{2.16}$$

The 3rd and 4th order TVD Runge-Kutta schemes are of 3 and 4 steps, respectively. Hence, they are computationally more demanding than the Adam-Bashforth scheme. On the brighter side they are more accurate due to the higher order of the scheme.

Adaptive Time Stepping

Implicit time steps are restricted by Courant condition where as explicit time steps are restricted by CFL condition to avoid numerical instabilities . With the use of time discretization schemes there are certain limitations for the size of the time step. Larger time step causes numerical instability and too small time step bears the danger on weighing heavily on the computational resources.

To ensure good numerical solution, Courant condition [20] is implemented in implicit time stepping algorithms. Courant condition implies that the fluid being simulated does not move a distance that is more than the computational grid size in one time step. It is written as in equation 2.17

$$\frac{u\Delta t}{\Delta x} \leq C \tag{2.17}$$

The most efficient solution to the problems of choosing time step in explicit time discretization is the use of adaptive time stepping. To implement this, a condition called the CFL criterion is applied, where the time step size for the next step is guided by the maximum values of velocities, viscosity and the volume and surface forces in the current time step, following the CFL condition proposed by Courant, Friedrichs

and Lewy [20]:

$$\delta t \leq 2 \left(\left(\frac{|u|_{max}}{\delta x} + V \right) + \sqrt{\left(\frac{|u|_{max}}{\delta x} + V \right)^2 + \frac{4\,|S_{max}|}{\delta x}} \right)^{-1} \tag{2.18}$$

with

$$V = max\,(\nu + \nu_t) \cdot \left(\frac{2}{(\delta x)^2} + \frac{2}{(\delta y)^2} + \frac{2}{(\delta z)^2} \right) \tag{2.19}$$

where, 'V' stands for the maximum viscosity and 'S_{max}' stands for source term contribution from surface and volume forces.

2.3   Solution of Navier-Stokes Equation

For a complete solution of Navier-Stokes equations, the pressure term in the equation 2.10 needs to be solved. The problem is that it cannot be derived directly from the generic equations. Pressure in Navier-Stokes equation is included as a source term and there is no definition for the advection of the pressure. Due to the absence of a definition for the evolution of the pressure, a direct approach to determine the pressure at the next grid point is not available. The presence of non-linear terms also pose a challenge to arriving at an analytical solution as it would involve the use of implicit methods which can be lengthy and computationally expensive.

REEF3D incorporates several algorithms for solution of pressure term. All the algorithms for dealing with the pressure have in common, that they employ the continuity equation to find the correct pressure field. Among different strategies (Projection Method, SIMPLE, SIMPLEC, SIMPLER and PISO), Projection method and SIMPLE are most widely used.

2.3.1   Projection Method

The projection method for solving pressure uses explicit time treatment of the Navier-Stokes equations proposed by Chorin [15] for incompressible flow. This method is straight forward as the velocity is computed using only values from the previous time step. In this method, an intermediate velocity field is first obtained by completely ignoring the pressure gradient. The intermediate velocity U_i^* is computed using the transient RANS equation:

$$\frac{\partial(U^* - U_i^n)}{\partial t} + U_j^n \frac{\partial U_i^n}{\partial x_j} = \frac{\partial}{\partial x_j} \left[\nu(\phi^n) \left(\frac{\partial U_i^n}{\partial x_j} + \frac{\partial U_j^n}{\partial x_i} \right) \right] + g_i \tag{2.20}$$

The intermediate velocity field U_i^* does not satisfy the continuity equation. In the second step, the projection step,the pressure is used to determine the velocity at the next time step, $n + 1$.

$$\frac{\partial(U_i^{n+1} - U_i^*)}{\partial t} + \frac{1}{\rho(\phi^n)}\frac{\partial P^{n+1}}{\partial x_i} = 0 \qquad (2.21)$$

To solve the equation 2.21, the value of the pressure term, P^{n+1} needs to be known. This is obtained by using the divergence operator on equation 2.21. A condition that the divergence of U_i^{n+1} is zero is applied. This is followed from the continuity equation, which provides a divergence free velocity field. With these definitions the Poisson equation for pressure is formed.

$$\frac{\partial}{\partial x_i}\left(\frac{1}{\rho(\phi^n)}\frac{\partial P}{\partial x_i}\right) = -\frac{1}{\Delta t}\frac{\partial U_i^*}{\partial x_i} \qquad (2.22)$$

In the current study, the Poisson equation is solved using the preconditioned BiCGStab [104] solver. Features of this pressure solver are discussed in 2.3.3 The new value of the pressure is then used in the equation 2.21 to find out the velocity at the new time step, which complies with the continuity equation. The solution scheme of the projection method cannot be used together with an implicit time discretization of the momentum equations. The reason is that the velocities used for the formulation of the Poisson equation are all from the new time step n + 1. After the correction of the velocities through the pressure, they are divergence free. But the newly obtained velocity field does not satisfy the Navier-Stokes equations anymore.

2.3.2   SIMPLE Method

SIMPLE algorithm is a widely used numerical procedure to solve the Navier-Stokes equations in CFD. SIMPLE stands for Semi-Implicit Method for Pressure Linked Equations. Prof. Brian Spalding and his student Suhas Patankar at Imperial College, London in 1972 proposed this method [82].

In the SIMPLE method, the pressure gradient instead of the pressure is used in the momentum equation. Then the pressure equation is replaced by a pressure correction equation. This equation is solved together with the momentum equations successively each time step. Figure 2.1 shows the flowchart of the SIMPLE algorithm.
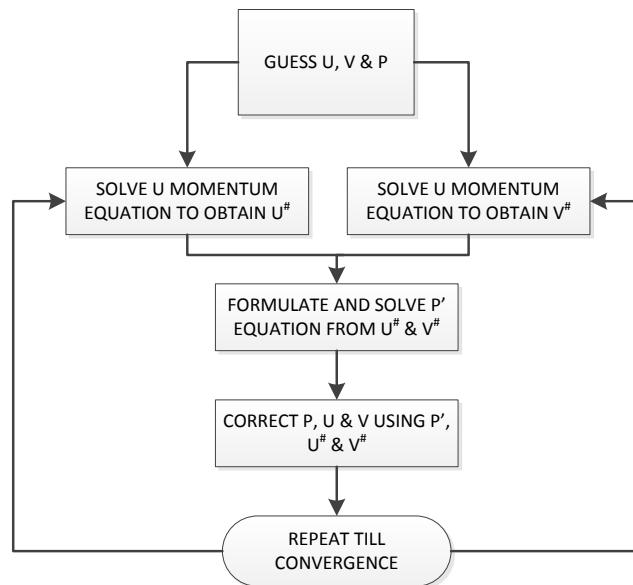
Figure 2.1: Flow chart showing the SIMPLE Algorithm in 2D

2.3.3   Poisson Solver

Numerical solutions of poisson equation (2.22) can be broadly divided into two major categories; namely direct method and iterative methods. Direct methods are computationally intensive which makes iterative solvers a preferred option for the solution of the poisson equation. Many iterative methods exists e.g. the Jocobi method, the Successive Over-Relaxation method, the Gauss-Siedel method, the Multigrid method, Conjugate gradient methods and their variations.

Among iterative solvers two approaches are famous: Newton-like solvers and Global solvers. Newton-like solvers arrive at the solution by linearizing it about an initial estimated value of solution using the TaylorÂťs expansion. The result is, however, dependent upon good initial estimate. Global solvers convert the problem into a minimization problem and tries to find the lowest point on the surface which lies in the opposite direction of the gradient of the function. This minimization is carried out iteratively until it converges to the solution. Global solvers hence do not rely on an initial estimate but the rate of convergence is slow. General iterative solvers search for the minima in just one direction so in event of function having two minima, the solver would oscillate between two successive minimas. Later in 1952 Hestenes and Stiefel developed the Conjugate Gradient (CG) method [49] which was able to minimize the function in several directions while searching in one direction. CG method was ap-

plicable when the directions were conjugate/ orthogonal vectors and in an symmetric systems only.

In 1976 Fletcher developed Bi-Conjugate Gradient (BiCG) method [37] which first converted the non-symmetric system into a symmetric system by the use of a transpose matrix. Because of this the computational demand is double compared to CG method but with same rate of convergence [84].

Van der Vorst in 1992 developed the Bi-Conjugate Gradient Stabilized (BiCGSTAB) method which converges faster and produces accurate solutions as BiCG method [104].

Current study utilizes the BiCGSTAB method to solve the Poisson equation.

2.4   Turbulence Model

The change in flow pattern caused by the interaction of structures with flow gives rise to turbulence. This in turn affects the sediment transport in the channel. To accurately calculate local scour, the modelling of high Reynolds number flows with rough boundaries over a relatively long time period is needed. This requires solving the Navier-Stokes equations directly which requires the resolution of all turbulence scales. The process of resolving all the resolution of turbulence could be achieved through Direct Numerical Simulation (DNS) which solves the Navier-Stokes equations without averaging or approximation other than numerical discretization.These errors can be estimated or controlled. Since the number of grid points that can be used in a computation is limited by the processing speed and memory of machine, DNS is possible only for flows at relatively low Reynolds number and for geometrically simple domains. The results of DNS contain very detailed information about the flow which is far more information than needed for engineering purposes. As a result, DNS is too expensive to be employed as a design tool.

Turbulent flows contain a wide range of length and time scale. The large scale motions are generally much more energetic than small scale motions. The size and strength of large scale makes them the most effective transporter of the conserved properties. A simulation which treats the large eddies in greater details is called Large eddy simulations (LES). LES is 3 dimensional, time dependent and expensive but much less costly than DNS. Consequently, LES is preferred method for flows in which Reynold number is too high or the geometry is too complex to allow the application of DNS. While LES is computationally less demanding then Direct Numerical Simulation (DNS), it is currently still too costly for most real-world cases encountered in the field of hy-

draulic engineering.

For real-life flows at moderate and high Reynolds numbers it is difficult to find a straightforward solution. This has to do with instabilities and the non-linear character of the solutions. One of the ways is to solve the equations numerically taking into account all or some of the length and time scales is by use of DNS and LES respectively. This requires computation and will only be possible for very simple flow geometries and low Reynolds numbers. A less accurate but more fruitful approach is via simplification of the Navier-Stokes equations. In many cases details of the separate fluctuations is not required and a proper prediction of the mean flow field suffices. In order to get to equations that describe the mean motion, the velocity vector and the pressure is decomposed in an ensemble average and a fluctuating component. This approach is called Reynolds-Average Navier-Stokes (RANS). The turbulence modelling approaches in this study make use of the RANS equations together with the widely tested and validated k-ω [115] and k-ϵ models [63]. Apart from k-ω and k-ϵ turbulence models REEF3D also has EARSM [109], SST [73] and LES models in the software.

2.4.1 k-ω Model

k-ω is a two equation model which includes two extra transport equations to represent the turbulent properties of the flow. These two equations lets the model account for effects like convection and diffusion of turbulent energy. The first transported variable is the turbulent kinetic energy k. The second transported variable is the specific turbulent dissipation ω, that determines the scale of the turbulence. The turbulent eddy viscosity ν_t is calculated using k and ω.

Using average and a fluctuating components in the Navier-Stokes equation (equation 2.10), yields after averaging of the equations, the Reynolds equation as in equation 2.23 below.

$$\frac{\partial U_i}{\partial t} + U_j \frac{\partial U_i}{\partial x_j} = -\frac{1}{\rho}\frac{\partial P}{\partial x_i} + \frac{\partial}{\partial x_j}\left[(\nu + \nu_t)\left(\frac{\partial U_i}{\partial x_j} + \frac{\partial U_j}{\partial x_i}\right)\right] + g_i \qquad (2.23)$$

The equations for turbulent kinetic energy k and the specific turbulent dissipation ω is as follows:

$$\frac{\partial k}{\partial t} + U_j \frac{\partial k}{\partial x_j} = \frac{\partial}{\partial x_j}\left[\left(\nu + \frac{\nu_t}{\sigma_k}\right)\frac{\partial k}{\partial x_j}\right] + P_k - \beta_k k\omega \qquad (2.24)$$

20

$$\frac{\partial \omega}{\partial t} + U_j \frac{\partial \omega}{\partial x_j} = \frac{\partial}{\partial x_j}\left[\left(\nu + \frac{\nu_t}{\sigma_\omega}\right)\frac{\partial \omega}{\partial x_j}\right] + \frac{\omega}{k}\alpha P_k - \beta \omega^2 \qquad (2.25)$$

P_k is the turbulent production rate given by equation 2.26, the coefficients in equation 2.24 and 2.25 have the values $\alpha=\frac{5}{9}$, $\beta_k = \frac{9}{100}$ and $\beta=\frac{3}{40}$.

$$P_k = \nu_t \frac{\partial U_i}{\partial x_j}\left(\frac{\partial U_i}{\partial x_j} + \frac{\partial U_j}{\partial x_i}\right) \qquad (2.26)$$

The eddy viscosity ν_t in the RANS-equations is obtained using the two-equation k-ω model [115] using equation . This limited formulation [29] avoids overproduction of turbulence in highly strained flow outside the boundary layer:

$$\nu_t = \min\left(\frac{k}{\omega}, \sqrt{\frac{2}{3}}\frac{k}{|\mathbf{S}|}\right) \qquad (2.27)$$

$\mathbf{S}$ is the mean rate of strain. The mean strain can be very large around the interface between water and air in the case for the oscillatory flow in a numerical wave tank. Under these circumstances the eddy viscosity limiter is no longer effective, and turbulence overproduction can be observed. To avoid this, free surface turbulence damping introduced by and Egorov [31] is used. It uses an additional source term in the ω-equation.

$$S_n = \left(\frac{6\ B\ \nu}{\beta\ dx^2}\right)^2 \beta\ dx\ \delta\left(\phi\right) \qquad (2.28)$$

where, model parameter $B= 100.0$, $dx=$ grid size and ϕ is the level set function. The source term is activated around the interface by multiplying the Dirac delta function $\delta\left(\phi\right)$ with the source term;

$$\delta\left(\phi\right) = \begin{cases} \frac{1}{2\epsilon}\left(1 + \cos\left(\frac{\Pi\phi}{\epsilon}\right)\right) & if\ |\phi| < \epsilon \\ 0 & else \end{cases} \qquad (2.29)$$

2.4.2 k-ϵ model

The structure of the k-ϵ model is similar to the k-ω model. The relation between the specific turbulent dissipation ω and the turbulent dissipation ϵ is:

$$\epsilon = k\omega \qquad (2.30)$$

The transport equation for the k-equation becomes:

$$\frac{\partial k}{\partial t} + U_j \frac{\partial k}{\partial x_j} = \frac{\partial}{\partial x_j}\left[\left(\nu + \frac{\nu_t}{\sigma_k}\right)\frac{\partial k}{\partial x_j}\right] + P_k - \epsilon \qquad (2.31)$$

And the transport equation for the dissipation ϵ is:

$$\frac{\partial \epsilon}{\partial t} + U_j \frac{\partial \epsilon}{\partial x_j} = \frac{\partial}{\partial x_j}\left[\left(\nu + \frac{\nu_t}{\sigma_\epsilon}\right)\frac{\partial \epsilon}{\partial x_j}\right] + c_{\epsilon_1}\frac{\epsilon}{k}P_k - c_{\epsilon 2}\frac{\epsilon^2}{k} \tag{2.32}$$

The formulations for the eddy viscosity and the rough wall functions can easily be changed using Eq.(2.30).

2.5 Free Surface

Many engineering applications deal with multi-phase flows having more than one incompressible and non-miscible fluid phase. This requires the knowledge of the free surface between these phases. In the field of coastal engineering, dealing with waves and sediment transport, the free surface of water is modelled by assuming a two phase flow with air and water.

Among several methods in literature, the major ones are discussed below.

- Lagrangian Approach
  In the Lagrangian approach, the numerical grid adjusts to the free surface. The grid deforms adaptively as the interface changes. Based on the water elevation, the vertical grid spacing changes, which is based on the computed pressure field. These types of method work efficiently as long as the local differences in the water level do not become too large and the free surface is not too complex. Supercritical flow and hydraulic jumps are very challenging for these methods.

- The Marker and Cell method (MAC)
  MAC is an interface capturing method. It was developed by Harlow and Welch [46]. In MAC massless marker particles represent the free surface on an Eulerian grid. Based on the velocity components the marker particles are moved in their vicinities. It allows for adjustments for the passage of marker particles across cell boundaries. It requires great computational effort as the grid needs to be refined around the free surface, in order to avoid a smeared-out solution and the number of particles to be calculated becomes very large [41].

- Volume of Fluid method
  The Volume of Fluid method [50] uses the volume fraction of one fluid for each discretization cell instead of markers for calculation of the free surface. A transport equation is solved to move the scalar field along with the external velocity field:

$$\frac{\partial F}{\partial t} + U_j \frac{\partial F}{\partial x_j} = 0 \tag{2.33}$$

It uses a reconstruction algorithm to extract a geometrical free surface from the fraction function. The accurate reconstruction of the interface is difficult as it effects the mass conservation. One of the major drawbacks of this method is that the free surface tends to get smeared over two to three cells due to the numerical diffusion resulting from the discretization of the fraction function and needs a local grid refinement to accurately represent the free surface. This effect is called foaming. This method is implemented in Ansys Fluent and OpenFOAM.

- Level Set Method
  Over the past several years, a class of numerical technique known as level set method has been built to tackle some of the most complex problems in fluid interface motion. The Level set method is a computational technique for tracking moving interfaces. It relies on an implicit representation of the interface whose equation of motion is numerically approximated using schemes built from those for hyperbolic conservation laws. The resulting technique is able to handle problems in which the speed of the evolving interface may sensitively depend on local properties such as curvature and normal direction, as well as complex physics of the front and internal jump and boundary conditions determined by the interface location. Level set method is particularly designed for problems in multiple space dimensions in which the topology of the evolving interface changes during the course of events, and problems in which sharp corners and cusps are present.

  The Level Set Method (LSM) is employed in REEF3D to model the free surface. This method was proposed by Osher and Sethian[80]. They devised it for computing and analysing the motion of an interface between two phases in two or three dimensions. This method is employed in the current study to model interface between water-air and water-sediments. More details are given below in subsection 2.5.1.

2.5.1 Level Set Method

The location of the interface is represented implicitly by the zero level set of the smooth signed distance function $\phi(\vec{x}, t)$. The level set function gives the closest distance to the interface in every point of the modelling domain. The phases are distinguished by the change of the sign. That results in the following properties:

$$\phi(\vec{x}, t) \begin{cases} > 0 \ if \ \vec{x} \in phase \ 1 \\ = 0 \ if \ \vec{x} \in \Gamma \\ < 0 \ if \ \vec{x} \in phase \ 2 \end{cases} \tag{2.34}$$

Since the interface Γ moves with the fluid particles, the evolution of ϕ is then given by a convection equation for the level set function.

$$\frac{\partial \phi}{\partial t} + U_j \frac{\partial \phi}{\partial x_j} = 0 \tag{2.35}$$

With the level set function in place the material properties of the two phases can be defined on the whole domain. The density and viscosity are constant in each fluid and take on two different values depending on the sign of ϕ. The sharp changes in ρ and ν across the front can present numerical difficulties. To alleviate these problems the interface is given a fixed thickness proportional to the spatial mesh size. The solution is to define the interface with the constant thickness 2ϵ. In that region smoothing is carried out with a regularised Heaviside function $H(\phi)$. The density and the viscosity can then be written as:

$$\begin{aligned} \rho(\phi) &= \rho_1 H(\phi) + \rho_2 (1 - H(\phi)), \\ \nu(\phi) &= \nu_1 H(\phi) + \nu_2 (1 - H(\phi)) \end{aligned} \tag{2.36}$$

and

$$H(\phi) = \begin{cases} 0 & if \ \phi < -\epsilon \\ \frac{1}{2}\left(1 + \frac{\phi}{\epsilon} + \frac{1}{\Pi} sin\left(\frac{\Pi\phi}{\epsilon}\right)\right) & if \ |\phi| < \epsilon \\ 1 & if \ \phi > \epsilon \end{cases} \tag{2.37}$$

The main advantage of using the level set method to calculate the interface between the fluids is that $\phi(\vec{x}, t)$ is smooth across the interface which makes it differentiable at the interface and avoids numerical instabilities.

2.5.2 Reinitialization

In the beginning, the level set function is a signed distance function, however, under the evolution of equation 2.35 it will not necessarily remain so. Therefore, at later times in the computation the level set function must be replaced by a signed distance function without changing its zero level set. When this is performed at the beginning of the calculation, it is called initialization, when performed during the course of the calculation, it is referred to as reinitialization. The level set function needs to be

reinitialized after a certain amount of time. In the present study, this is scheduled after each time step. The quality of the reinitialization has a strong influence on the overall accuracy of the LSM and its mass conservation.

There are several ways to perform this step. One is a straightforward approach; simply evaluate each computational mesh point geometrically and find the signed distance to the front; however, this can be time-consuming. There are two other well established methods to approach reinitialization, the Fast Marching Method (FMM) and the partial differential equation (PDE) approach . This study uses the PDE based reinitialization procedure presented in [102].

$$\frac{\partial \phi}{\partial \tau} + S\left(\phi\right)\left(\left|\frac{\partial \phi}{\partial x_j}\right| - 1\right) = 0 \tag{2.38}$$

$S\left(\phi\right)$ is the smoothed sign function by Peng et al. [83].

$$S\left(\phi\right) = \frac{\phi}{\sqrt{\phi^2 + \left|\frac{\partial \phi}{\partial x_j}\right|^2 \left(\Delta x\right)^2}} \tag{2.39}$$

Equation 2.38 is solved until steady state using an artificial time step $\partial \tau$ which restores the signed distance property. The sign function $S\left(\phi\right)$ returns the value 0 on the interface using the equation 2.39 , which theoretically guarantees the location of the interface to be unchanged. The values for the rest of the domain are assigned according to equation 2.34.

2.6 Numerical Wave Tank

Simulation of wave propagation using CFD is enabled by the implementation of a numerical wave tank. The simulations using the CFD based numerical wave tank mimic the experiments carried out in a wave flume in the laboratory. There has been a strong growth in the availability and capabilities of numerical wave tank models in recent years based on different approaches. The two major approaches involve RANS and potential theory. The numerical treatment coupled with these approaches provide many combinations for the implementation of numerical wave tank in the field of CFD. Some of the possible combinations are;

- Potential Theory with Finite Element discretization
  A Fully Non-linear Potential Flow (FNPF) model was proposed by Grilli [43] to implement the potential theory approach for numerical modelling of waves. Green's identity has been used to transform the Laplace equations for velocity

25

potential (Φ) and its time derivative ($\frac{\partial \Phi}{\partial t}$) to obtain two Boundary Integral Equations (BIE). The Boundary Element Method (BEM) is used to obtain the solution for BIEs. The FNPF model describes the domain through shape functions or splines and the boundary is divided into a finite number of elements. The BIEs yield a finite number of linear algebraic equations. The system of equations is then solved and the values of the unknowns is then determined. After this solution, the unknowns inside the domain can be calculated.

- RANS equations with the free surface description by the VOF method
  An attempt to develop such a numerical wave tank model using the open source CFD software OpenFOAM is presented in [2]. The spatial discretization was carried out by finite volume approach and the free surface was determined by the VOF method. In a further development, a wave generation toolbox was also developed for OpenFOAM with a new method for the wave generation and absorption in the wave tank[52].

- RANS equations with free surface description by the Level Set Method
  The current study uses the Navier Stokes equations and the free surface is obtained using the level set method. The current study uses the domain discretization technique for the implementation of wave tank unlike potential theory approach. The method has also been used by Kamath [55].

- Combination of Potential Theory and RANS equations
  The combination of both the methods is a possible research area as reported by [16]. The use of potential theory with the method of finite elements results in a fast and accurate solution, though RANS equations are preferred for the simulation of wave-structure interactions.

2.6.1 Relaxation Method

The relaxation method is a technique used for the implementation of a numerical wave tank with three relaxation zones. Relaxation functions are used to generate the waves at the beginning, absorb the waves at the end and prevent reflected waves from affecting the wave generation as shown in Figure 2.2. Each zone has its own relaxation function associated with it. Zone 1 takes care of wave generation, Zone 2 prevents reflected waves from affecting the wave generation and the third zone is the numerical beach, which absorbs the waves at the end of the tank. Absence of zone 3 leads to wave reflection and hence, can be used to simulate the formation of standing waves. The relaxation in zone 1 and 2 is achieved using the following rules
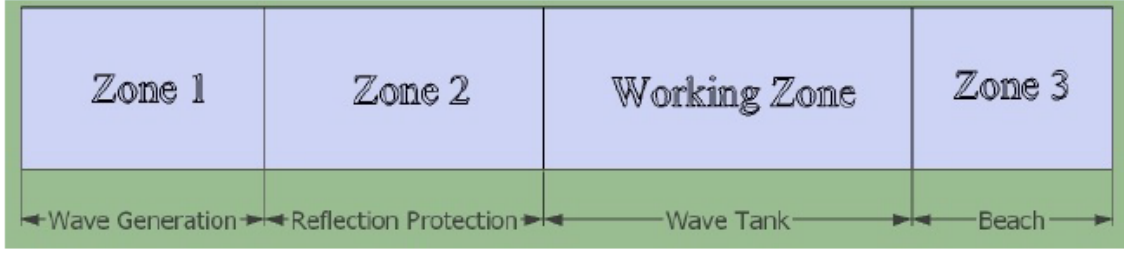
Figure 2.2: Sections of a Numerical Wave Tank (as in [55])

on pressure and velocity in the zone

$$U_{relaxed} = \Gamma(x)U_{analytical} + (1 - \Gamma(x))U_{computational}$$
$$P_{relaxed} = \Gamma(x)P_{analytical} + (1 - \Gamma(x))P_{computational}$$

$$(2.40)$$

Similarly, the relaxation in zone 3 is achieved by the following set of rules for pressure and velocity.

$$U_{relaxed} = \Gamma(x)U_{computational} + (1 - \Gamma(x))U_{analytical}$$
$$P_{relaxed} = \Gamma(x)P_{computational} + (1 - \Gamma(x))P_{analytical}$$

$$(2.41)$$

The function $\Gamma(x)$ changes its value based on the zone to which the relaxation is being applied. The values for the velocities and the free surface are ramped up from the computational values to the the values obtained by wave theory in the wave generation relaxation zone. The computational values for the velocities, pressure and the free surface are smoothly reduced to zero in the numerical beach relaxation zone. This absorbs the wave energy and prevents reflections simulating a beach.

A set of relaxation functions as proposed by Engsig-Karup [34] for the wave absorption and generation, respectively are as follows

$$\Gamma(x) = (1 - x)^p \tag{2.42}$$

$$\Gamma(x) = -2x^3 + 3x^2 \tag{2.43}$$

Using $(1 - x)$ in equation (2.43), produces the function for absorbing reflected waves, so as not to affect the wave generation,

$$\Gamma(x) = -2(1 - x)^3 + 3(1 - x)^2 \tag{2.44}$$

The steepness of the relaxation function is determined using the term p in equation (2.42). For current study a value of $p = 6$ has been used similar to [55]. The figure 2.3 illustrates the shapes of the relaxation functions in their respective zones. A rule of
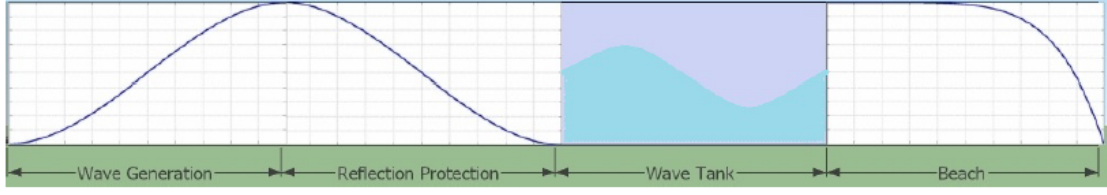
Figure 2.3: Form of Relaxation Functions in the Wave Tank (as in [55])

thumb suggested in [34] is to extend the relaxation zone over 1-2 times the wavelength of the wave being simulated.

Another set of relaxation functions were proposed by Jacobsen et.al. [52] for wave generation and absorption.

$$\Gamma_R(\chi_R) = 1 - \frac{exp(\chi_R^{3.5}) - 1}{exp(1) - 1} \; for \; \chi_R \in [0; 1] \tag{2.45}$$

The form of relaxation function proposed by [52] is used in the current study. The wave generation zone for this study has the length of one wavelength, the numerical beach extends over two wavelengths.

2.7   Immersed Boundary

REEF3D uses a cartesian grid which is not very flexible and cannot be wrapped around a complex geometry. This becomes a problem when an irregular structure is placed in the fluid domain. To deal with this problem a ghost cell immersed boundary method [5] is employed in REEF3D. The cut cells and complex geometries can be accounted for using this method. This method extrapolates the solution into the solid region. The cells in the solid region are fictitious and are called ghost cells. This ensures that boundary conditions are enforced implicitly and numerical discretization does not need to account for boundary conditions explicitly. Figure 2.4 shows the extrapolation along orthogonal lines across the solid boundary using the ghost cell immersed boundary method.
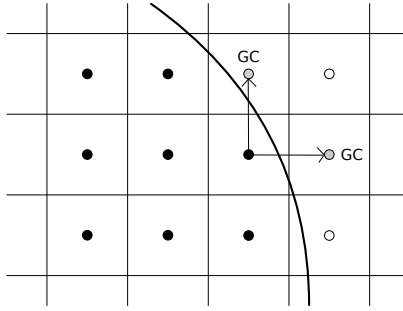
Figure 2.4: Ghost Cell Immersed Boundary (from [6])

2.8 Parallelization

REEF3D makes use of multiple processors for the computation to improve the efficiency of the numerical simulation. This is achieved through the division of a large problem into smaller parts and solving them simultaneously which is called domain decomposition.
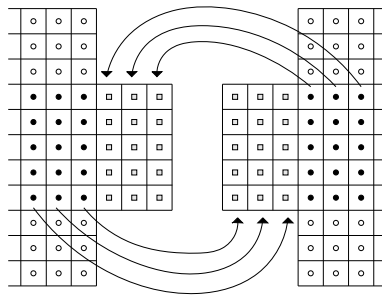
Figure 2.5: Ghost cells of two neighboring processes, the arrows indicate the direction of the update with MPI (from [6])

The domain decomposition results into smaller domains for the problem in consideration and are assigned to different processors. The communication with the neighbours is done through ghost cells. This becomes straightforward as REEF3D uses the ghost cell method for solid boundaries. Ghost cell value exchange is implemented using a method called Message Passing Interface (MPI). The values at the boundaries of each smaller domain is shared among the neighbouring domain during the simulation. Figure 2.5 illustrates working of MPI. The current study has made use of a 12-core workstation for parallelization.

Chapter 3

Sediment Transport

The collective movement of solid particles along a bed of a flowing water body (oceans and rivers) is usually composed of fine cohesion-less loose sediments. This movement of the sediment that happens under the influence of currents and waves is termed as sediment transport. When the bed cannot resist the wall shear stress caused by the flow and the waves, sediment is entrained and transported downstream and the process is called erosion. In the areas of weaker flow the force of gravity on the particles prevails and the suspended sediment settles at the bed surface. This is called deposition. The deposition and erosion deform the river and ocean bed, which affects the flow field and the associated sediment transport in a strongly coupled manner.

In the case of ocean beds in coastal zones where waves are important, the wave stirs up sediment and current transports it. It is established that in combined action of waves and currents, the wave boundary layer remains thin and the current boundary layer fulfils the whole flow depth [66]. In the coexistence of wave and current, even if the current velocity is much larger than the wave-induced velocity near the water surface, the wave-induced velocity will dominate the situation close to the bottom and will cause an increased bed shear stress which in turn will start the initiation of motion. However, because of the one step forward and one step backward nature of water particle movement due to waves, current will usually be the main transporter of the sediments stirred up by the waves, except for wave breaking zones, where a longshore current is produced due to wave breaking [66] .

3.1   Overview of Sediment Transport Models

Flows in rivers and oceans are described by a set of partial differential equations for computer simulations of hydrodynamic and sediment processes. Numerical methods are used to solve these equations. An efficient way to estimate the time and space-

dependent sediment processes are mathematically represented simulations [108]. There are numerous mathematical models available to simulate sediment transport and depositions in one-dimension (1D), two-dimension (2D), and three-dimension (3D).

3.1.1 One Dimensional (1-D) Models

In one-dimensional models the parameters are horizontally and vertically averaged over a cross-section of the water body to achieve a practical solution of the governing equations. The model parameters have the same value over the entire width of the cross section. Two of the most widely used 1-D models to study sediment transport, scour and deposition in large and small rivers are MIKE 11 by DHI and HEC-6 by USACE.

To simulate morphological changes occurring over years in rivers, 1-D models are virtually the only numerical tool available [108]. They are relatively easy to set up and calibrate quickly on desktop computers. Assumptions of 1D flow may not be valid in many situations. Flow in a channel along varying cross-section, changing alignment, or complex tidal flow in the estuaries are some of these examples.

3.1.2 Two Dimensional (2-D) Models

Two-dimensional models are of two major types namely laterally or vertically (depth) integrated. A laterally integrated model solves the laterally integrated momentum and continuity equations for the fluid and the sediment phases [95]. They find applications in the design of pipelines, tunnel trenches and settling traps for irrigation canals [108][12].

2-D(depth integrated) sediment transport models are based on the depth-integrated equations of motion and continuity linked to a depth-integrated sediment transport model. The water surface elevation, velocity, sediment concentration, deposition or scour is computed at each of several points across the cross-section. The model parameters however, are assumed to be uniform through out the water column at each computational point. A 2-D model is required if the problem involves complicated circulation patterns and unsteady flows within the model domain. However, these models are more time consuming to set up than 1-D models, and require much more computer time to run. Therefore, careful planning and analysis is needed to develop the optimum trade-off between the density of the computational mesh or grid and the resulting run times, requirements for computer memory, and storage. One of the disadvantage of 2D models compared to 3D models is that in 2D models the

parameters like velocity are averaged out and hence, might not capture the actual physical process like turbulence. This is based on assumption that one length scale is significantly lower than the others.

Two of the most widely used 2-D models to study sediment transport, scour and deposition in large and small rivers and coastal areas are MIKE 21 by DHI and TABS-MD by USACE.

3.1.3   Three Dimensional (3-D) Models

These models are based on the three dimensional mass balance equations or the convection diffusion equations for suspended sediment transport [108]. In three-dimensional models, both the horizontal and the vertical components of the sediment transport processes are considered. They provide the most complete quantitative representation of any hydrodynamic system. The calibration data requirements are more extensive and expensive [108] as it requires large computational power to capture the complexities of flow in three directions. The application of a 3D model is necessary near or around a hydraulic structure where flow separation and vortex characteristics are truly three-dimensional, and sedimentation processes are complex [108].

Examples of some of the most widely used 3D models for sediment transport are RMA11 (Resource Management Associates, Inc., 2003), ECOMSED (HydroQual, Inc, 2003), CH3D-SED[14], Delft-3D (Delft Hydralics, 2003), SSIM and MIKE 3 (DHI, 2003).

3.2   Sediment Transport Modeling

3.2.1   Modes of Sediment Transport

Erosion of materials of many different shapes and particle sizes and their transport constitutes the mechanism of sediment transport. The mode in which the sediments will be transported downstream depends upon the ratios of the settling velocity of the sediment to the critical bed shear stress[60]. If the wall shear stress exceeds a critical value, the sediment is eroded and suspended. It will be transported in suspension, until it comes to a position where the local flow conditions can not further transport it and will then settle again. Based on this ratio, there are two types of sediment transport modes; suspended load and bed load.

- Suspended load Transport
  Suspended load is composed of fine-sediment particles suspended and trans-

ported through the fluid flow. It is the part of the total sediment load which is moving without continuous contact with the bed as the result of the agitation of the fluid turbulence. The suspended load is related to the total bed shear stress.

- Bed load Transport
  The bed load rolls along the flow bed. This includes the larger and heavier materials. The bed load must be determined in relation to the effective shear stress which acts directly on the grain surface.
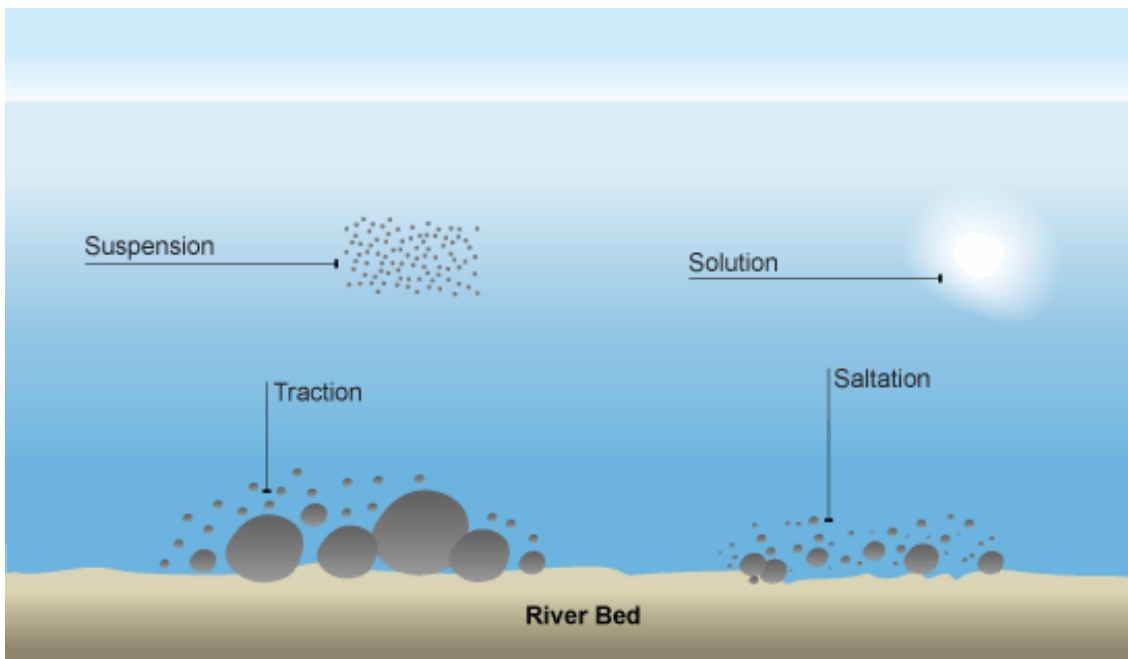
Figure 3.1: Modes of Sediment Transport

3.2.2 Bed shear stress formulations

Bed shear stress is a fundamental quantity in hydraulic and coastal engineering which links the flow conditions and wave motion to sediment transport. The bed shear stress and shear velocity are used to calculate the transport field and the scour, deposition and channel changes [114]. In a complex flow field where both current and waves interact, it is extremely difficult to estimate the correct bed shear. The difficulty of estimating the bed shear stress, particularly in complex flow field when flow is highly three dimensional, has been recognised. Some of the bed shear stress formulations, which are available in literature for estimation of bed shear stress, are discussed. Among these, REEF3D has four bed shear stress formulations (Wall function, friction

33

based, turbulent viscosity/velocity based and turbulent kinetic energy based) which can be used.

Reach-Average Bed Shear Stress

This is the oldest and most popular method for estimation of bed shear stress in rivers [3]

$$\tau = \rho g R S_f \tag{3.1}$$

where τ is bed shear stress, ρ is water density, g is acceleration due to gravity, R is hydraulic radius and S_f is the energy slope. This method is not suitable for small-scale and local estimates of the variation bed shear stress as it gives average bed shear stress of the entire stretch of the river.

Quadratic Stress Law

This is a method to obtain a local estimate of bed shear stress which relates the average bed shear stress to the square of the average fluid velocity U [91].

$$\tau = \rho C_d U^2 \tag{3.2}$$

where C_d is the drag coefficient. The drag coefficient is, however, not constant and is therefore, difficult to estimate [25].

Friction Based

This method makes use of bed friction in calculation of bed shear stress which depends upon the flow regime(smooth or rough).

$$\tau = \frac{1}{2}\rho f U^2$$

$$f = \frac{2g}{C^2} = \begin{cases} \frac{0.06}{(log(\frac{12h_s}{3.3\nu})^2} & if \ \frac{u^* k_s}{\nu} < 5 \\ \frac{0.06}{(log(\frac{12h_s}{k_s})^2} & if \ \frac{u^* k_s}{\nu} > 70 \end{cases} \tag{3.3}$$

Here f is friction coefficient of the bed, which is a dimensionless parameter, k_s is bed roughness parameter generally given by van rijn formulation (k_s=3d_{90} [106]), C is Chezzy coeffecient. u^* is shear velocity and ν is viscosity of the fluid.

Wall function

In this method the local bed shear stress is calculated from the logarithmic relation between the shear velocity and variation of velocity with height [91]

$$\frac{u}{u_*} = \frac{1}{\kappa} ln \frac{z}{z_0}$$
$$u_* = \sqrt{\frac{\tau}{\rho}} \tag{3.4}$$
$$\tau = \rho u_*^2$$

Where u is the velocity, u* is the shear velocity, z is the height above the bed and z_0 is the characteristic roughness length denoted by $k_s/30$. k_s is the bed roughness which is dependent upon the grain size. The most commonly used formulation for k_s is that of van Rijn [106] which uses $k_s = 3d_{50}$ [116].

This is among the most widely used method but there are many uncertainties related to it. In complex flow fields, the velocity profile may not be logarithmic.

Turbulent viscosity/velocity based

The turbulent bed shear stress by definition can be written as

$$\tau = -\rho(\nu_t + \nu)\frac{\partial u}{\partial z} \tag{3.5}$$

Here ν_t is turbulent viscosity obtained from turbulence models (k-ω or k-ϵ) [119].

Reynold stress based

The local bed shear stress can be estimated from the reynold stress if the turbulence parameters/measurements are available inside a numerical or a physical model.

$$\tau = \frac{1}{2}\langle \tilde{u} \rangle \langle \tilde{w} \rangle \tag{3.6}$$

Here $\tilde{u}$ and $\tilde{w}$ are the velocity fluctuations of the stream wise and vertical component and $\langle \rangle$ stands for an average [85].

Turbulent kinetic energy based

This formulation relates bed shear stress to total turbulent kinetic energy. Total kinetic energy (TKE or k) is the product of the absolute intensity of velocity fluctuations from the mean velocity, i.e., the variances of the flow within XYZ coordinate

system, and is defined as;

$$k = \frac{1}{2}\rho(\langle \tilde{u}^2 \rangle + \langle \tilde{v}^2 \rangle + \langle \tilde{w}^2 \rangle) \tag{3.7}$$

Here $\tilde{u}$, $\tilde{v}$ and $\tilde{w}$ are velocity fluctuations in x, y and z direction respectively, and $\langle \rangle$ stands for an average. Simple relationships between k and shear stress have been formulated in turbulence models [39], but further studies have shown that the ratio of k to shear stress is constant [96] [97].

$$\frac{\tau}{k} = \sqrt{c_\mu} \tag{3.8}$$

The proportionality constant $\sqrt{c_\mu}$ was found to be 0.2 by Soulsby [96] while $\sqrt{c_\mu}$= 0.19 has been adopted by Huntley [97]. The current study uses c_μ value of 0.09.

3.2.3 Bed Load Transport

There are many formulations available in literature for the calculation of the bed load transport rate. Most of these formulations relate the transport rate to the bed shear stress. The majority of the formulations use the dimensionless form of sediment transport and bed shear stress rather than their absolute value.

$$\tau^* = \frac{\tau}{(\rho_s - \rho)g d_i}$$
$$\tau_{c,i}^* = \frac{\tau_{c,i}}{(\rho_s - \rho)g d_i} \tag{3.9}$$
$$q_{b,i}^* = \frac{q_{b,i}}{\sqrt{\frac{(\rho_s - \rho)g}{\rho}} d_i}$$

Here ρ_s is the density of the sediment, ρ the density of the water, g is the gravity, d_i the sediment particle diameter. $q_{b,i}^*$ is the dimensionless bed load transport rate also called Einstein number[32], τ^* is the dimensionless shear stress and $\tau_{c,i}^*$ is dimensionless critical shear stress.

The Bed load transport formulations available in current software package REEF3D are discussed below.

van Rijn

The bed load transport rate $q_{b,i}$ was formulated by van Rijn [106] in his publication from 1984.

$$\frac{q_{b,i}}{d_i^{1.5}\sqrt{\frac{\left(\rho_s-\rho\right)\cdot g}{\rho_s}}} = 0.053 \cdot \frac{\left(\frac{\tau-\tau_{c,i}}{\tau_{c,i}}\right)^{2.1}}{\left(d_i\left(\frac{\rho_S/\left(\rho-1\right)\cdot g}{\nu^2}\right)^{1/3}\right)^{0.3}} \tag{3.10}$$

The critical bed shear stress $\tau_{c,i}$ is calculated from the Shields diagram [93] and then multiplied with the reduction factor r in order to take the sloping bed into account. Here ρ_s is the density of the sediment, ρ the density of the water, g is the gravity, d_i the sediment particle diameter, ν the kinematic viscosity of water.

Meyer-Peter and Muller

The earliest bed load equation was developed by Meyer-Peter and associates [74].It is an empirical formulation which was developed using flume measurements of a sediment bed made up of grains sized d = 0.03 −2.9 cm, with varying sediment densities with both well-sorted and naturally sorted material. During the experiments it was noticed that the bed load transport ceased at dimensionless shear stress $\tau^* < 0.047$. The original formula proposed was:

$$q_{b,i}^* = 0; \tau^* < \tau_{c,i}^*$$
$$q_{b,i}^* = \alpha_s(\tau^* - \tau_{c,i}^*)^n; \tau > \tau_{c,i}^* \tag{3.11}$$

Here $\tau_{c,i}^*$ is dimensionless critical shear stress which has a value of 0.047 in original formulation of Meyer-Peter and Muller. α_s is taken to be 8 in the formulation and n as 3/2 in their original formulation. The variations in the coefficient α_s were later generalized as a function of dimensionless shear stress [113].

$$\alpha_s = 1.6\ln\tau^* + 9.8 \tag{3.12}$$

Engelund and Fredsoe

The formulation of Engelund and Fredsoe [33] is based on the dimensionless shear stress and the Einstein number.

$$q_{b,i}^* = 0; \tau^* < \tau_{c,i}^*$$
$$q_{b,i}^* = 18.74(\tau^* - \tau_{c,i}^*)(\tau^{*0.5} - 0.7\tau_{c,i}^{*0.5}); \tau > \tau_{c,i}^* \tag{3.13}$$

3.2.4 Suspended Load Transport

The governing equation for suspended load is a standard convection diffusion equation. The numerical treatment for this transport equation is done in a similar fashion as the momentum equations.

$$\frac{\partial c}{\partial t} + U_j \frac{\partial c}{\partial x_j} + w_S \frac{\partial c}{\partial z} = \frac{\partial}{\partial x_j}\left(\Gamma \frac{\partial c}{\partial x_j}\right) \tag{3.14}$$

The fall velocity of the sediment particles is denoted w_S. The value of the diffusion coefficient Γ is assumed to be equal to the eddy viscosity. The values of the suspended load concentration in the bed cell is used as a boundary condition for the convection-diffusion equation, which is applied in the rest of the computational domain. The deposition rate D at the bed is;

$$D = w_S c_b \tag{3.15}$$

Here c_b is the sediment concentration near the bed calculated using the equation 3.14. In the current model, the concentration at the nearest cell centre is used in equation 3.15. The entrainment rate E is calculated with van Rijn's suspended load formula [107].

$$c_{bed,susp.load,i} = \frac{E}{w_S}$$

$$c_{bed,susp.load,i} = 0.015 \frac{d_i}{a} \cdot \frac{\left(\frac{\tau - \tau_{c,i}}{\tau_{c,i}}\right)^{1.5}}{\left(d_i \left(\frac{\rho_S/\left(\rho_W - 1\right)\cdot g}{\nu^2}\right)^{1/3}\right)^{0.3}} \tag{3.16}$$

The entrainment rate is given at some reference level a very near the bed to avoid singularity. The reference level a in van Rijn [107] is 0.05 times the water depth from bed.

3.2.5 Bed Morphology Model - Level Set Method

The level-set method is employed in REEF3D model to track the movable sediment surface. This technique has also been implemented by Kraft in her paper on large eddy simulation of sediment deformation in a turbulent flow [60]. The evolving bed is represented implicitly by the zero level set of the smooth signed distance function $\phi(\vec{x}, t){=}0$. The equation for the evolution $\phi(\vec{x}, t)$ of corresponding to the motion of the interface is given by;

$$\frac{\partial \phi}{\partial t} + F|\nabla \phi| = 0 \tag{3.17}$$

Here F is propagating velocity of the interface along its normal direction given by:

$$F = \frac{\partial z_b}{\partial t} \tag{3.18}$$

Here z_b is the local bed surface elevation. The velocity of the sediment surface F is determined by the mechanism of sedimentation and erosion due to bed load and suspended load transport, which particularly is dependent of the local wall shear stress. This is known as Exner equation (as in 3.19)

$$(1 - p')F = -\frac{\partial q_{B,x}}{\partial x} - \frac{\partial q_{B,y}}{\partial y} - E + D \tag{3.19}$$

Here p' is the porosity of the bed layer. The terms on RHS of equation 3.19 are evaluated in the direction normal to the sediment surface. In the model, the flow field is first calculated by solving Navier-Stokes equation. Then the obtained flow field and the turbulent eddy viscosity are employed to solve for the bed load and suspended load. By solving the level set equation 3.17, the position of the sediment surface, indicated by the zero level set $\phi(\vec{x}, t)=0$ is updated for each morphological time step.

3.2.6   Bed Shear Stress reduction

The threshold of sediment motion is one of the most important mechanism that determines the bed load transport rate occuring under stream flow. This threshold of motion is defined by Shield's diagram [93] which uses a semi-empirical approach, combining the equilibrium of forces on a sediment particle with his experimental observations. This diagram does not take into account the effect of bed slope. On a sloping bed, the incipient motion of sediment particles is not only a function of hydrodynamic forces, but also additional gravity and tractive components have to be included, in order to correct the critical shear stress obtained from the Shields diagram. One such example is scour hole. To calculate the reduced shear stress (Eq. 3.20), initially the critical shear stress τ_0 is calculated for a flat bed. Then a reduction factor r, based on formulations given in literature[62][59][51][23], is calculated which takes the slope of the bed into account. Fig. 3.2 shows the two angles for a tilted bed cell. The reduction factor r is multiplied with τ_0 to give the final critical shear stress τ_c.

$$\tau_c = r \cdot \tau_0 \tag{3.20}$$

The CFD model used in current study includes formulations by Kovacs and Parker [59] and Dey [23] [24] to account for the reduced critical shear stress on a sloping bed.
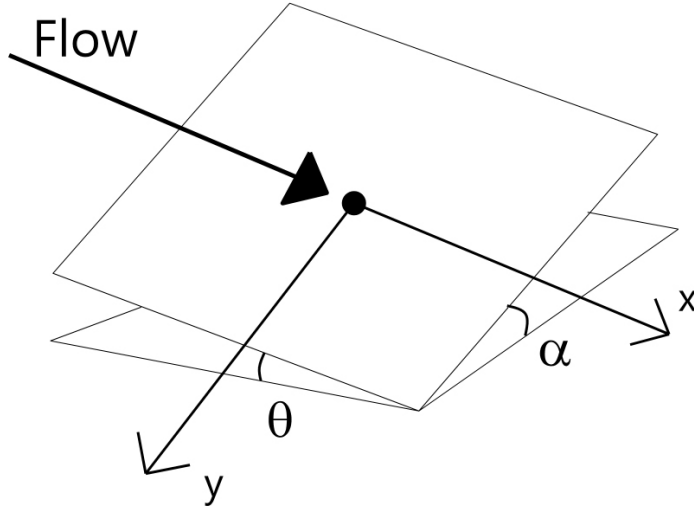
Figure 3.2: Tilted bed cell with the longitudinal angle θ and the transversal angle α (as in [6])

Kovacs and Parker

The first research work on the impact of sloping beds on the incipient motion on sediment particles was done by Lane [62]. His focus was exclusively on the effect due to side slopes, but he did not include the longitudinal angle. Side slope is the angle perpendicular to the flow direction, the transversal angle α and angle in flow direction is the the longitudinal angle θ. The angle φ is the angle of repose which is a material parameter. Kovacs and Parker [59] developed a vectorial equation for the threshold for a combined transversal and longitudinal sloping bed. The parameter Δ represents the effect of the lift force and can be approximated with $\eta \tan \varphi$ The equation was analytically solved by Seminara [92] as a quadratic equation (Eq. 3.21).

$$(1 - \Delta)\, r^2 + 2 \left(\frac{\Delta}{\sqrt{1 + \tan^2 \theta + \tan^2 \alpha}} + \frac{\sin \theta}{\tan \varphi} \right) r$$

$$+ \frac{1 + \Delta}{1 + \tan^2 \theta + \tan^2 \alpha} \left(\frac{\tan^2 \theta + \tan^2 \alpha}{\tan^2 \varphi} - 1 \right) = 0$$

(3.21)

Dey

Dey [23] found an empirical expression (Eq. 3.22). It included both the transverse angle α and the longitudinal angle θ. As a result of further research Dey [24] derived

40

an analytical form of the formula (Eq. 3.23). Besides α and θ, the lift/drag force ratio η was also included in this formula.

$$r = 0.954 \left(1 - \frac{\theta}{\varphi} \right)^{0.745} \left(1 - \frac{\alpha}{\varphi} \right)^{0.372} \tag{3.22}$$

$$
\begin{aligned}
r = &\frac{1}{\left(1 - \eta \tan \varphi \right) \tan \varphi} \Big\{ -\Big(\sin \theta + \eta \tan^2 \varphi \sqrt{\cos^2 \theta - \sin^2 \alpha} \Big) \\
&+ \Big[\Big(\sin \theta + \eta \tan^2 \varphi \sqrt{\cos^2 \theta - \sin^2 \alpha} \ \Big)^2 \\
&+ \Big(1 - \eta^2 \tan^2 \varphi \Big) \Big(\cos^2 \theta \tan^2 \varphi - \sin^2 \alpha \tan^2 \varphi - \sin^2 \theta - \sin^2 \alpha \Big) \Big]^{0.5} \Big\}
\end{aligned} \tag{3.23}
$$

3.2.7 Sandslide

The start of erosion in individual bed cells results in tilted bed cells. At the next time step the critical shear bed stress is reduced. As a result there is more erosion in the cell. The slope of the cell will become even steeper, leading again to a smaller r in the following time step. Hence, without taking special care the erosion of bed cells will never stop. To this effect, the implementation of a sand slide algorithm is necessary. The sand slide algorithm thus acts as limiter for the bed shear stress reduction in erosion process. Some of the previous studies [77] [88] implemented the sand slide algorithm by correcting the slope of the bed when it became larger than the constant angle-of-repose under air φ. Some studies [77] made use of a constant φ where others [88] [6] made use of the sand slide algorithm that gives all bed cells the same slope, namely φ-2°, giving the scour hole a very uniform look.

The current study utilizes the sand slide algorithm as presented in [11]. When the slope of the bed becomes larger than φ, the slope of the concerned bed cell is readjusted by redistributing the volume of sediment in all the 8 neighbouring cells of the plane. The slope limiter algorithm is implemented for a particular bed cell when:

$$
\begin{aligned}
h_{i,j} - h_{1+1,j} &> tan(\alpha) \cdot \Delta x \\
h_{i,j} - h_{1,j+1} &> tan(\alpha) \cdot \Delta y
\end{aligned} \tag{3.24}
$$

If the condition given in equation 3.24 is found true then redistribution takes place in such a way that the height of lateral and longitudinal cells increase/decrease by dh/24 and the cell concerned height is reduced/increased by the same amount. In case of diagonal cells this value is found out to be dh/48. dh is the difference in height of the two adjacent cells. This process is continued until the bed angle becomes equal to the angle of repose. Figure 3.3 shows a plan view of cells undergoing sand slide

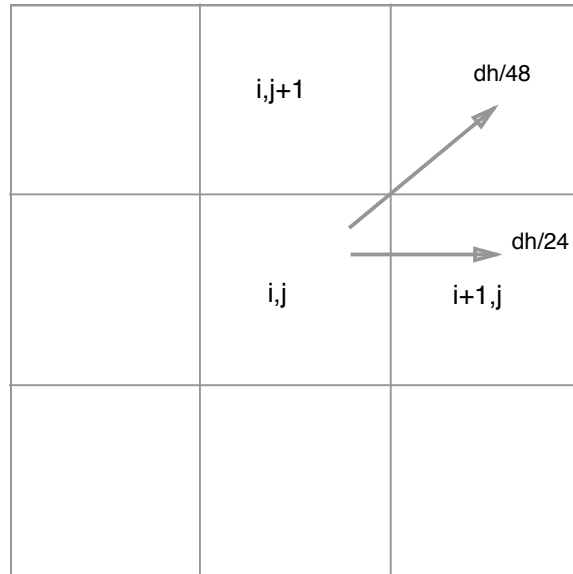redistribution. This process gives a uniform look to the scour hole.

Figure 3.3: Plan view of cells undergoing the sand slide process

3.2.8 Time Step Decoupling

Numerical modelling of erosion and deposition is a very complex process. It involves the correct prediction of the flow conditions coupled with the sediment transport modelling and the bed evolution. The movement, erosion and deposition of the sediments are extremely sensitive to slight changes in the flow conditions and leads to evolution of the bed. As these processes are interdependent, the numerical models should ideally use same time step for the bed evolution as for the hydrodynamic solver. This fully coupled approach for the bed evolution is computationally very expensive [119]. As a result most of the existing numerical models make use of either semi-coupled or fully decoupled approach.

A semi-coupled approach assumes that the flow and the suspended sediment transport have same time scale whereas the bed level changes and the bottom roughness redistribution have much larger time steps than the one used for the flow and suspended sediments. It solves the flow and suspended sediment transport first at each flow time step and then uses the updated flow fields to calculate bed load transport and bed evolution using a larger (morphological) time step. This is based on the assumption that suspended sediments has a negligible influence on the flow.

A fully decoupled approach is implemented in REEF3D. It assumes no interaction

of flow with suspended load, the bed load or the bed level changes. The morphological time step, which is much larger than the hydrodynamic time step, is used for the computation of the suspended sediment transport, the bed load transport and evolution of the bed. This assumption is valid in cases where suspended sediment concentration is too low to alter the flow conditions forming a feedback process. This approach for REEF3D is further strengthened by the fact that in the numerical model the morphology and the bed load transport processes are calculated in terms of bed load layer and not individual sediment particle.

Chapter 4

Scour under uniform flow conditions

The first task of the current study is to test and validate the sediment transport module of CFD code with abutment scour (section 4.1). To this effect, the results obtained from the CFD code are compared against experimental data for comparison. The test cases in this section have constant inflow as the boundary condition. The effect of the variation of different parameters on the abutment local scour development is observed. Two more test cases namely 3D numerical modelling of pier scour (section 4.2) and contraction scour (section 4.3) are studied under uniform flow conditions and compared with experimental results for comparison.

To simulate the test cases, a three dimensional channel with different length, width and depth is used along with an abutment, pier or contraction depending on the experimental setup used for the respective test cases. To compare the results with experiments two features have been studied; The scour hole pattern (the depth and its location) and the time development of the scour for these cases.

4.1 Abutment

Failure of bridges due to local scour has motivated many investigators to explore the causes of scouring and to predict the maximum scour depth at abutments. The flow field at an abutment embedded vertically in a loose sediment bed of an open channel is complex in nature; and the complexity increases with the development of a scour hole involving separation of flow to form a three-dimensional vortex flow system at the base of the abutment. Some promising theoretical and experimental studies [86] [61] [75] have been done in the past to study the scouring pattern around the abutment which bring us closer to better understanding of the problem. It is revealed that the

exact scour mechanism and effect of different parameters on the scour depth are yet to be fully understood or explored. The study of this case is thus an attempt to test a numerical model which can represent the process of abutment scour.

4.1.1 Experimental Setup

The physical experimental study [71] was conducted at Politecnico di Milano, Dept. I.I.A.R., Milan, Italy. The experiment reported herein was performed in a rectangular channel, 15 m long and 0.6 m wide. The channel was filled with approximately uniform natural sediments of mean diameter $d_{50} = 1.9$ mm. The rectangular abutment model was made of PVC and its dimensions were b = 20.2 cm and L = 10.2 cm, respectively, in the transverse and in the stream-wise directions. The test parameters were: uniform water depth h = 9.5 cm; mean flow velocity U = 0.47 m/s; longitudinal slope S = 0.0012. This corresponded to nearly incipient condition for the undisturbed bed with a shields parameter of 0.03. The duration of the experiment was 2 hours. This experiment is considered in the study for the validation of REEF3D code.

4.1.2 Numerical Model Setup

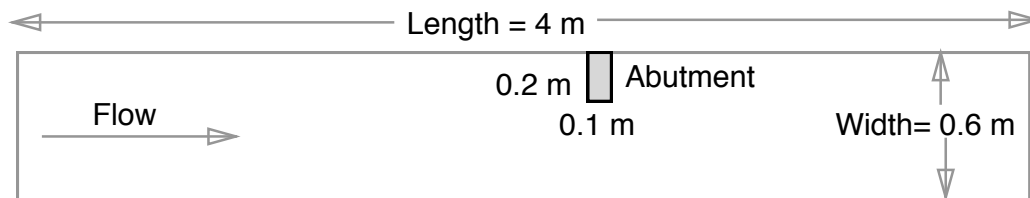The numerical model setup for abutment scour case is as shown in figure 4.1.

Figure 4.1: Abutment: Numerical Setup

For the investigation of the abutment scour, the sediment transport module of REEF3D [6] has been used. The Reynolds- Averaged Navier-Stokes (RANS) equations are solved in all three dimensions, making it fully three-dimensional. The eddy viscosity ν_t in the RANS equation is determined by the use of the two-equation k-ω model [115] and k-ϵ model [63]. Using the conservative finite-difference framework on a structured-staggered grid, convective terms of RANS equation is discretized with the fifth-order WENO (weighted essentially non-oscillatory) scheme [53]. The pressure gradient term in the RANS equation is modelled using Chorinấts projection method [15]. For time treatment Adam Bashforth, a third-order accurate TVD Runge-Kutta

scheme [94] and 4th order accurate TVD Runge-Kutta scheme is employed . The location of the free surface is represented using level set method. The Engelund and Fredsøe [33] sediment transport formula is used to calculate the bed load. Van Rijn's [107] formula for the suspended load is used to account for suspended load transport. Bed shear stress formulation based on turbulent viscosity as presented in section 3.2.2 have been used. The bed changes for erosion and deposition are calculated from the exner equations using the level set method [60]. Kovacs and Parker [59] and Dey [23] [24] formulations of bed shear stress reduction due to the sloping bed is implemented along with the sand slide algorithm as in [11] to take care of erosion of individual bed cells.

4.1.3   Numerical Results

A three Dimensional tank 4 m long, 0.6 m wide and 0.5 m deep with 0.095 m water depth is used. The location of the centre of the abutment is 2.25 m, 0.5 m and -0.05 m in x, y and z direction, respectively. The abutment is 20.2 cm wide and and 10.2 cm long. A 0.30 m thick sediment layer has been used in the numerical model setup. Parameters like grid size, turbulence models (k-ω and k-ϵ), time discretization schemes, porosity and sloping bed formulations are varied to test the performance of the REEF3D sediment transport module. To this effect, the bed elevation changes along with the time development obtained using the numerical model are compared against the experimental results.

Figure 4.2 shows bed elevation changes of the scour hole after 2 hours of the experiment. For the sake of better visualisation the figure shows 4m of tank length with adjusted bed elevation for this configuration with location of abutment as reference. Other dimensions are same as in the experiment. The maximum scour depth after 2 hours of experiment is found to be 20.5 cm.
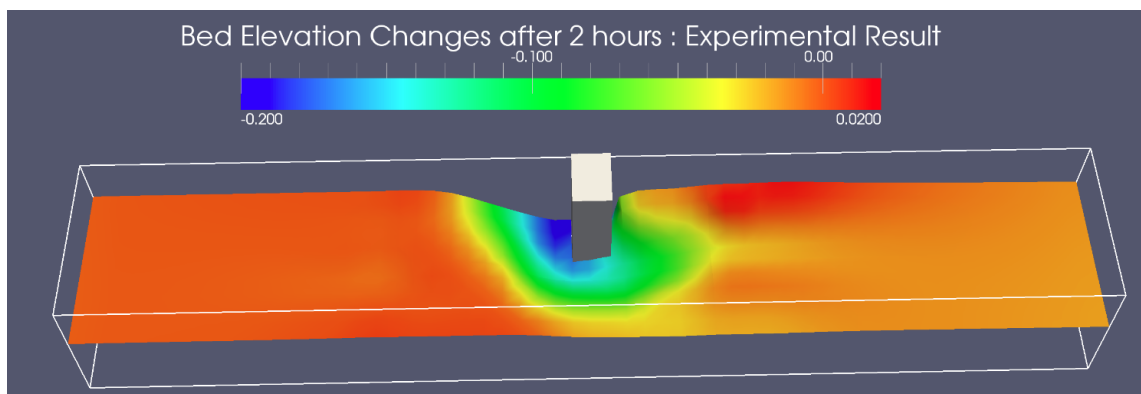

Figure 4.2: Abutment: Experimental Result

Effect of Grid Size

The grid size of the computational mesh is one of the important factors that affects the performance of the numerical model. A smaller grid width (dx) would implies more number of cells in the computational domain and provide better solutions. This however, results in higher computational time. A trend of improved results that matches experimental data is expected with reducing grid size. It is also important to arrive at an optimum grid size which ensures accurate results without being too expensive with regards to computation time.

In this subsection, the model runs are carried out with WENO spatial discretization scheme and 3rd order Runge-Kutta time discretization scheme. Turbulence model used is k-ω. The porosity of the bed layer is kept at 0.75. Kovacs and Parker [59] formulation of bed shear stress reduction due to sloping bed is implemented along with the sand slide algorithm. To test the performance based on grid size model tests have been carried out with dx= 0.05 m, 0.025 m and 0.015 m.

Figure 4.3 presents the solution obtained with grid cell size of 0.05 m. A difference in prediction of scour depth (19.2 cm) compared to experimental result is observed. The scour depth near the nose of the abutment is under-predicted and the scouring pattern does not match the experimental result accurately. The scouring hole location is however accurately predicted. Figure 4.4 and 4.5 presents the solution obtained with grid cell size of 0.025 m and 0.015 m respectively. An error is still observed with 2.5 cm mesh size but the scour hole looks more similar to the experimental results compared to the 5 cm mesh size results. With a mesh size of 0.015 m the scour hole depth, scouring pattern and scour hole location is in close match with the experimental result. The maximum scour hole depth with grid size of 0.025 m is 16.5 cm where as with grid size of 0.015 cm is 20.8 cm similar to the experimental result.
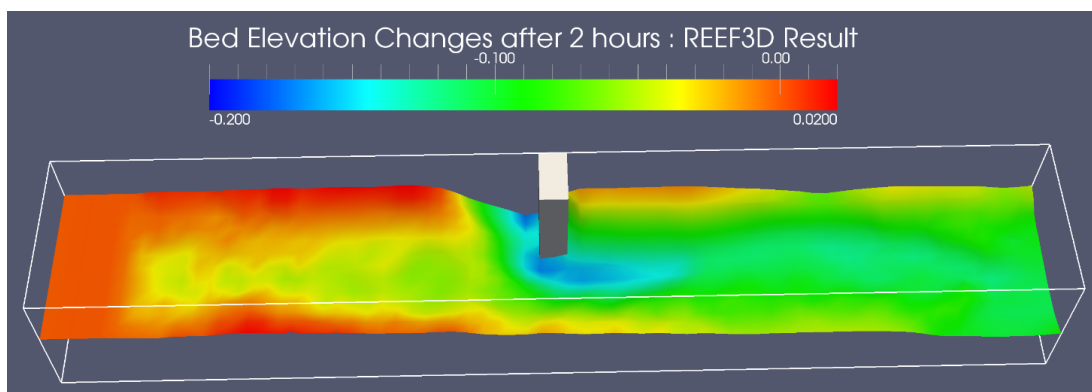

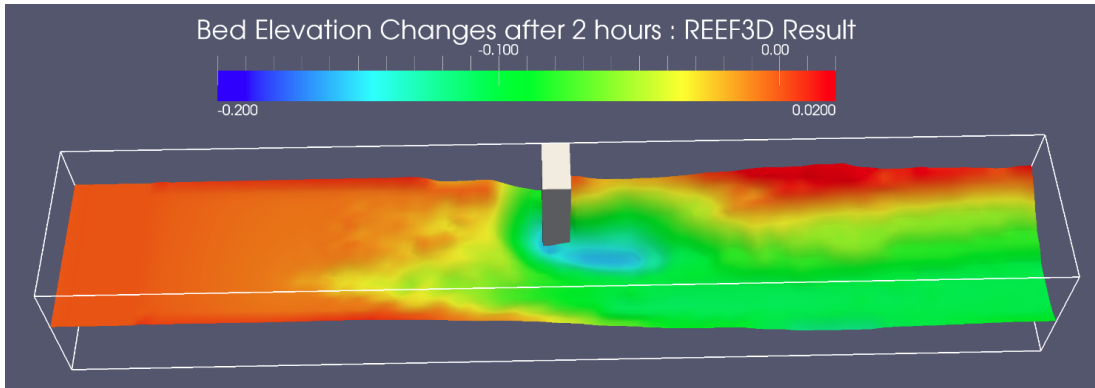Figure 4.3: Abutment: Model result with 0.05 m grid size

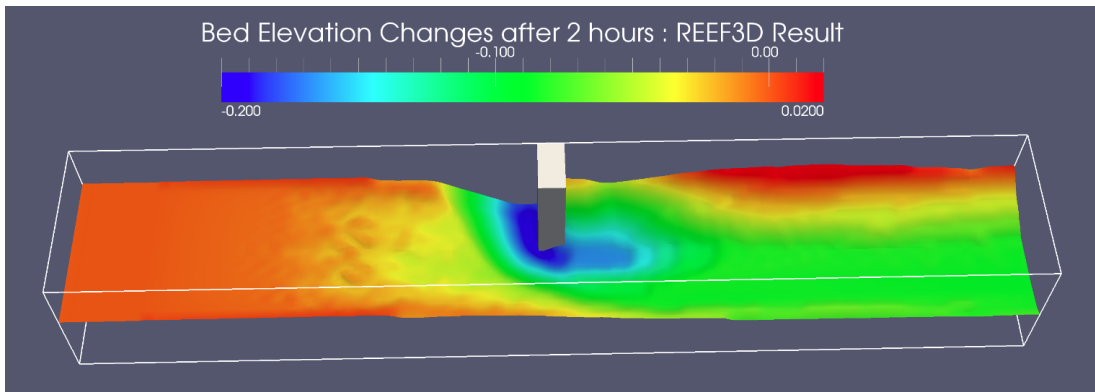Figure 4.4: Abutment: Model result with 0.025 m grid size

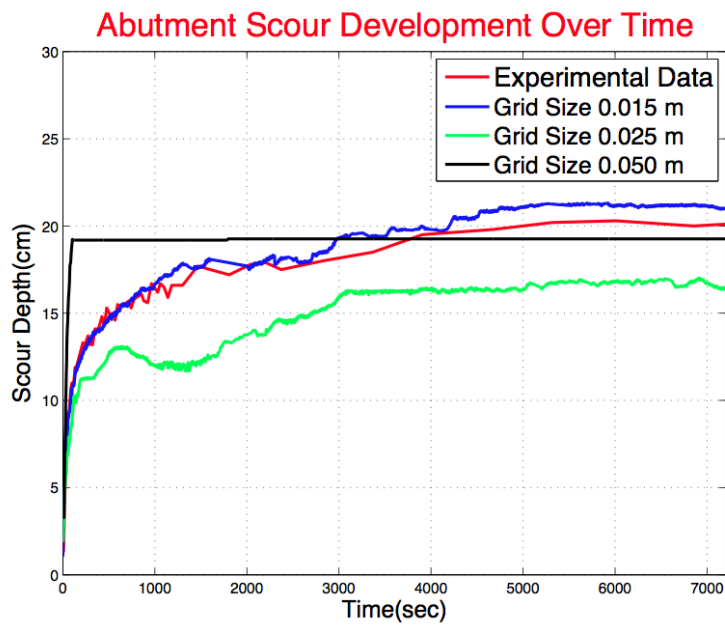Figure 4.5: Abutment: Model result with 0.015 m grid size

Figure 4.6: Abutment: Time Development of Scour with varying grid sizes

48

It is seen that the numerical solutions start to match the experimental result with decreasing dx. The time development of the scour hole using the three grid cell sizes are compared against experimental results as shown in figure 4.6. It is noticed that the time development of the scour matches experimental result with decreasing mesh width. Mesh width of 5 cm fails to capture the time development of the scour hole where as the time development improves with decreasing grid size. The main reason for better result with decreasing grid size is better discretization which avoids numerical diffusion and models the real physical process accurately.

Performance of Turbulence models

Two turbulence models (k-ω and k-ϵ) out of many that are available in REEF3D were presented in section 2.4. The performance of these two models are tested by comparing the time development of scour with the experimental result. The model runs are carried out with WENO spatial discretization scheme and 3rd order Runge-Kutta time discretization scheme. The mesh width used is 0.015 m. Kovacs and Parker [59] formulation of bed shear stress reduction due to sloping bed is used.

Figure 4.7 presents the solution obtained using the k-ω turbulence model. A small difference in prediction of scour depth (20.8 cm) compared to experimental result is observed. The scour depth near the nose of the abutment is well predicted and the scouring pattern matches the experimental result accurately. The scouring hole location is also well predicted.

Figure 4.8 presents the solution obtained using k-ϵ turbulence model. Scour depth in this case is over predicted (22.8 cm) and the scouring pattern does not match match the experimental result accurately. The scour hole location near the abutment is more or less well predicted. An additional scour hole at the end of the tank is observed which is absent in the experimental results and the numerical results with the k-ω turbulence model. This outcome is not that surprising, since the bed shear stress formulation (based on shear velocity given in section 3.2.2) used is directly proportional to ν_t, which can be slightly over predicted with the k-ϵ turbulence model. This leads to increased shear stress at the bed causing more erosion. The time development of the scour hole using the two turbulence model against experimental results is shown in figure 4.9. It is noticed that the time development of scour matches the experimental results using the k-ω model compared to the k-ϵ model.
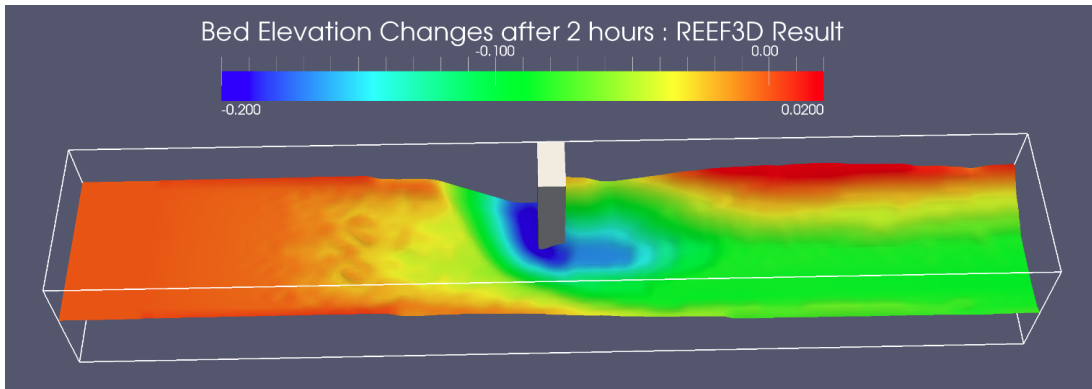
Figure 4.7: Abutment: Model result with k-ω turbulence model
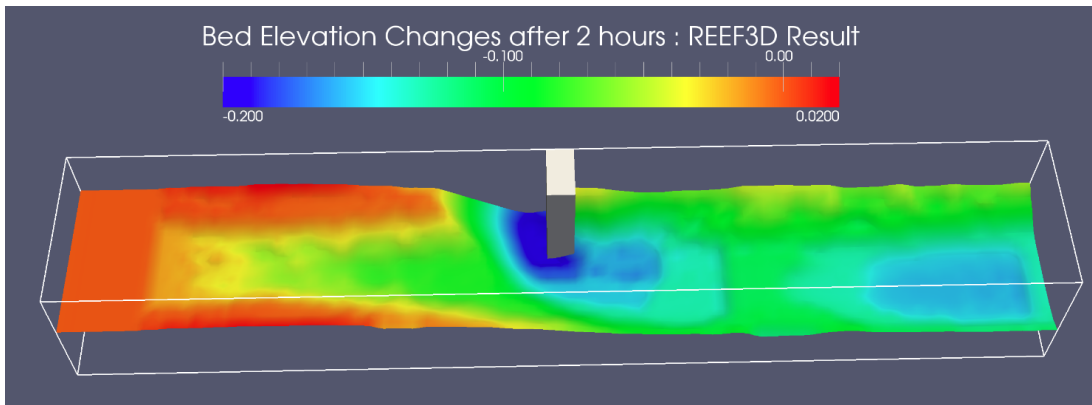

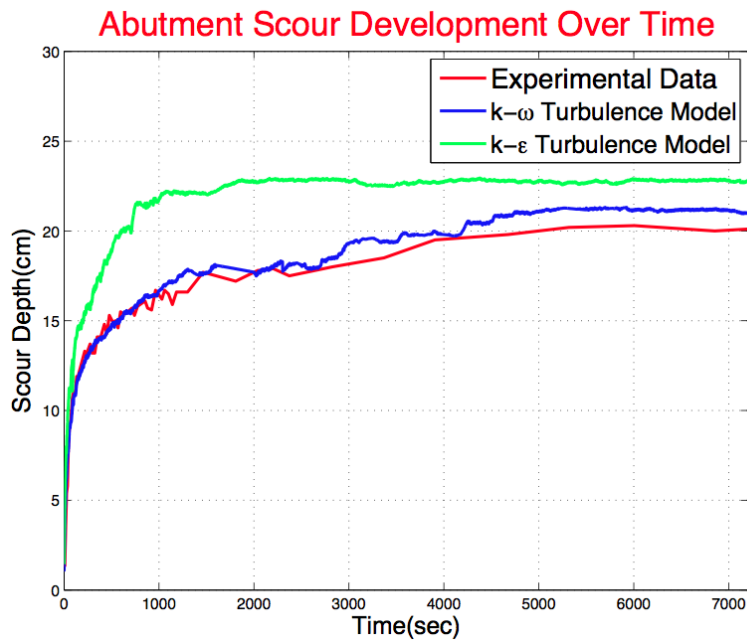Figure 4.8: Abutment: Model result with k-ϵ turbulence model

Figure 4.9: Abutment: Time Development of Scour with different turbulence models

Performance of different time discretization schemes

In this part the effect of higher order time discretization of the momentum equation and the level set function is explored. The time discretization schemes described in section 2.2.2 are employed to observe the difference in the solution among methods with Adam Bashforth (second order), 3rd and 4th order TVD Runge-Kutta time discretization schemes. The turbulence model used is k-ω. The mesh width used is 0.015 m. Kovacs and Parker [59] formulation of bed shear stress reduction due to sloping bed is used.
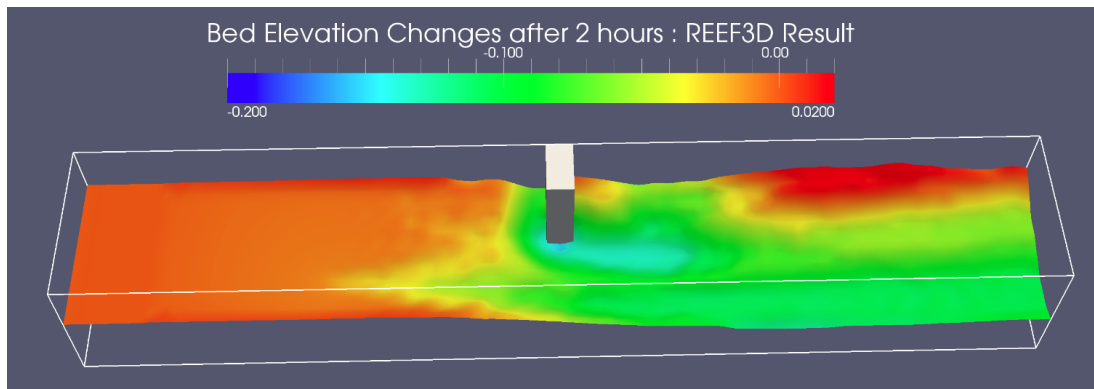
Figure 4.10: Abutment: Model result with 2nd order Adam-Baschforth time discretization scheme

Figure 4.11: Abutment: Model result with 3rd order Runge Kutta time discretization scheme

Figure 4.10 presents the solution obtained using the 2nd-order Adam-Baschforth time discretization scheme. A big difference in prediction of scour depth (16.2 cm) compared to experimental result is observed. The scour depth near the nose of the abutment is very much under predicted but the scouring pattern more or less matches the experimental result. The scouring hole location is predicted correctly.
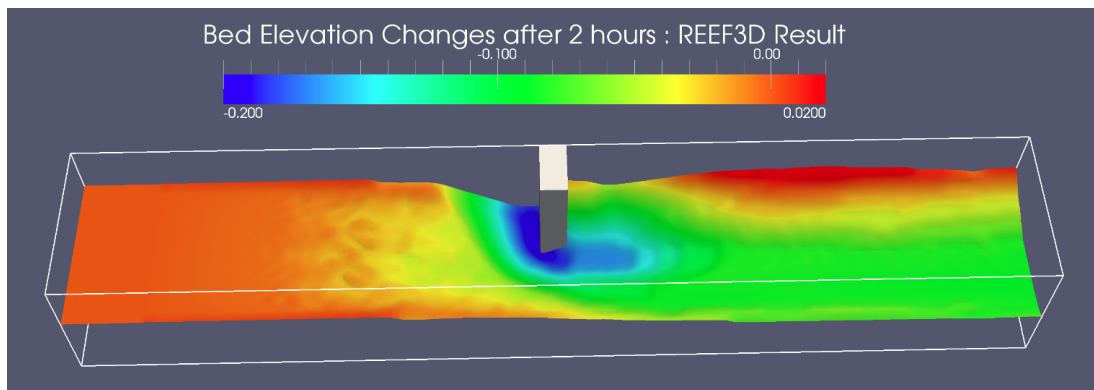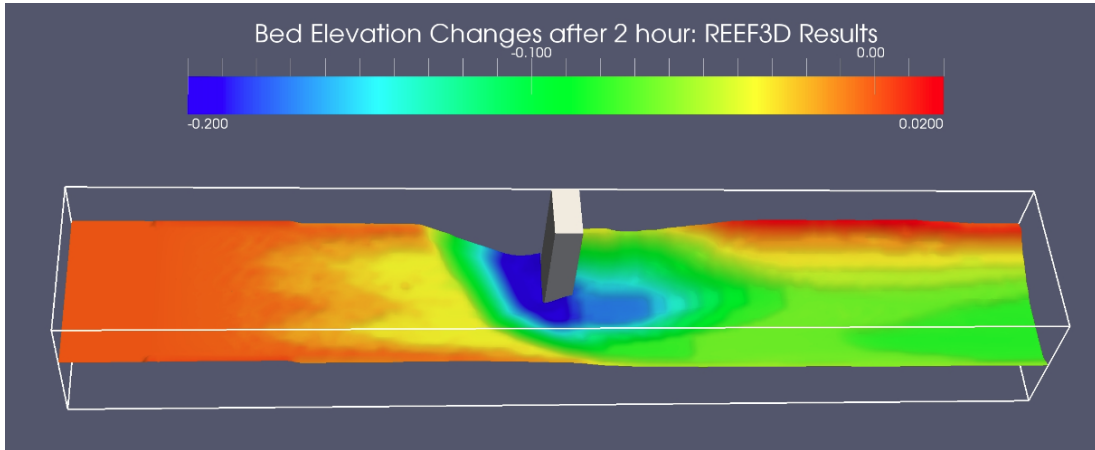
Figure 4.12: Abutment: Model result with 4th order Runge Kutta time discretization scheme

Figure 4.11 presents the solution obtained using 3rd order Runge-Kutta time discretization scheme. A small difference in the scour depth (20.8 cm) compared to experimental result is observed. The scour depth near the nose of the abutment is well predicted and the scouring pattern matches the experimental result accurately. The scouring hole location is also well predicted. Figure 4.12 presents the solution obtained using 4th order Runge-Kutta time discretization scheme. The location of the scour hole using this scheme is well predicted and the scour pattern does not show erosion near the abutment wall as depicted in the experimental result. However, the maximum scour depth (21 cm) is well predicted which is close to the experimental result.

The time development of scour hole using the three different time discretization schemes against experimental results is shown in figure 4.13. It is noticed that the time development of scour closely matches experimental result using the 3rd and 4th order Runge-Kutta time discretization scheme compared to Adam-Baschforth time discretization schemes. This outcome is not that surprising, since higher order time discretization ensures better numerical results. It is to be mentioned that even though both 3rd and 4th order Runge-Kutta time discretization scheme predict the time development of scour accurately, a 3rd order Runge-Kutta scheme is preferred, since it requires less run time to achieve the same accuracy compared to the 4th order Runge-Kutta time discretization scheme.
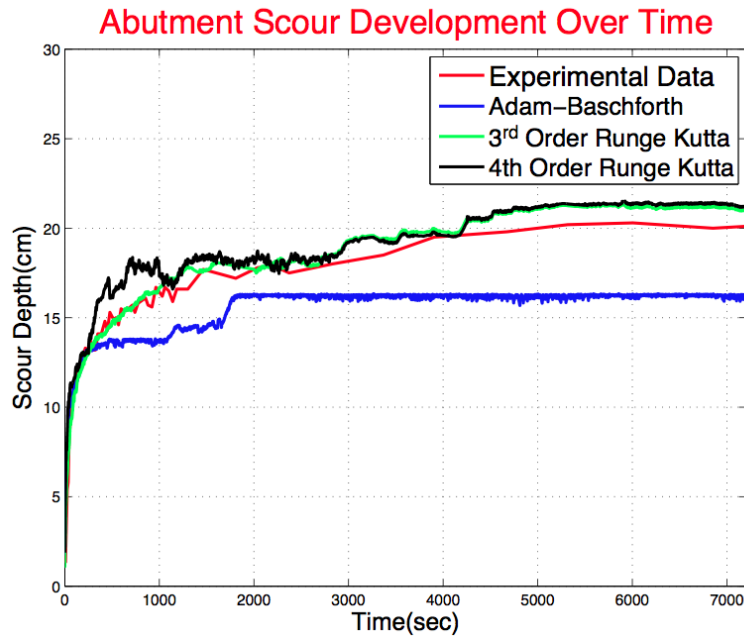
Figure 4.13: Abutment: Time Development of Scour with different time discretization schemes

Performance of different formulations for critical shear stress reduction for sloping bed

When modelling local scour, steep bed slopes up to the angle of repose occur. In order to be able to predict the depth and the shape of the local scour correctly, the reduction of the critical shear stress due to the sloping bed has to be taken into account. The focus of the current section is to investigate different formulas for the threshold of non-cohesive sediment motion on sloping beds. Some of the formulae only take the transversal angle (perpendicular to the flow direction) into account, while others consider the longitudinal angle (stream wise direction) as well. It has been established [7] that formulae which take both transversal and longitudinal angle into account predict better results. This section investigate three different formulae for the reduction of critical shear stress due to sloping bed; Kovacs and Parker [59], Dey' Analystical [24] and Dey's Empirical [23] formulation.

Figures 4.14 , 4.16 and 4.15 present the solution obtained using Kovas and Parker, Dey's Analytical and Dey's Empirical formulation for reduction of critical shear stress on sloping bed respectively.
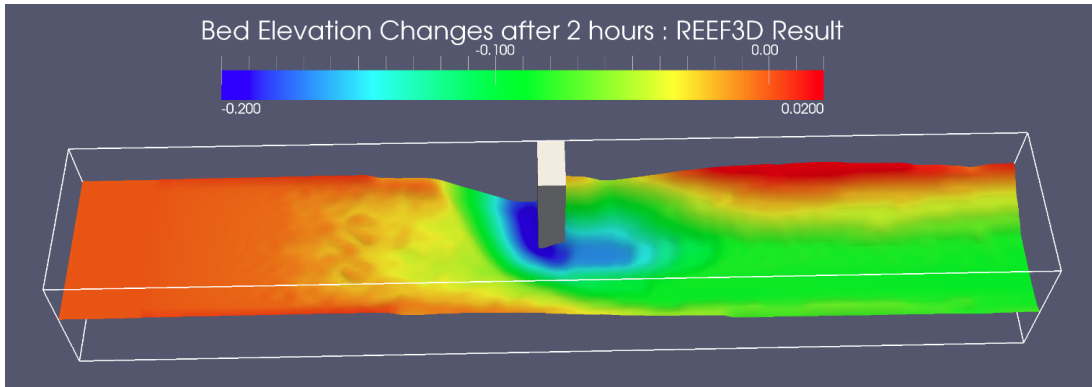
Figure 4.14: Abutment: Model result with Kovas and Parker formulation for reduction of critical shear stress on sloping bed
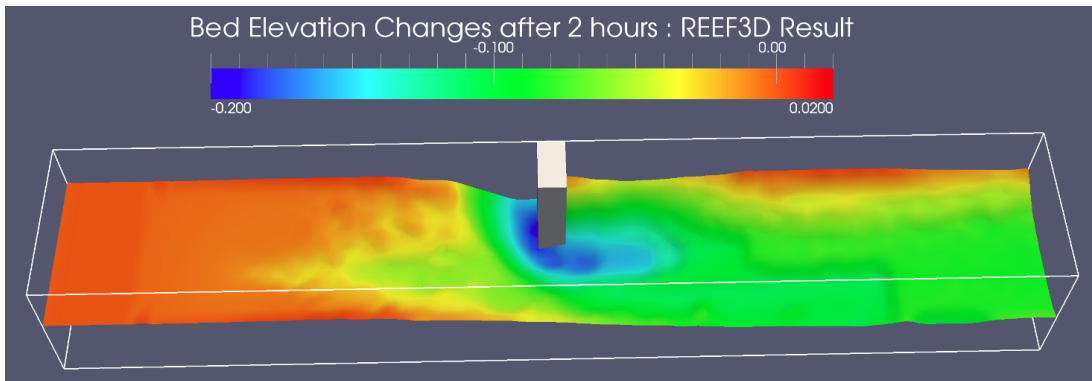

Figure 4.15: Abutment: Model result with Dey's Empirical formulation for reduction of critical shear stress on sloping bed
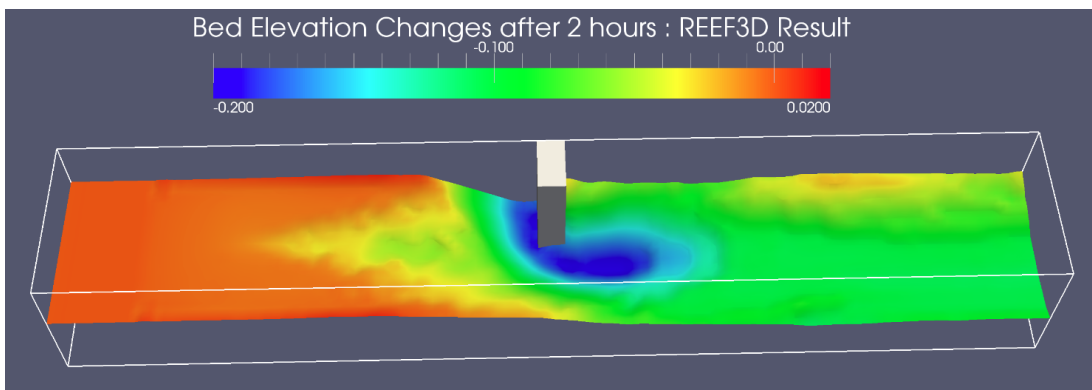

Figure 4.16: Abutment: Model result with Dey's Analytical formulation for reduction of critical shear stress on sloping bed

In the experiment the maximum scour depth was 20.5 cm. It was located on the upstream side of the abutment close to the side wall. The maximum scour depths are 20.6 cm with DeyâĂŹs empirical and 20.3 cm with DeyâĂŹs analytical approach. With the Kovacs and Parker formula 20.8 cm maximum depth was obtained. It can be seen that maximum scour depth is very well predicted using all the three formulations. In general the scouring pattern and location of scour hole is also well predicted by all the three methods. The maximum scour depth, the erosion pattern and the geometry of the scour appear to match well with the experiment. Small deviations occur when it comes to the location of the maximum scour. With DeyâĂŹs analytical formula the maximum scour is about 0.2 cm deeper at the tip of the abutment than close to the wall. For DeyâĂŹs empirical formula the formula by Kovacs and Parker predicts the location of the maximum scour accurately.

To have better insight into scouring process, the time development of scour process using the three formulations have been compared for the first 1500 sec simulation. This is shown in figure 4.17. The time development process is best predicted by Dey's Analytical formulation, however there is very minor difference among all the three methods. So the performance of all the three methods can be assumed to be satisfactory.
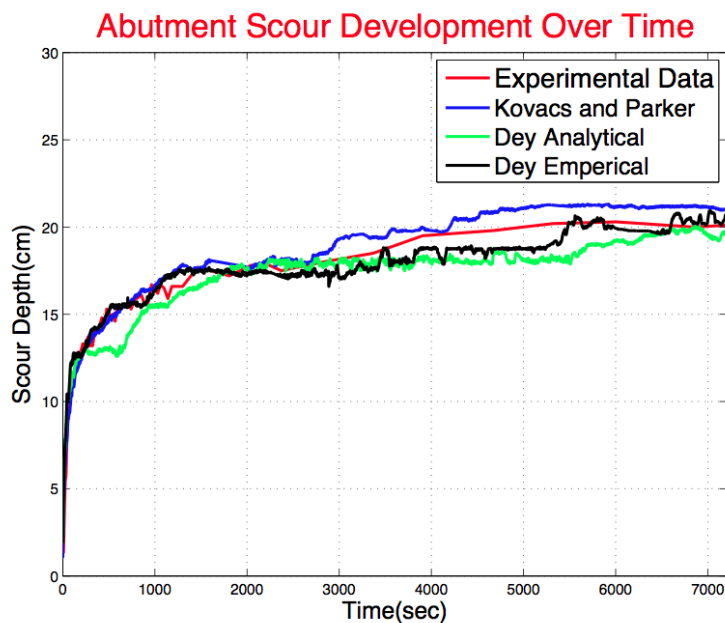

Figure 4.17: Abutment: Time Development of Scour with different formulations for critical shear stress reduction for sloping bed

Effect of Porosity

The porosity of bed layer is one of the terms that appear in the Exner's equation which is used to calculate the bed changes for erosion and deposition using the level set method [60]. Porosity is used as an input in the REEF3D sediment transport module. Studies have indicated that porosity of bed layer may change rapidly during the scouring process and may not remain constant as assumed in the model setup. To study this aspect, test runs have been carried out with porosity value of 0.60, 0.75 and 0.85. These are compared against the experimental results. The time development of the scour hole using the three different porosity against experimental results for the first 1500 sec is shown in figure 4.18.
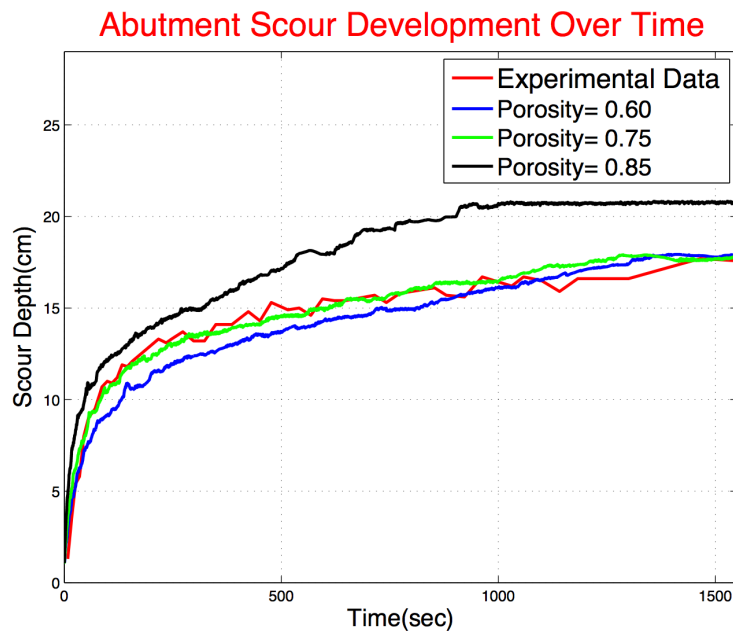
Figure 4.18: Abutment: Time Development of Scour with varying porosity of bed layer

It is seen from the figure 4.18 that with increasing porosity the scour development is increased. The best result is predicted using porosity of 0.75 and 0.6. However, the result using porosity of 85 is found to be satisfactory and predicts the time development well within limits.

4.1.4 Discussion

A study of local abutment scour has been performed to test and validate the sediment transport module of REEF3D. The numerical model predicts the general evolution (geometry, location and maximum scour depth) and time development of the scour

hole accurately. Slight difference in scouring pattern downstream of the abutment is noticed in the numerical model which shows an extended scour hole compared to the experimental result which shows a uniform circular scour hole. This is because in the experiments the bed topography outside the actual scour hole is not measured. It is noticed that the improved resolution of the mesh improves the result as finer meshes result in better discretization.
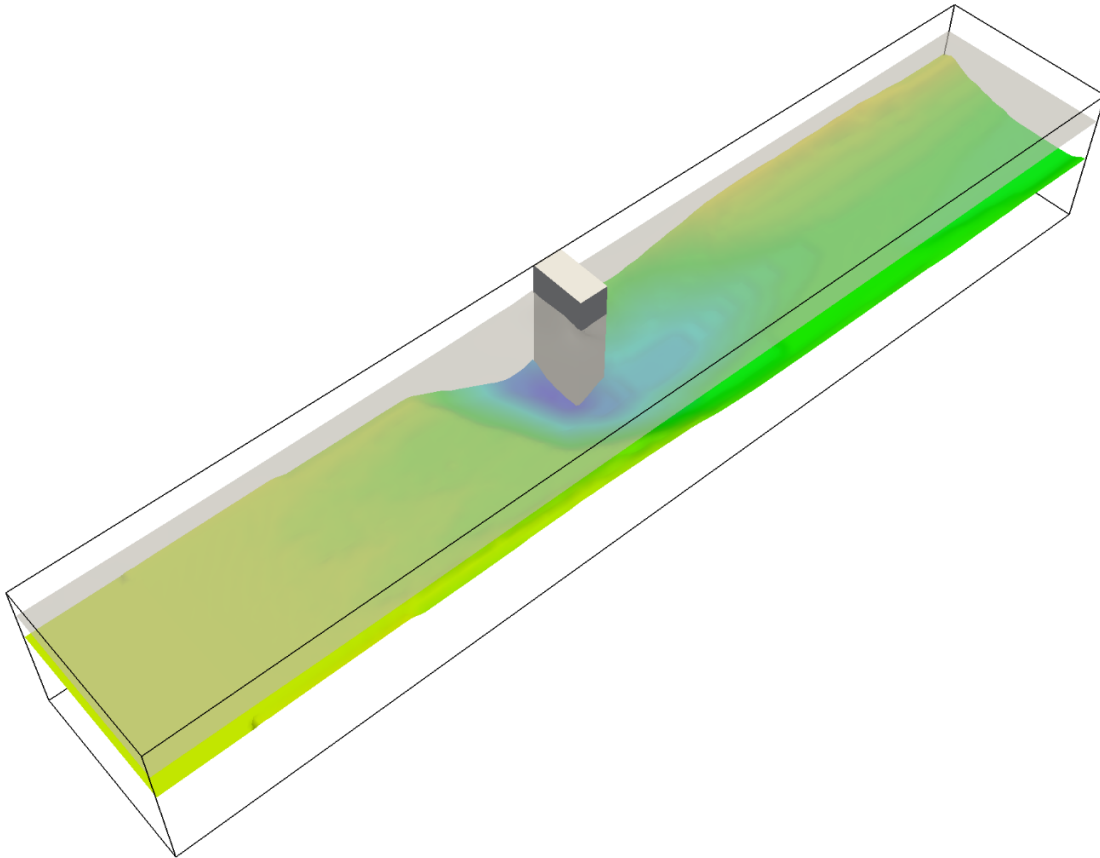
Figure 4.19: Abutment: 3D Model result under constant discharge showing free surface and topography (REEF3D)

The performance of the k-ω turbulence model is found to be better than k-ϵ model. This is due to the fact that the shear velocity based bed shear stress formulation is used in the study that uses turbulent viscosity to predict the bed shear stress. Both the models share the theoretical rationale of two-equation eddy-viscosity models, but turbulent viscosity can be slightly over predicted in k-ϵ model compared to k- model which results in higher bed shear stress and hence, more erosion. A better performance of the k-ω model near the wall has been reported [28] earlier which is seconded by the current study. The time discretization study reveals that higher order time discretization results in better numerical solutions. It is found out that both the

3rd and 4th order Runge-Kutta time discretization scheme give good results. The 3rd order TVD Runge Kutta scheme is preferred due to the fact that higher order time discretization (4th order Runge-Kutta) result in longer computation times. The study emphasised the importance of incipient motion on sloping beds and sand slide algorithm for the correct prediction of the abutment scour. To this effect, three different formulations (Kovacs and Parker, Dey's Analytical and Dey's Empirical) for the critical shear stress reduction for sloping bed are tested. Geometry and location of the scour hole is well predicted using all the three formulations. Careful investigation of the time development reveals that the numerical results with Dey's empirical formulation shows best agreement with the experiment. The affect of porosity has also been studied by comparing time development of scour hole using three different values for the porosity of bed layer. The results indicate that higher porosity results in greater scour depth. This is not surprising, as the porosity appears in the Exner's equation which is used to move the zero level set function of the interface between water and the sediment phase.

The numerical model is also able to represent the complex free surface and topology using the level set method. Figure 4.19 shows the bed elevation changes in combination with representation of the complex free surface under constant discharge conditions in a very realistic manner using a three dimensional plot of the numerical model result after 2 hours of simulation.

4.2   Pier

Stability of hydraulic structures is threatened by local scouring which could lead to their failure, hence, knowledge of mechanism of scouring and accurate prediction of the characteristic scour geometry is very important during the design phase of such structures. Flow pattern investigation around such structures has, hence, been a topic of research in the field of hydraulics in the past. In the event of a high flow discharge in a river, a scour hole appears around bridge piers. The local scour depth develops in high flows and if it is not predicted correctly the bottom level of local scour hole will exceed the original level of the pier foundation. In this case the safety and stability of the bridge will be in danger. The flow field around a pier is extremely complex, three dimensional and turbulent due to separation and generation of multiple vortices [42]. The complexity of the flow field is further magnified due to the dynamic interaction between the flow and the moveable boundary during the development of a scour hole.

This section will present the investigation of 3D numerical modelling of pier scour under uniform flow conditions using the validated sediment transport module of REEF3D. The investigation is compared against the pier scour experiments.

4.2.1   Experimental Setup

The pier scour experiments were conducted in the hydraulic laboratory of the Technical University Darmstadt [65]. The flume used for the experiments had a rectangular cross section with a length of 37 m, width of 2 m and depth of 1 m. The side walls were confined by plexiglass walls. The pier, made of plexiglass, was placed in the flume centre, 16m away from the inflow. The pier diameter was 0.2 m. The stretches 1.5 m before and after the pier were filled with sediment. The rest of the flume consisted of concrete. The boundary between sediment bed and concrete floor was sealed with aluminium plates in order to prevent horizontal water flow through the sediments. The bed material consisted of natural sand with a d_{50} of 0.97 mm, density of $2.65 t/m^3$ and an angle-of-repose of 29^0 in air. From a total of eleven runs, the one with a discharge of 0.18 m^3/s and a water level of 0.3 m was chosen for the comparison in the present study. The duration of the run was 21 hours.

4.2.2   Numerical Model Setup

The numerical model setup for pier scour case is as shown in figure 4.20.

For the investigation of local scour due to pier, the sediment transport module of
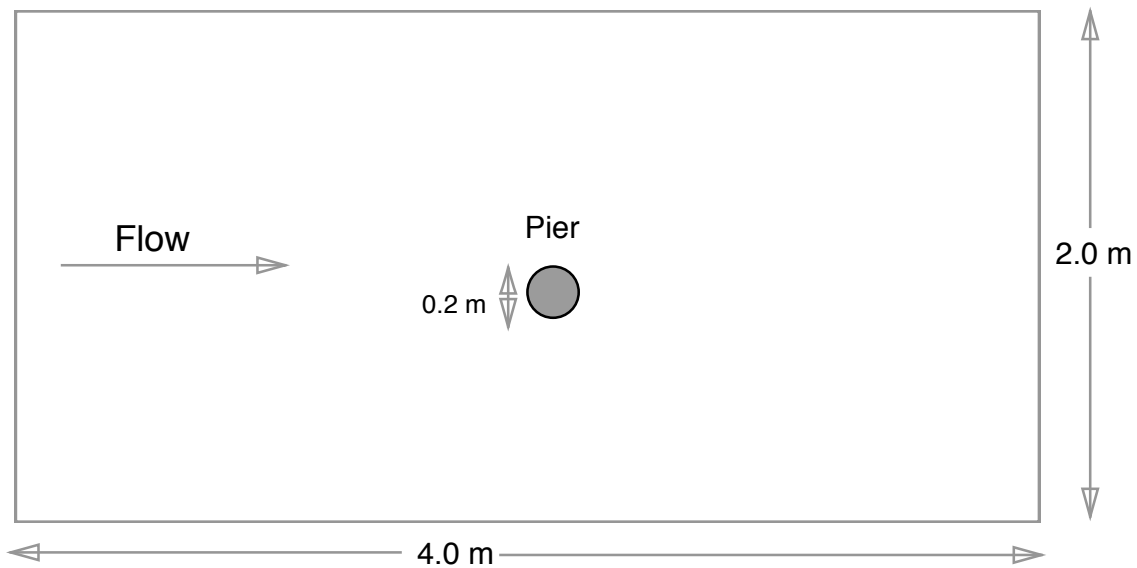
Figure 4.20: Pier: Numerical Setup

REEF3D [6] has been used. The eddy viscosity ν_t in the RANS equation is determined by the use of the two-equation k-ω model [115]. Engelund and Fredsøe's[33] sediment transport formula is used to calculate the bed load. Van Rijn's [107] formula for the suspended load is used for suspended load transport. The bed shear stress formulation based on turbulent viscosity as presented in section 3.2.2 has been used. Dey's empirical [23] formulation of bed shear stress reduction due to sloping bed is employed.

4.2.3 Numerical Results

A three Dimensional channel which is 4 m long, 2.0 m wide and 0.8 m deep with 0.30 m water depth is used. The location of centre of the pier is 2.50 m and 1.0 m in x and y direction respectively. The pier diameter is 0.20 m. A 0.30 m thick sediment layer has been used in the numerical model setup. The test has been performed with a mesh width of 0.025 m. The bed elevation changes along with the time development obtained using the numerical model are compared against the experimental results.

Figure 4.21 shows the measured scour geometry in the form of a contour plot from 21 hours after the start of the experiment. The maximum scour depth after 21 hours is 15 cm and is located on the upstream side of the pier.
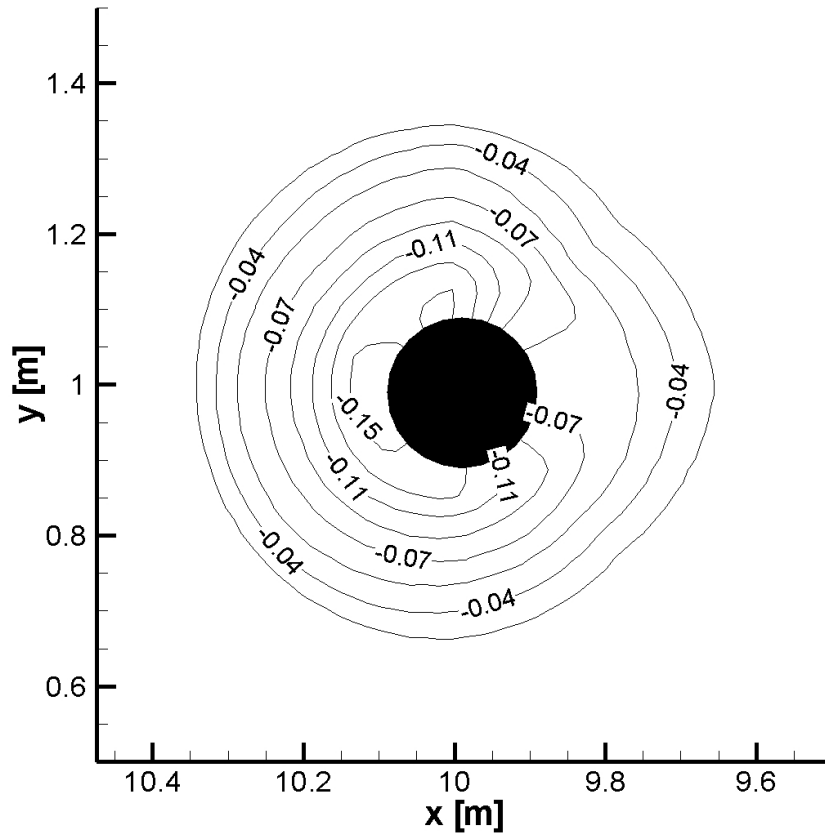
Figure 4.21: Pier: Contour Plot of Experimental Result (as in [6])

Figure 4.22 shows the modelled scour geometry with Dey's empirical formula and the k-ω model after 75,600 sec. Here the maximum depth is 15 cm. This corresponds well with the experimental results. As a major difference between the two Figures, the bed elevation on the downstream side of the pier can be noted. The numerical results show an arrow shaped scour hole on the downstream side. The measured scour hole is very even shaped and forms a full circle. This happens because in the experiment the scour hole was measured from within the translucent pier. The major constraints of this method is that the bed topography outside the actual scour hole is not considered which results in an even shaped full circle contour in the experiment.In order to investigate the influence of the formulas for the reduction of the critical shear stress on sloping beds, computations with Kovacs and Parker formula has also been carried out. Figure 4.23 shows the modelled scour geometry with Kovacs and Parker formula and the k-ω model after 75,600 sec.

61
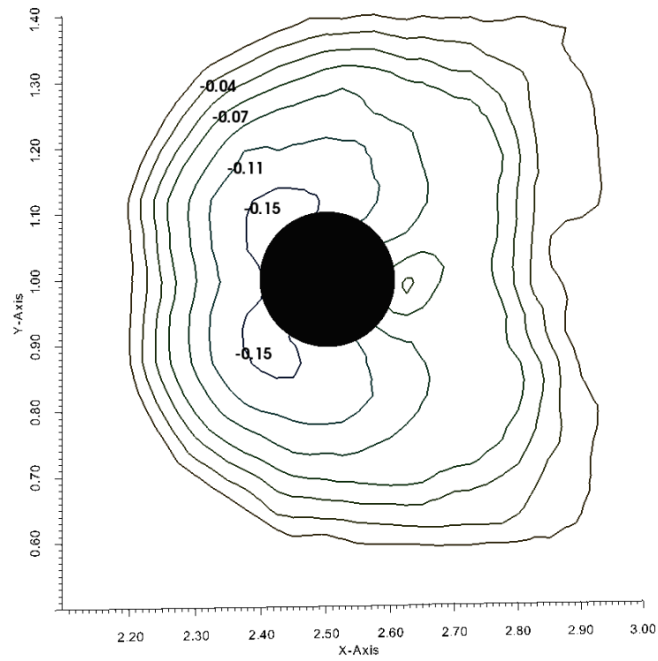
Figure 4.22: Pier: Model Result with k-ω model and Dey's empirical formula(Contour Plot)
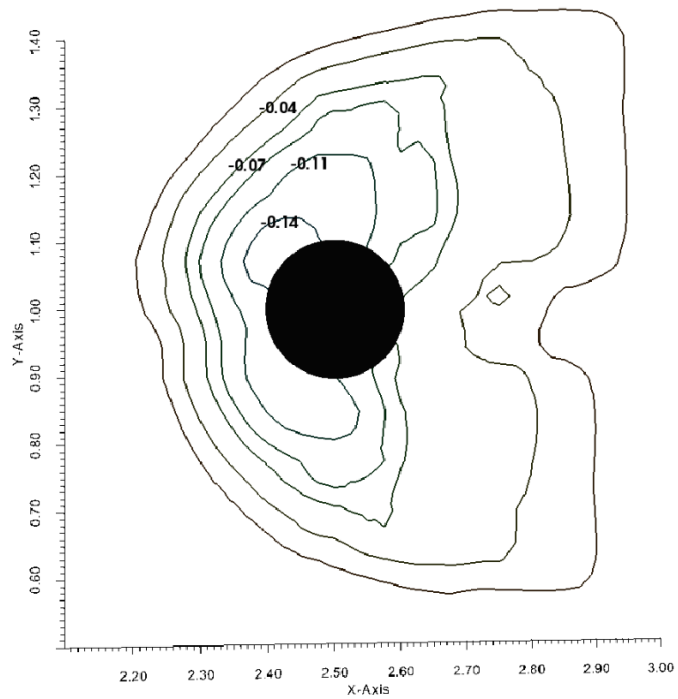
Figure 4.23: Pier: Model Result with k-ω model and Kovacs-Parker formula(Contour Plot)

The scour hole contour lines appear to be somewhat mollified. Here the maximum depth is 14 cm. The scour hole roughly resembles that of experimental result (Figure 4.21) and the scour hole is 1 cm less deep compared to Dey's empirical formulation. The reason for this behaviour can be attributed to physics behind these formulations. For larger longitudinal bed cell angles the critical shear stress reductions is intensified with DeyâĂŹs empirical formula. Slight difference in shape of contour plot is also noticed downstream of the pier with this formulation.
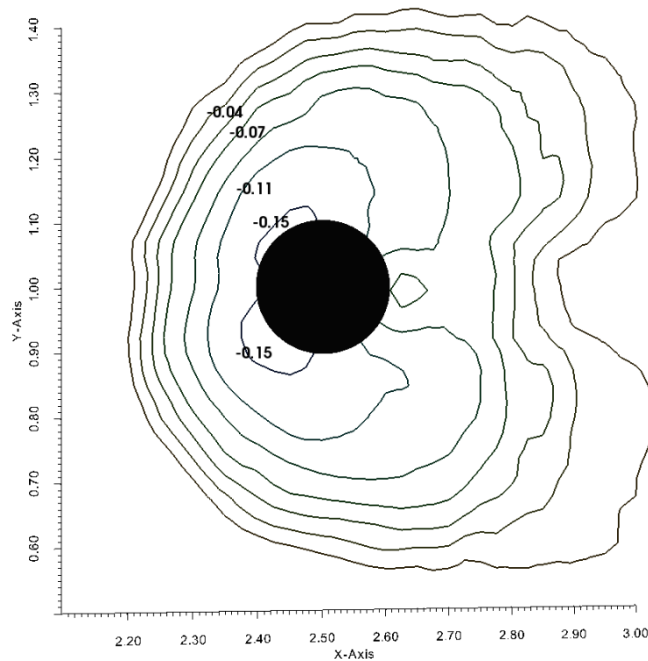
Figure 4.24: Pier: Model Result with k-ϵ model and Dey's empirical formula(Contour Plot)

The performance of the turbulence model was studied by comparing the results of the k-ϵ model with the k-ω model. Figure 4.24 shows the modelled scour geometry with Dey's empirical formula and the k-ϵ model after 75,600 sec. The results using the k-ϵ model show good agreement with the experimental result. The magnitude of the scour hole and the location of the maximum scour are identical. Since these two characteristics are most relevant in hydraulic engineering applications, the performance of both the turbulence model is considered satisfactory and no preference to either of the models can be expressed for this case. This outcome is expected, since both models share the theoretical rationale of two-equation eddy-viscosity models. This is different from abutment case where the results using the k-ϵ model is different from the k-ω model. This happens because in abutment case the turbulent eddy viscosity is over-predicted near the walls as the width of the channel is less. In current case, the pier is placed at the centre and the channel is wide compared to the abutment

case.
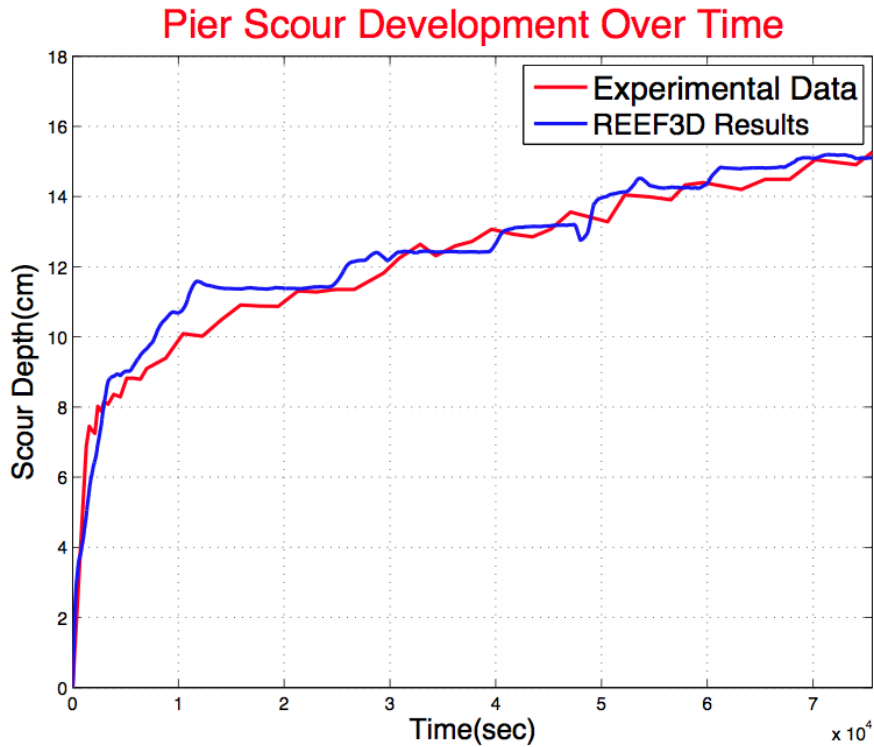
Figure 4.25: Pier: Time Development of Scour, numerical model with Dey's empirical formula and k-ω model

The development of the maximum scour depth over time is shown in figure 4.25. The numerical result use Dey's empirical formula and the k-ω model. The overall tendency is strong erosion in the beginning and less in the end. In the first 7000 seconds the erosion predicted by the numerical model is similar to the experiments. For next 15000 seconds the simulated scour depth grows more rapidly than the experiment until both lines meet up near the 25000 s mark after which there is a very close match of the numerical simulation with the experiment. The shape of both curves indicates, that the equilibrium scour depth has not yet been reached.

4.2.4 Discussion

A study of local pier scour has been performed using the sediment transport module of REEF3D. The numerical model predicts the general evolution (geometry, location and maximum scour depth) of the scour hole accurately. Best agreement has been found using Dey's empirical formulation for the reduction of critical bed shear stress due to sloping beds coupled with the k-ω turbulence model. The time development

of the maximum scour depth also matches the experimental results.
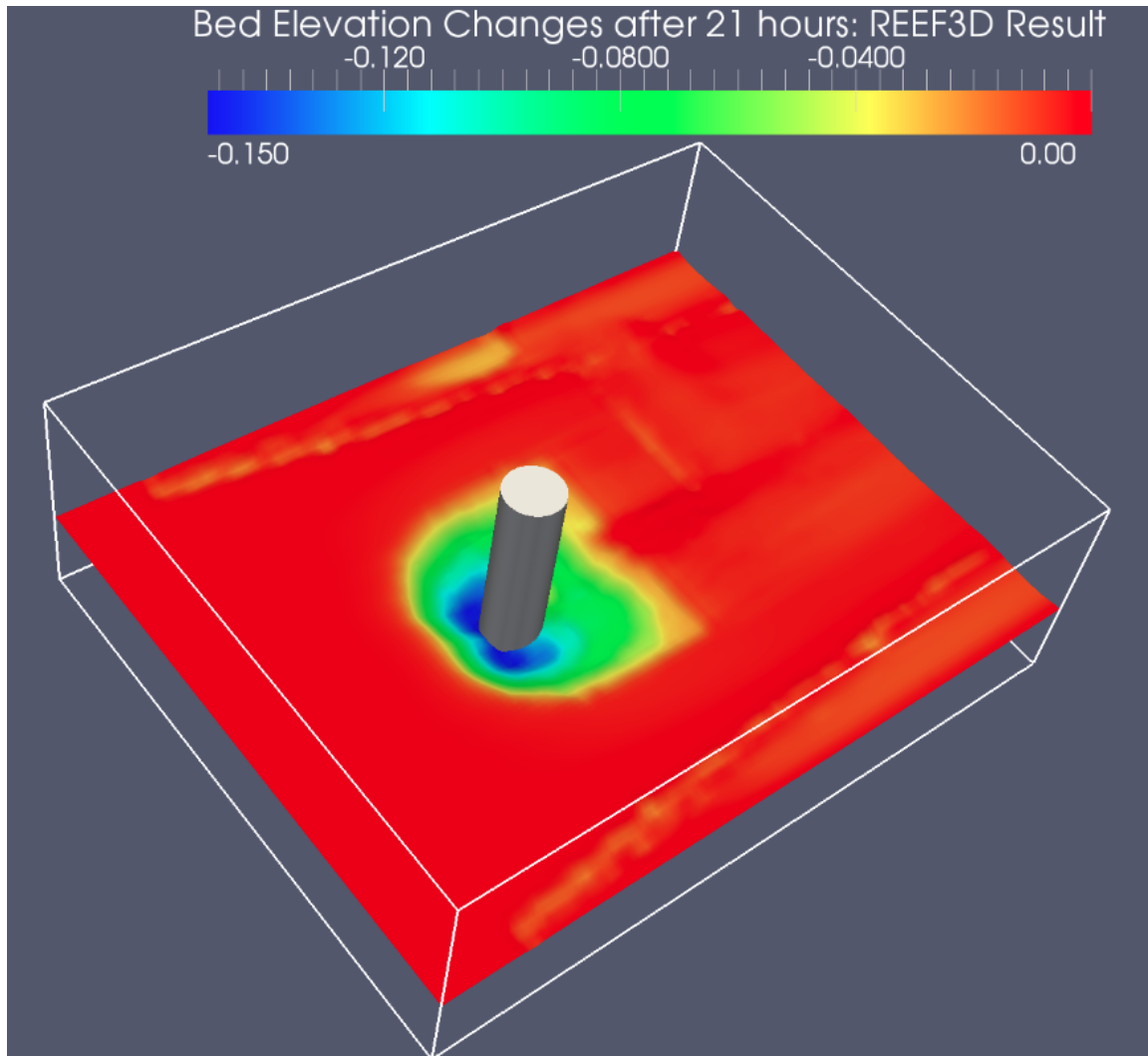
Figure 4.26: Pier: 3D Model Result with k-ω model and Dey's empirical formula(REEF3D)

Figure 4.26 shows the bed elevation changes in a three dimensional plot of the numerical model setup after 21 hours simulation using Dey's empirical formulation coupled with the k-ω turbulence model. Some difference in scouring pattern downstream of the pier is noticed in the numerical model which shows an arrow shaped scour hole on the downstream side compared to the experimental result which shows a uniform circular scour hole. This can be attributed to the measurement procedure adopted during the experimental investigation which is unable to capture the topography outside the actual scour hole. The performance of both the k-ω and k-ϵ turbulence model is found to be satisfactory and no preference to either turbulence model could

be expressed. This happens because in large-scale flow situation with high Reynolds numbers these differences are very small when accounting for the scouring process. Implementation of the sand slide algorithm and correct formulation for critical shear stress reduction for sloping bed are important factors that determine the accurate prediction of a scour hole in a numerical model. The comparison of numerical results using Kovacs-Parker and Dey's empirical formulations for the critical shear stress reduction for sloping beds were done. Geometry and location of the scour hole is slightly better predicted using the Dey's empirical formulation which showed best agreement with the experiment.

Figure 4.27: Pier: 3D Model result under constant discharge showing free surface and topography (REEF3D)

The numerical model is also able to represent the complex free surface using the level set method. Figure 4.27 shows the bed elevation changes in combination with free surface under constant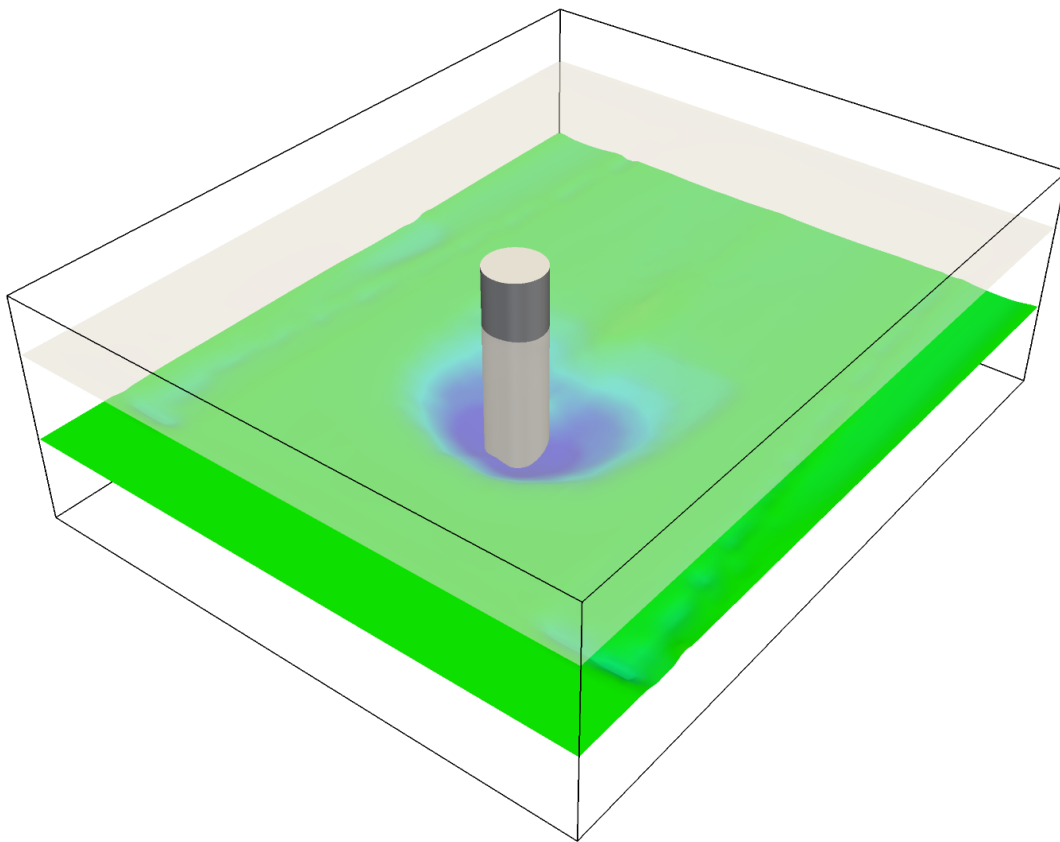 discharge conditions in a very realistic manner using a three dimensional plot of the numerical model result after 21 hours.

4.3   Contraction

The process of scouring is removal of sediments from river bed caused due to moving water or waves. Scour can be classified into two broad categories: General scour and local scour. Contraction scour is a type of general scour which occurs due to a reduction in channel cross-sectional area. Local scour on the other hand occurs due to the direct effect of an obstruction on the flow field. The two scour cases in previous sections 4.1 and 4.2 are examples of local scour. This section deals with study of contraction scour.

Contraction scour is observed where the flow is constricted due to the placement of structures like bridges etc. The flow accelerates in constriction which increases the the bed shear stress and the turbulence associated with it. The development of contraction scour is noted when the critical shear stress of the bed materials is overcome by the bed shear stress. This could lead to the failure of the structure if too much sediment is eroded near the it. Accurate predictions of scour processes is hence, necessary to assist the design engineers in monitoring and correcting the aforementioned problems before the structures fail or become unsafe.

In literature, the generalised scour due to channel constriction is not very well documented. Among the one dimensional models, HEC-18 [22] has been used to estimate the mean water velocity in the contracted channel by using the velocity in the uncontracted channel and the contraction ratio. Here an empirical analytical formula was used for estimation of scour parameters. Among the two dimensional models Weise in 2002 [111] and Marek and Dittrich in 2004 [72] deserve to be mentioned. They used 2D numerical morpho-dynamic models to simulate the details of the erosion process in the open-channel contraction laboratory experiment. They concluded that the flow in the contraction domain had dominant 3D flow effects hence, a 2D model could not accurately reproduce the flow. Later Bihs and Olsen in 2007 [8] and Duc and Rodi in 2008 [26] modelled the contraction scour case using their respective 3D models. They used the same experimental data for validation which is utilised in the current study.

The current section presents the application of the REEF3D sediment transport module by modelling a contraction flow situation in an alluvial laboratory channel with non-cohesive bed, for which experiments have been carried out at the Federal Waterways Engineering and Research Institute Karlsruhe (Bundesanstalt fuÌĹr Wasserbauâ ĂŤBAW) [4]. The same study has been used by Weise in 2002 and Marek and Dittrich in 2004 for their 2D numerical modelling study. Later this study was used by Bihs and Olsen and Duc and Rodi in their paper for 3D numerical modelling study.

4.3.1 Experimental Setup

The experimental data is obtained from physical experiments of the contraction case conducted at the laboratories of the BAW (Federal Waterways Engineering and Research Institute) in Karlsruhe, Germany [4]. The flume was 16.50 m long and 1 m wide. The contraction was 0.5 m wide. The left side wall (in stream wise direction) was an alternation of glass and concrete. A brick wall separated the contraction geometry from the rectangular flume on its right side. This caused a slight difference between the roughnesses of the two side walls. The average size of the sediments in the flume was d_{50}= 5.5 mm. The bed sediment layer was 20 cm thick. The experiments were run with three different discharges: 80 l/s, 130 l/s and 150 l/s. There was no erosion with the 80 l/s discharge. With the discharges of 130 l/s and 150 l/s erosion occurred with different intensities. In the current section the scour pattern obtained due to the discharge of 150/s is compared with the numerical model results.

4.3.2 Numerical Model Setup

The numerical model setup for contraction scour case is as shown in figure 4.28.
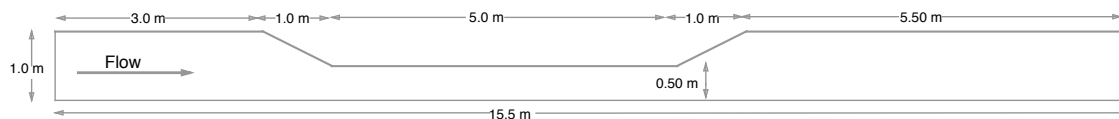
Figure 4.28: Contraction: Numerical Setup

The length of rectangular flume in numerical setup is chosen to be 15.5 m by excluding the 1.0 m entrance section. The eddy viscosity ν_t in the RANS equation is determined by the use of the two-equation k-ω model [115]. For time treatment a third-order accurate TVD Runge-Kutta scheme [94] is used. Engelund and Fredsøe's [33] sediment transport formula is used to calculate the bed load. Van Rijn's [107] formula for the suspended load is used to account for suspended load transport. Bed shear stress formulation based on wall law as presented in section 3.2.2 has been used. This being a general scour case where there is no steep bed slope formation, formulation of bed shear stress reduction due to sloping bed is not considered. Only the sand slide algorithm as in [11] has been used.

4.3.3 Numerical Results

A three dimensional tank 15.5 m long, 1.0 m wide, 0.5 m contraction and 0.8 m deep with constant water depth of 0.268 m at exit for 80 l/s discharge case and 0.275 m water depth at exit for 150 l/s discharge case is used. A 0.20 m thick sediment layer

has been used in the numerical model setup. The numerical model has a mesh size of 0.05 m

The visual observations in the laboratory have shown that no sediment transport occurred at flow discharge of 80 l/s. Since no sediment transport occurred in the physical experiment, this run was used investigate the ability of the numerical model to compute the hydraulic situation in the contraction geometry. To this effect, the velocity at free surface of the model is compared against the experimental observations. This test case is specifically used to calibrate the numerical model for equivalent roughness height to get good agreement between calculation and measurement. Figure 4.29 and 4.30 show free stream velocities measured in the experiment and calculated by the numerical simulations until steady state.
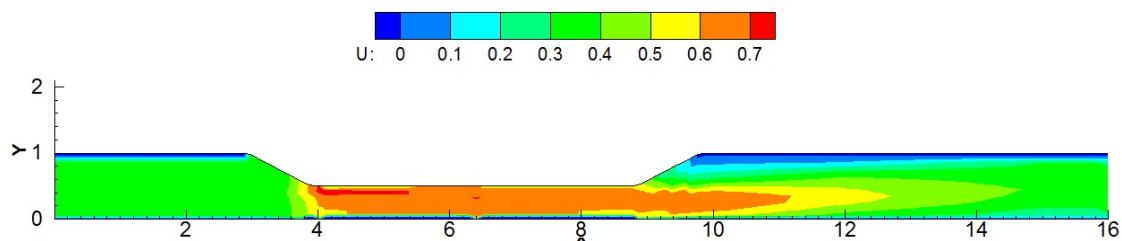
Figure 4.29: Contraction: Mean velocity at free surface for Q=80 l/s (Experiment from [8])
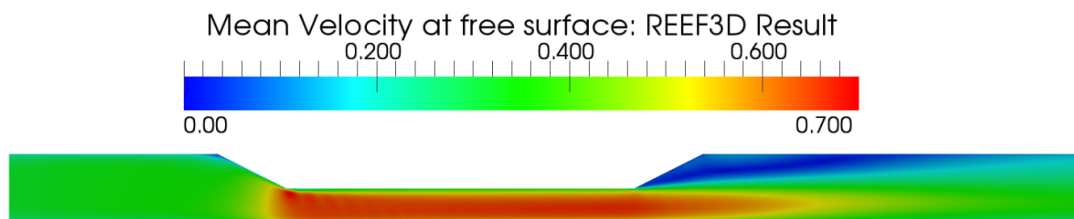
Figure 4.30: Contraction: Mean velocity at free surface for Q=80 l/s (REEF3D)

The computed flow pattern is quite similar to that observed in the laboratory experiment. As expected, the velocity increases in the contracted channel since water elevation and width decrease. The water slows down in the expansion. High velocities up to 0.70 m/s is noticed in the numerical simulation which is very close to the one obtained in the experimental results. However, at this flow discharge, the bed shear stress does not exceed the critical shear stress of the channel bed, so that no

69

scour occurs in the channel. Recirculation zone was present during the numerical simulation at the free surface and at the bed. The area of high velocities due to the contraction is identical to experimental result.

Now the case with a discharge of 150 l/s is discussed. Figure 4.31 shows shows bed elevation changes after 150 minutes of the experiment. The color legends of the figure 4.31 are similar to those of figure 4.32. The scour occurs first at the beginning of the contraction and then develops downstream, along the contraction part of the channel. The eroded sediment from the scour hole settles down as it moves downstream into the expansion region with lower velocity and bed shear stress to form a deposition area downstream of the scour hole. The observed maximum scour hole in the experiment extends along the contracted bank.
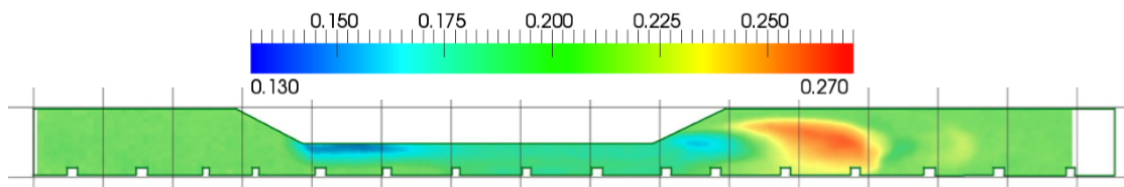
Figure 4.31: Contraction: Bed elevation changes after 150 mins for Q=150 l/s (Experiment (from [4]))

Figure 4.32 shows shows bed elevation changes after 150 minutes of the numerical simulation.
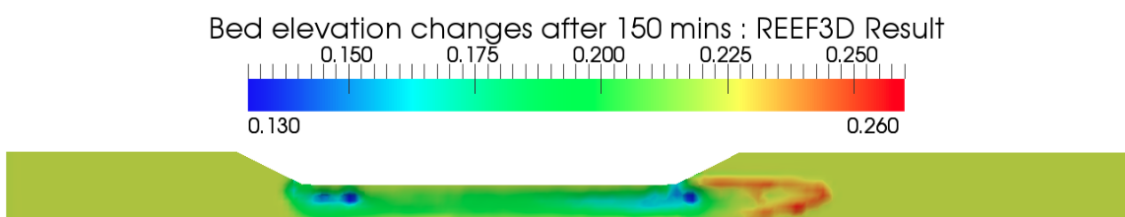
Figure 4.32: Contraction: Bed elevation changes after 150 mins for Q=150 l/s (REEF3D)

The predicted maximum scour depth (7 cm) occurs at the location close to and behind the start of the contraction and also near the end of contracting extending to the beginning of the expansion. This corresponds well with the experimental results which has a scour depth of 7 cm. The scour depth after the contracted part is well predicted too (7 cm). In the numerical model the eroded sediment is deposited around

70

1.5 m after the start of expansion. This behaviour correspond well with the physical experiments where the sediment was transported through the expansion and settles about 1.5 m further downstream. There is slight difference in deposition height. The numerical results predicted deposition of 6 cm compared to experiments (7 cm).The numerical model predicted a recirculation near the bed in the expansion which is similar to the experimental results. Scour depth, its location, deposition height and its location are predicted well with the numerical model.

4.3.4 Discussion

A study of contraction scour has been performed using the sediment transport module of REEF3D. The numerical model predicts the general evolution (geometry, location and maximum depth) of scour, deposition height and its location accurately with very minor differences. Since these characteristics are most relevant in hydraulic engineering applications, the performance of the numerical is assumed to be satisfactory in prediction of contraction scour. The results predicted by numerical model are better than found by Bihs and Olsen [8].
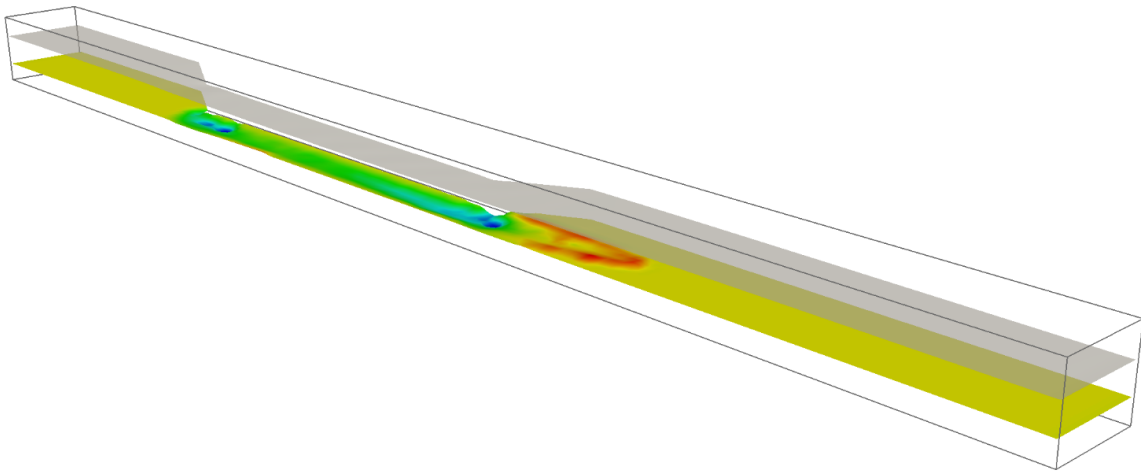
Figure 4.33: Contraction: 3D Model result under constant discharge showing free surface and topography (REEF3D)

The numerical model is also able to represent the complex free surface using the level set method. Figure 4.33 shows the bed elevation changes in combination with representation of the complex free surface under constant discharge conditions in a very realistic manner using a three dimensional plot of the numerical model result after 150 minutes of simulation.

Chapter 5

Scour under waves

With the growth and the expansion of the offshore industry into new geographic and physical environments, the evolution of new technologies is necessary to cope with engineering problems which have not been understood in the past. One such problem is the development of scour holes around ocean structures embedded in the sea floor. The scour problem in sea and estuarine climate exists mainly because of two reasons: current and waves. The previous chapter discussed the scour process under current conditions. This chapter focusses on scour under waves.

It has been established in the field of hydraulic engineering that transport of sediment occurs when the fluid shear stresses acting on the bottom exceed the values needed to initiate entrainment of sediments. In case of waves the resulting bottom shear stress is much higher compared to that of steady currents. Hence, the expected scour is also higher. The situation becomes grave when both current and waves act in combination, resulting into even higher bed shear stress and in more scouring around the structure. As a benchmark, the present thesis will investigate scour under waves only. The combined action of waves and current could be a possible area of research for the future.

In this chapter, the performance of the sediment transport module of CFD code is tested with a test case of pier scour under waves (section 5.1). To this effect, the results obtained from the CFD code are compared against the experimental data. The effect of variation of the sediment time stepping with the decoupling of the hydrodynamic and the morphodynamic time step is tested.

5.1 Pier

Piers find application in large marine structures as platform legs and bridge piers which are generally exposed to waves and currents. Observations have shown that the stability of these structures are in constant danger due to scouring near the structure at the ocean bed. The solution to this technique is the provision of scour protection, a design which is very much dependent upon a clear understanding of the physics behind the scour process and its correct prediction. Hence, for the past two decades, the study of pier scour under wave conditions have been a research topic among scientists. There have been many studies performed in the past that investigates this issue. The studies done by Wang and Herbich 1983 [110], Herbich et al. 1984 [48], Kobayashi 1992 [57], Sumer et al. 1992 [101], 1993 [98], Kobayashi and Oda 1994 [58] and Whitehouse 1998 [112] focussed on scour pattern around small vertical cylinders under waves where-as Toue et al. (1992) [103] and Sumer and Fredsøe (2002) [100] studied large cylindrical piers. They tried to relate the scouring process to either vortex shedding in the case of small cylinders where as in case of large cylinders, where the vortex shedding is not present, to the wave induced steady streaming near the cylinder. Some analytical and theoretical work has also been carried out [90] [79]. The work by Ong and Myrhaug deserves special mention, as they derived maximum equilibrium scour depth around vertical piles exposed to long-crested (2D) and short-crested (3D) nonlinear random waves plus current [79]. The approach was based on assuming the waves as a stationary narrow-band random process, adopting the Forristall (2000) [38] wave crest height distribution representing both 2D and 3D nonlinear random waves and using the formulas for the scour depth by Sumer and Fredsøe (2002) [100].

This section starts with a theoretical discussion on mechanics of pier scour in oscillating flow (waves) and then present the investigation of 3D numerical modelling of pier scour under waves using the validated sediment transport module of REEF3D. The investigation is validated against the pier scour experiments conducted in the Department of Hydrodynamics and Water Resources (ISVA), Technical University of Denmark [99] by Sumer and Fredsøe.

5.1.1 Mechanics of scour in oscillating flow

The wave orbital velocities are simple oscillating flows parallel to the seafloor near the seabed. On neglecting higher order effects like mass transport and wave asymmetry, the flow can be described as simple sinusoidal oscillation at the wave period. Such flows are capable of developing scour around seafloor obstructions. The flow/structure interaction produces changes in the primary flow field, as well as significant secondary

flow which is caused by interaction of a boundary layer or shear flow with the obstruction. The mechanisms for the scour hole development due solely to waves is substantially different than the mechanisms for the scour hole development due to steady or slowly varying currents [81].

There have been studies [81] in the past that report the observations of scour development from oscillating flows. In general the scour hole development depends on the cylinder diameter, intensity of the oscillating flow and the sediment transport on the surrounding seafloor area. The qualitative description of the scour development around a pier under waves based on their observations is discussed.
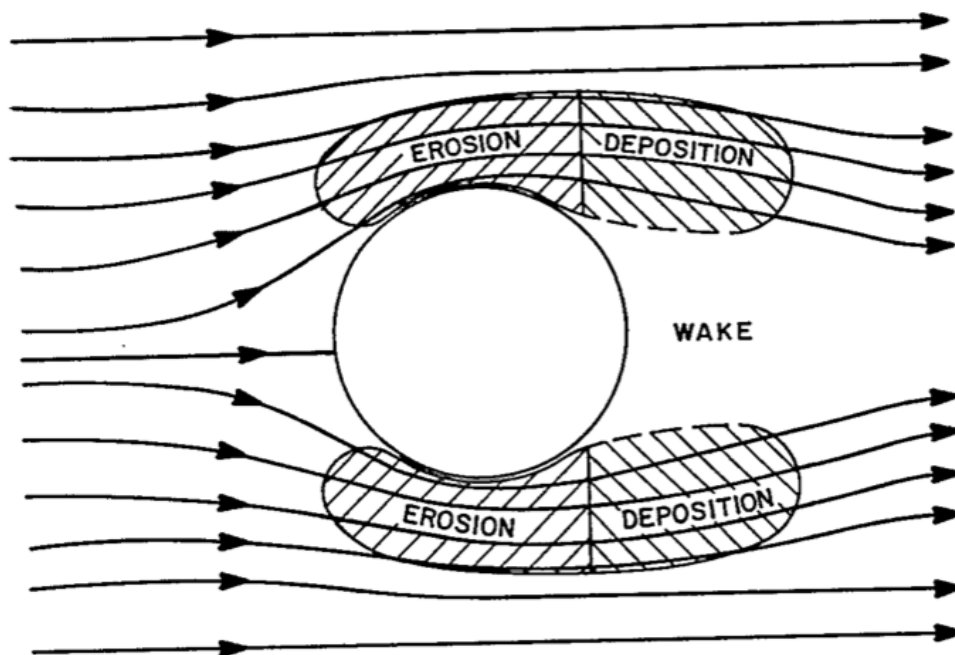
Figure 5.1: Pier: Flow and scour due to oscillating flow (from [81])

The scour hole initiates at the sides of cylinder on the side facing the incoming waves and some deposition is noted against the lee side of the cylinder. As the scour hole continues to develop, the deposition is removed, and the shifts to a rim outside the scour hole. The scour hole is a radially symmetric frustum of an inverted cone with side slopes at the angle of repose of the sediment when it is fully developed. This generalised description indicates that an important transition occurs between the initial scour hole shape and its final shape. This is quite different from the steady current case where the shape of the scour hole remains unchanged from the beginning until the end. In oscillating flow past a cylindrical obstruction, the horseshoe vortex is insignificant as the orbital boundary layer is thin and thus the scour initiates from the concentration of the bottom fluid shear stress produced by the acceleration of

the primary flow by the obstruction. A positive bottom fluid shears stress gradient develops from upstream of the cylinder to the point of maximum velocity. A negative gradient exists from this point to the downstream limit of the disturbed flow. If the maximum bottom shear fluid shear stresses are above the critical threshold, then erosion will occur from upstream of the cylinder to the point of maximum velocity and deposition will occur downstream from this point in the shadow zone. Figure 5.1 shows the flow and scoring pattern due to an oscillating flow.

One of the important parameter which determines the erosion and scouring pattern around the cylinder under waves is the Kuelegan-Carpenter (KC) number [70]. The dominant mode of sediment transport is suspension when KC number is high. If the KC number is high then even the sand size sediment can be suspended and convected away from the cylinder. Thus, during the initial stages of scour formation deposits will form only if KC number is low.

5.1.2   Experimental Setup

The pier scour experiments under were conducted in the Department of Hydrodynamics and Water Resources (ISVA), Technical University of Denmark [99] by Sumer and Fredsøe. These experiments were carried out in a wave flume that was 12.5 m long and 23.5 m wide. The water depth used for the experiments was 40 cm. In the flume two type of experiments were conducted: rigid bed and actual scour experiments. The basin floor was made up of concrete in rigid bed experiments and the cylindrical base was sealed along its periphery at the floor. Velocity and particle tracking measurements were done for the rigid bed setup. The scour experiments on the other hand used a rectangular shaped sand pit in the basin. The pit was 5.6 m long, 3.6 m wide and 0.14 m deep. Three cylinders with diameters of 0.54 m, 1.0 m and 1.53 m were used for the scour experiments. The same cylinders were also used for rigid bed experiments. The cylinder was placed in the sediment bed extending down to the bottom of the sand pit. The bed material consisted of natural sand with a d_{50} of 0.20 mm and a density of 2.65 t/m^3.

Several tests with varying cylinder diameter and varying wave properties were conducted. For the current study, at first test from the set of experiment had to be chosen for comparison with the numerical results from REEF3D. This test had a wave period of 3.5 sec, a wave height of 12.0 cm and wave length of 6.79 m. The type of wave in consideration is cnoidal. The cylinder diameter was kept at 1.0 m. A maximum scour depth of 47 mm was observed after 8 hours of experimental testing.

5.1.3 Numerical Model Setup

The numerical model setup for pier scour under waves is as shown in figure 5.2.
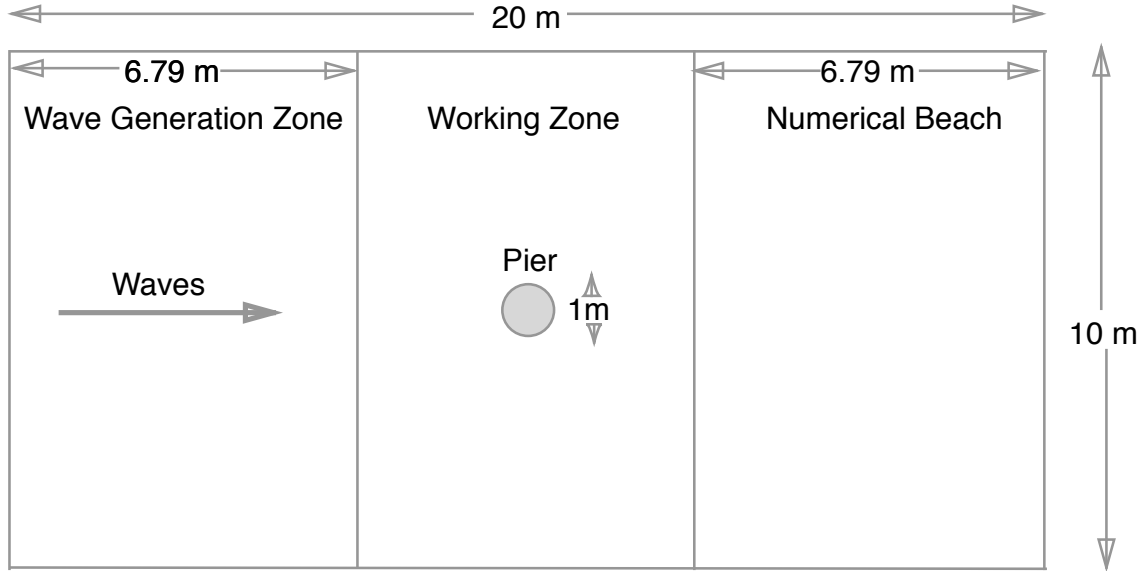
Figure 5.2: Pier: Numerical Setup under waves

For the investigation of local scour due to pier, the sediment transport module of REEF3D [6] has been used. Cnoidal waves with an amplitude of 0.06 m are generated in the wave tank having a wave length of 6.79 m. Jacobsen's relaxation function has been used for the generation of the wave, thus the wave tank has one wave generation zone and one numerical beach. The eddy viscosity ν_t in the RANS equations is determined by the use of the two-equation k-ω model [115]. For time treatment a third-order accurate TVD Runge-Kutta scheme [94] is used. Engelund and Fredsøe's [33] sediment transport formula is used to calculate the bed load. Van Rijn's [107] formula for the suspended load is used to account for suspended load transport. Bed shear stress formulation based on logarithmic wall law as presented in section 3.2.2 has been used. Dey's empirical [23] formulation for the bed shear stress reduction due to sloping bed is used.

5.1.4 Numerical Results

A three dimensional numerical wave tank 20 m long, 10 m wide and 1.1 m deep with 40 cm water depth is used. The location of the centre of the pier is 10.0 m and 5.0 m in x and y direction, respectively. The pier diameter is 1.0 m. A 0.30 m thick sediment layer has been used in the numerical model setup. The test has been performed

with grid size of 0.10 m. Evaluation of the de-coupled approach for the simulation of hydrodynamic and sediment transport processes using different time steps for flow and morphodynamic is tested by comparing the time development of the scour. For this, three different relaxation factors for the sediment time step were chosen while keeping the same hydrodynamic time step relaxation factor.

Figure 5.3 shows the bed elevation changes after 8 hours of numerical simulation with the numerical setup mentioned in section 5.1.3. Here the relaxation factor for the time step sediment transport is 0.10.
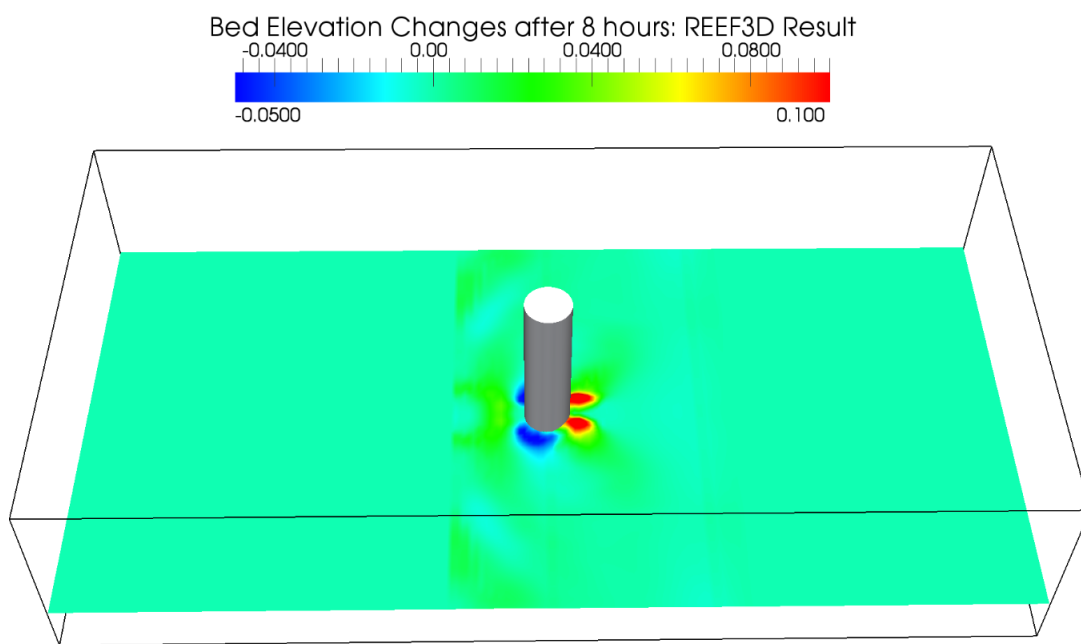
Figure 5.3: Pier: Bed Elevation Changes under waves (REEF3D)

Visual investigation of figure 5.3 shows close match with a generalised erosion and deposition pattern as shown in figure 5.1. It was also mentioned in section 5.1.1 that this pattern is more applicable for scenarios with a low KC number as the dominant mode of sediment transport is bed load transport which results in this type of erosion and deposition pattern. The experimental result chosen for comparison has a KC value of 1.1 which is identical with the numerical result observations. Figure 5.3 shows that a maximum scour hole of 54 mm is reached after 8 hours of numerical simulation. This is in good agreement with the experimental result which indicated a maximum scour depth of 47 mm.

Figure 5.4 shows the contour plot of bed elevation change at the equilibrium stage in experiment under consideration (after 8 hours test time) [99]. The sediments up-

stream of the cylinder are stirred by waves and brought in suspension and transported by wave-induced steady streaming near the bed outwards towards the shadow region (downstream). This results in formation of scour (erosion) hole in this area near the cylinder. The sediment that is transported will eventually end up in the shadow area (downstream) causing the observed deposition pattern. This is quite evident from figure 5.4. Figure 5.5 shows the contour plot of bed elevation change at the equilibrium stage obtained from numerical simulation using REEF3D after 8 hours of simulation. The pattern of erosion and deposition is similar to that of the experimental result.
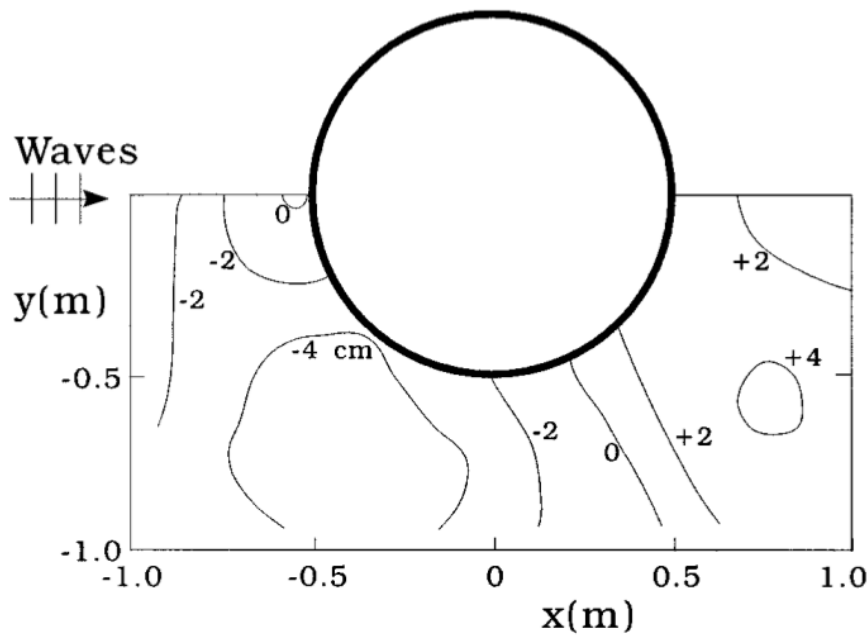
Figure 5.4: Pier: Contour plot of Bed Elevation Changes under waves (Experimental from [99])

There is very slight difference in shape of the contour obtained from numerical solution in comparison to the experiment and its looks somewhat mollified. But more importantly the magnitude of the scour hole, the location of the maximum scour and the location of the deposition are identical to that of the experiment. The development of the maximum scour depth over time is shown in figure 5.6. The overall tendency is strong erosion in the beginning and less in the end. In the first 5000 seconds the erosion predicted by the numerical model is less than the experiments. After that the simulated scour depth grows more rapidly than the experiment until the end of the simulation. The shape of both curves indicates, that the equilibrium scour depth has been reached at 15000 seconds. The maximum scour depth of the numerical solution is slightly over-predicted.
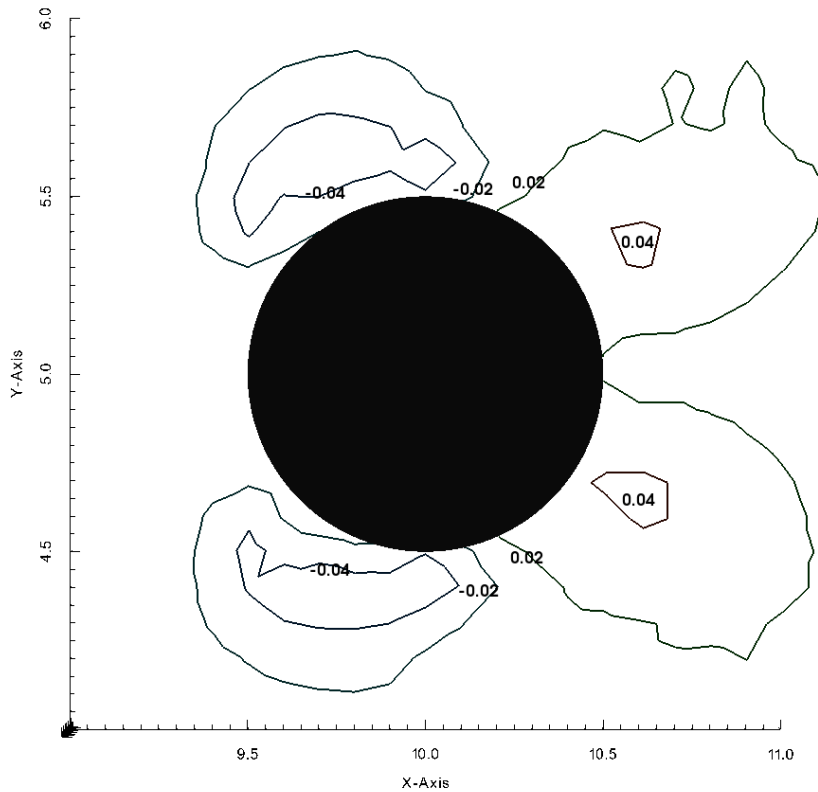
Figure 5.5: Pier: Contour plot of Bed Elevation Changes under waves (REEF3D)

One of the important issues with sediment transport modelling is whether or not to decouple hydrodynamic and morpho-dynamic time step. This aspect also has been studied using this test case by varying the relaxation factor for time step size for sediment transport. The values for relaxation factor used are 0.05, 0.1 and 0.3 while keeping the same relaxation factor for hydrodynamic time step. Figure 5.7 shows time development of scour under three different sediment time step relaxation factors. The time development indicates that there is no difference in scour development over time using these three values. This means that the approach to de-couple hydrodynamic and morphodynamic time step is a reasonable assumption. The conclusion is not surprising, since the major mode of transport in this case is the bed load transport and the CFD code does not calculate the morphology and bed load transport processes in terms of individual sediment particle movement. Rather, the bed level changes and bottom roughness redistribution are calculated via an Eulerian approach using a much larger time step than the one used for the flow and suspended sediment transport solvers.

79
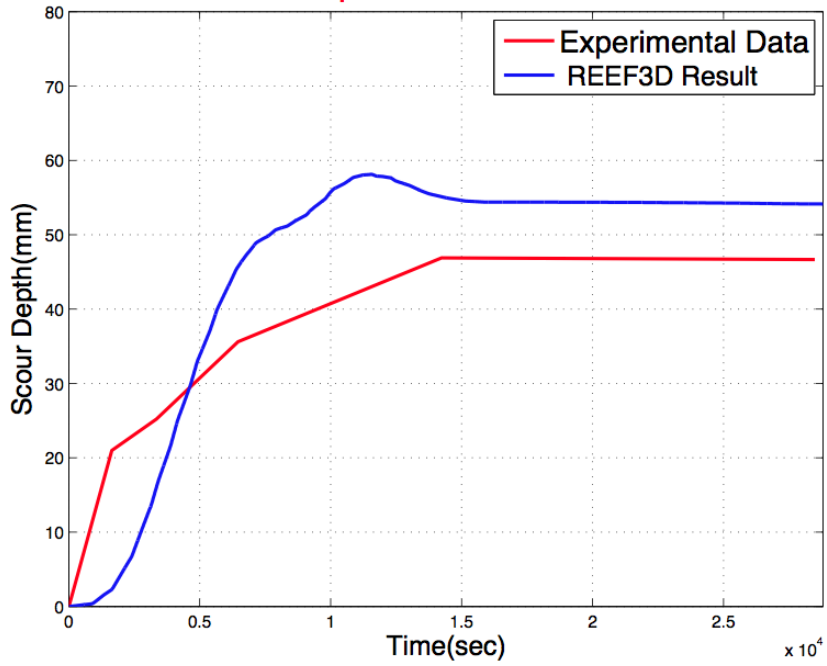
Figure 5.6: Pier: Time Development of Scour under waves
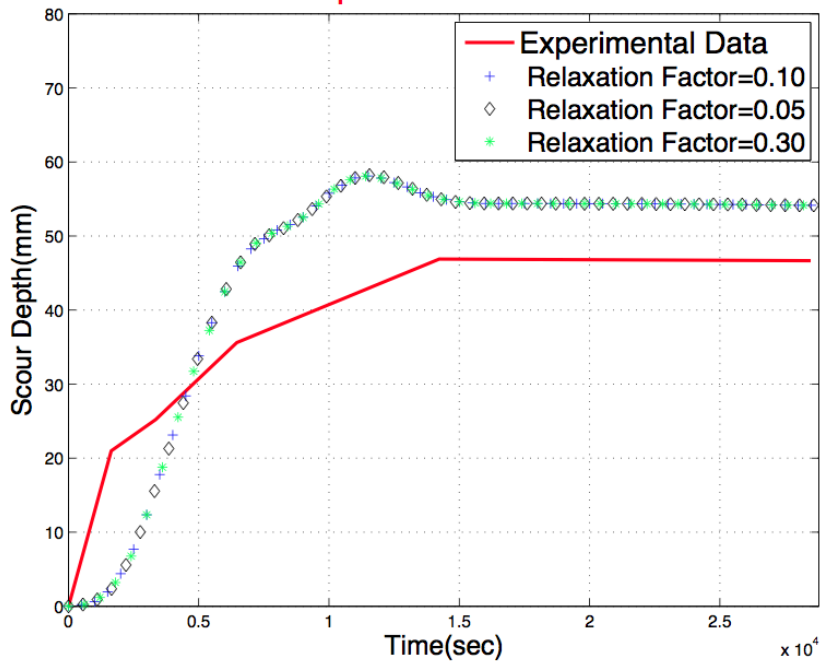
Figure 5.7: Pier: Time Development of Scour under waves by varying relaxation factors for sediment time step

5.1.5 Discussion

A study of local pier scour under waves has been performed using the sediment transport module of REEF3D. The numerical model accurately predicts the general evolution of scour (geometry and location) and the deposition location when compared to the experiment and theoretical erosion and deposition pattern given in [81]. Very small difference is noted in maximum scour depth values predicted by the numerical model when compared to the experimental results. The bed elevation changes contour is slightly mollified. Since the location and magnitude of scour and deposition are the most important parameters in the field of marine civil engineering, the results obtained through the numerical simulation are considered satisfactory. There is a slight variation in time development but the overall trend of accelerated erosion in the beginning with decreasing rate of erosion with time matches the experimental time development well. Numerical as well as experimental result show that the equilibrium scour depth is reached at the same time.
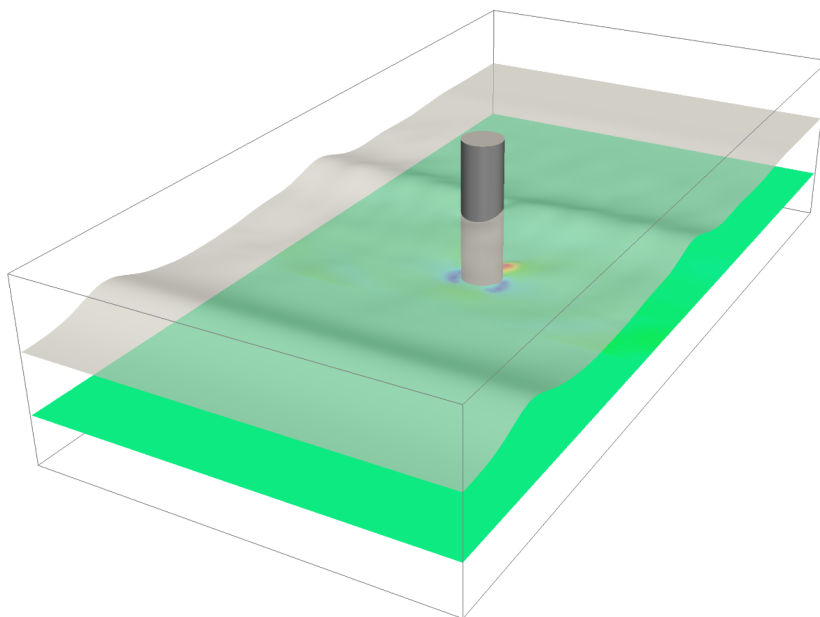
Figure 5.8: Pier: 3D Model result under waves showing free surface and topography (REEF3D)

The numerical model is also able to represent the complex free surface and topology using the level set method. Figure 5.8 shows the bed elevation changes in combination with representation of the complex free surface with waves in a very realistic manner using a three dimensional plot of the numerical model result after 8 hours of simulation. The study also shows that the de-coupled approach for simulation of hydrodynamic and sediment transport processes is a reasonable assumption.

Chapter 6

Conclusions and Recommendations

6.1 Conclusions

The sediment transport module of REEF3D is used to calculate the scour, the deposition pattern and time development of scour for different cases under current and waves. The numerical results for all the four test cases show good agreement with the experiments, which confirms that the numerical model is able to predict the general evolution (geometry, location and maximum scour depth) and time development of the scour hole accurately. Very slight difference in scour pattern is noticed for the abutment and the pier under constant discharge compared to the experiments. This is because in the experiments the bed topography outside the scour hole is not measured. The contour plot was slightly mollified in the pier scour experiments both under waves and currents. Since the location and magnitude of scour and deposition are the most important parameters in the field of marine civil engineering, the results obtained through the numerical simulation are considered satisfactory. Very minor differences in result predicted by numerical model and the experiments is noted for the contraction case, where the scour depth, its location, deposition height and deposition location are well predicted. Its worth mentioning that the result for this case using the current numerical model is better than found by Bihs and Olsen [8].

The impact of mesh resolution upon the numerical results has been tested in the abutment scour. For this case three different mesh widths (5cm , 2.5 cm and 1.5 cm) are used. It is noted that finer mesh resolution gives better results. Comparison in performance of k-ω and k-ϵ turbulence models is done for abutment and pier scour under constant discharge. The results reveals that performance of the k-ω model is similar to the k-ϵ model in the pier scour case since both the models share the theoretical rationale of two-equation eddy-viscosity models and there in no wall effect as the pier was situated in the middle of the tank. In case of the abutment, the k-ω model

gives better results because the bed shear stress formulation is used in the study that uses turbulent viscosity which can be slightly over predicted in k-ϵ model compared to the k-ω model resulting in higher bed shear stress and hence more erosion. The performance of time discretization schemes (Adam Bashforth, a third-order accurate TVD Runge-Kutta and fourth-order accurate TVD Runge-Kutta) reveals that higher order time discretization gives better results. However a balance needs to maintained in the quality of the results and simulation time. It is concluded that a third-order accurate TVD Runge-Kutta scheme gives satisfactory result while keeping the simulation time low. The performance of different formulations for the critical shear stress reduction for the sloping bed in cases of pier and abutment under constant discharge and pier under waves is done. It is concluded that all the three formulations (Kovacs-Parker, Dey Empirical and Dey Analytical) give satisfactory results. However, the best result is predicted by Dey Analytical formulation. The time development of scour is observed for varying porosity of bed layer for the abutment scour case. It is noted that with increasing porosity the scour depth is larger. This is expected, since the porosity is used in Exner's equation to calculate the bed level changes.

A 3D pier scour case is tested by using the CFD code as a numerical wave tank. Use of wave generation and numerical beach is made. The numerical model accurately predicts the general evolution of scour (geometry and location) and the deposition location when compared to the experiment and theoretical erosion and deposition pattern. This study also confirms that the de-coupled approach for the simulation of hydrodynamic and sediment transport processes in REEF3D is a reasonable assumption. The numerical model in all the four test cases represents the complex free surface and the bed topology using the level set method.

6.2 Recommendations

The implementation of sediment transport cases under current (abutment, pier and contraction) and waves (pier) using REEF3D has shown accurate and promising results. This numerical model incorporates more physics in its calculations with lesser amount of simplification compared to other 2D and 3D numerical modelling tools which results in a more detailed description of the flow and sediment transport phenomena. The following section discusses the improvements that could be made to the existing REEF3D module.

- Multi-block or Nested Grids
  The current version of REEF3D supports only uniform grid size throughout the domain. As a result, implementation of grid resolution enhancement at specific regions of interest is not possible. The implementation of nested or

multi-block grids can be a good addition to the code. This would enable the user to enhance the grid resolution at required locations like near the bed and at the free surface or near the structure where more detailed insight into the wave-current-structure interaction is needed. This will lead to efficient computation and more accurate results in the areas of interest.

- Integration with other numerical models
  On of the major criticism of CFD program is that it is resource intensive and effective over smaller temporal and spatial domains compared to the other 2D and 3D numerical modelling programs. To address this criticism, room for expanding the computational domain to include larger areas similar to other modelling programs exit. This could be done by coupling the REEF3D program with spectral or Boussnesq wave model. With this integration, these wave models can be used to solve flow, wave and sediment transport in larger domain and the CFD code can be used in localised area of interest where the fluid interaction phenomena have to be studied in more detail. An attempt to do this is already in progress at the Department of Civil and Transport Engineering at NTNU. This will result in more effective handling of the practical marine civil engineering problems.

- Modelling bed load sediment transport as individual sediment particle
  The current version of REEF3D models the bed load sediment transport as bed layer. For better understanding of the sediment movement an attempt to model the bed load transport on individual sediment particle scale could be undertaken. This could improve our understanding of the physics behind the incipient motion of particles.

- Inclusion of time varying porosity
  Porosity is included in the Exner's equation to model the bed elevation changes. An assumption of constant porosity is made in the current version of REEF3D. With the formation of scour hole and varying situation of saturation of sediment particles and option for varying porosity should be included based on the flow regime and the stage of sediment transport. This would improve the prediction of scour process to a great extent.

Bibliography

[1] S. Abdelaziz, M. D. Bui, and P. Rutschmann. River flow 2010. In *Proc. of the Intern. Conf. on Fluvial Hydraulics, 2:1597-1604*, 2010.

[2] M. A. Afshar. Numerical wave generation in OpenFOAM. Master's thesis, Chalmers University of Technology, 2010.

[3] K. Babaeyan-Koopaei, D. Ervine, P. Carling, and Z. Cao. Velocity and turbulence measurements for two overbank flow events in river severn. *Journal of Hydraulic Engineering*, 128(10):891–900, 2002.

[4] BAW. Morphologische versuche an einer rinne mit ein- schnuÌĹrung mittel- bis feinkiessohle. Company report: Baw-nr: A39530110064-01, 2009.

[5] P. A. Berthelsen and O. M. Faltinsen. A local directional ghost cell approach for incompressible viscous flow problems with irregular boundaries. *Journal of Computational Physics*, 227:4354–4397, 2008.

[6] H. Bihs. Three-dimensional numerical modeling of local scouring in open channel flow. PhD thesis, 2011.

[7] H. Bihs and N. Olsen. Numerical modeling of abutment scour with the focus on the incipient motion on sloping beds. *Journal of Hydraulic Engineering*, 137(10):1287–1292, 2011.

[8] H. Bihs and N. R. B. Olsen. Three-dimensional numerical modeling of contraction scour. In *Proc., 32st Cong. of IAHR, Venice, Italy*, 2007.

[9] H. Bihs and N. R. B. Olsen. Three dimensional numerical modeling of pier scour. In *Fourth International Conference on Scour and Erosion, ICSE 4, Tokyo, Japan*, 2008.

[10] H. Bihs, M. Ong, A. Kamath, and Ø. A. Arntsen. A level set method based numerical wave tank for calculation of wave forces on horizontal and vertical cylinders. In *Proc., Seventh National Conference on Computation Mechanics MekIT'13, Trondheim, Norway*, 2013.

[11] M. Burkow. Numerische simulation stromungsbedingten sedimenttransports und der entstehenden gerinnebettformen. Master's thesis, Mathematisch-Naturwissenschaftlichen Fakultat der Rheinischen Friedrich-Wilhelms-Universitat Bonn, 2010.

[12] I. Celik and W. Rodi. Modeling suspended sediment transport in nonequilibrium situations. *Journal of Hydraulic Engineering, ASCE*, Vol. 114, No. 10., 1988.

[13] H. Chanson. The hydraulics of open channel flow: An introduction. *Elsevier Butterworth-Heinemann*, 2004.

[14] J. B. Chapman, R. S. and S. Vemulakonda. "userâĂŹs guide for the sigma stretched version of ch3d-wes." technical report hl-96-21. Technical report, US Army Engineer Waterways Experiment Station, Vicksburg, MS, 1996.

[15] A. Chorin. Numerical solution of the navier stokes equations. *Math. Comput.*, 22:745–762, 1968.

[16] G. F. Clauss, G. E. Schmittner, and R. Stück. Numerical wave tank- simulation of extreme waves for the investigation of structural responses. In *Proc., 24th International Conference on Offshore Mechanics and Arctic Engineering, Greece*, 2005.

[17] R. Clough. *The Finite Element Method in Plane Stress Analysis.* American Society of Civil Engineers, 1960.

[18] S. E. Coleman, C. S. Lauchlan, and B. W. Melville. Clear-water scour development at bridge abutments. *Journal of Hydraulic Research*, 41(5):521–531, 2003.

[19] R. Courant. Variational methods for the solution of problems of equilibrium and vibrations. *Bulletin of the American Mathematical Society*, (49):1–23, 1943.

[20] R. Courant, K. Friedrichs, and H. Lewy. On the partial difference equations of mathematical physics. *IBM Journal of Research and Development*, 11:215–234, 1967.

[21] R. Courant, E. Isaacson, and M. Rees. On the solution of nonlinear hyperbolic differential equations by finite differences. *Comm. Pure Appl. Math*, (5):243–255, 1952.

[22] R. Croce, M. Griebel, and M. A. Schweitzer. Evaluating scour at bridges. Preprint, Federal Highway Administration, Hydraulics engineering circular No. 18, Publication FHWA HI-96âĂŞ031, Washington, D.C, 1995.

[23] S. Dey. Experimental studies on incipient motion of sediment particles on generalized sloping fluvial beds. *Journal of Sediment Research*, 16(3):391–398, 2001.

[24] S. Dey. Threshold of sediment motion on combined transverse and longitudinal sloping beds. *Journal of Hydraulic Research*, 41(4):405–415, 2003.

[25] W. E. Dietrich and P. Whiting. Boundary shear stress and sediment transport in river meanders of sand and gravel. *River Meandering, American Geophysical Union Water Resources Monograph*, 12:1–50, 1989.

[26] B. Duc and W. Rodi. Numerical simulation of contraction scour in an open laboratory channel. *Journal of Hydraulic Engineering*, 134(4):367–377, 2008.

[27] B. Duc, T. Wenka, and W. Rodi. Numerical modeling of bed deformation in laboratory channels. *Journal of Hydraulic Engineering*, 130(9):894–904, 2004.

[28] P. A. Durbin. Turbulence closure models for computational fluid dynamics. 2004.

[29] P. A. Durbin. Limiters and wall treatments in applied turbulence modeling. *Fluid Dynamics Research*, 41:1–18, 2009.

[30] W. Eggenberger and R. MuÌĹller. *Experimentelle Und Theoretische Untersuchungen UÌĹber Das Kolkproblem*. Leemann, 1944.

[31] Y. Egorov. Contact condensation in stratified steam-water flow. *Validation of CFD codes with PTS-relevant test cases - EVOL-ECORA âĂŞ D 07*, 2004.

[32] H. A. Einstein. The bed-load function for sediment transportation in open channel flows. *Technical Bulletin 1026, U.S. Dept. of the Army, Soil Conservation Service*, 1950.

[33] F. Engelund and J. Fredsøe. A sediment transport model for straight alluvial channels. *Nord. Hydrol.*, 7(5):293–306, 1976.

[34] A. P. Engsig-Karup. *Unstructured Nodal DG-FEM Solution of High-order Boussinesq-type Equations*. PhD thesis, Technical University of Denmark, Lyngby, 2006.

[35] C. Escauriaza and F. Sotiropoulos. The dynamics of bed-forms around scour holes. In *IAHR Conference*, 2009.

[36] C. Field, V. Barros, T. Stocker, D. Qin, D. Dokken, K. Ebi, M. Mastrandrea, K. Mach, G. Plattner, S. Allen, M. Tignor, and P. M. (eds.). Managing the risks of extreme events and disasters to advance (summary for policymakers) climate change adaptation. a special report of working groups i and ii of the intergovernmental panel on climate change. Technical report, Cambridge University Press, Cambridge, UK, and New York, NY, USA, 2012.

[37] R. Fletcher. Conjugate gradient methods for indefinite systems. In G. Watson, editor, *Numerical Analysis*, volume 506 of *Lecture Notes in Mathematics*, pages 73–89. Springer Berlin Heidelberg, 1976.

[38] G. Z. Forristall. Wave crest distributions: observations and second-order theory. *J. Phys. Oceanogr.*, 30:1931–1943, 2000.

[39] B. Galperin, L. H. Kantha, S. Hassid, and A. Rosati. A quasi-equilibrium turbulent energy model for geophysical flows. *Journal of Atmospheric Sciences*, 45:55–62, 1988.

[40] P. H. Gaskell and A. K. C. Lau. Curvature-compensated convective transport:SMART, a new boundedness-preserving transport algorithm. *International Journal for Numerical Methods in Fluids*, 8:617–641, 1988.

[41] E. v. d. Giessen and H. Aref. *Advances in Applied Mechanics p.86.* Academic Press., 2003.

[42] W. Graf and I. Istiarto. Flow pattern in the scour hole around a cylinder. *Journal of Hydraulic Research*, 40(1):13–20, 2002.

[43] S. T. Grilli and J. Horrillo. Numerical generation and absorption of fully nonlinear periodic waves. *Journal of Engineering Mechanics*, 123(10):1060–1069, 1997.

[44] E. Hairer. *Solving ordinary differential equations.* Springer-Verlag, Berlin New York, 1993.

[45] F. Harlow and M. Evans. A machine calculation method for hydrodynamic problems. *Los Alamos Scientific Laboratory report LAMS Report No. LA-2*, 1957.

[46] F. Harlow and J. Welch. Numerical calculation of time dependent viscous incompressible flow of fluid with a free surface. *Physics of Fluids*, 8:2182–2189, 1965.

[47] A. Harten. High resolution schemes for hyperbolic conservation laws. *Journal of Computational Physics*, 49:357–393, 1983.

[48] J. Herbich and M. T. Society. *Seafloor scour: design guidelines for ocean-founded structures.* Ocean engineering. M. Dekker, 1984.

[49] M. Hestenes and E. Stiefel. Methods of conjugate gradients for solving linear systems. *The Journal of Research of the National Institute of Standards and Technology*, 49:409, 1952.

[50] C. Hirt and B. Nichols. Volume of fluid vof method for the dynamics of free boundaries. *Journal of Computational Physics*, 39:201–225, 1981.

[51] S. Ikeda. Incipient motion of sand particles on side slopes. *Journal of the Hydraulics Division ASCE*, 108(1):95–114, 1982.

[52] N. G. Jacobsen, D. R. Fuhrman, and J. Fredsøe. A wave generation toolbox for the open-source cfd library: Openfoam. *International Journal for Numerical Methods in Fluids*, 2011.

[53] G. S. Jiang and C. W. Shu. Efficient implementation of weighted eno schemes. *Journal of Computational Physics*, 126:202–228, 1996.

[54] A. Kamath, H. Bihs, and Ø. A. Arntsen. Application of porous media flow relation to simulate pressure drop across a nozzle in a two dimensional numerical wave tank. In *Proc., Seventh National Conference on Computation Mechanics MekIT'13, Trondheim, Norway*, 2013.

[55] A. M. Kamath. Calculation of wave forces on structures using reef3d. Master's thesis, Norwegian University of Science and Technology, 2012.

[56] G. Kirkil, S. G. Constantinescu, and R. Ettema. Coherent structures in the flow field around a circular cylinder with scour hole. *Journal of Hydraulic Engineering*, 134(5):572–587, 2008.

[57] T. Kobayashi. 3d analysis of flow around a vertical cylinder on a scoured bed. *Coastal Engineering Proceedings*, 1(23), 1992.

[58] T. Kobayashi and K. Oda. Experimental study on developing process of local scour around a vertical cylinder. *Coastal Engineering Proceedings*, 1(24), 1994.

[59] A. Kovacs and G. Parker. A new vectorial bedload formulation and its application to the time evolution of straight river channels. *Journal of Fluid Mechanics*, 267:153–183, 1994.

[60] S. Kraft, Y. Wang, and M. Oberlack. Large eddy simulation of sediment deformation in a turbulent flow by means of level-set method. *Journal of Hydraulic Engineering*, 137(11):1394–1405, 2011.

[61] R. T. F. Kw An and B. W. Melville. Local scour and flow measurements at bridge abutments. *Journal of Hydraulic Research*, 32(5):661–673, 1994.

[62] E. W. Lane. Design of stable channels. *Transactions, ASCE*, 120(1):1234–1260, 1955.

[63] B. Launder and B. Sharma. Application of the energy-dissipation model of turbulence to the calculation of flow near a spinning disc. *Letters in Heat and Mass Transfer*, 1(2):131 – 137, 1974.

[64] B. Leonard. A stable and accurate convective modelling procedure based on quadratic upstream interpolation. *Computer Methods in Applied Mechanics and Engineering*, 19(1):59 – 98, 1979.

[65] O. Link. Untersuchung der Kolkung an einem schlanken zylindrischen Pfeiler in sandigem Boden. *Wasser Abwasser GWF*, 147(6):421–422, 2006.

[66] X. Liu and M. Garcia. Three-dimensional numerical model with free water surface and mesh deformation for local sediment scour. *J. Waterway, Port, Coastal, Ocean Eng.*, 134(4):203–217, 2008.

[67] X.-D. Liu and S. Osher. Convex eno high order multi-dimensional schemes without field by field decomposition or staggered grids. *Journal of computational physics*, 142(2):304–330, 1998.

[68] X. D. Liu, S. Osher, and T. Chan. Weighted essentially non -oscillatory schemes. *Journal of Computational Physics*, 115:200–212, 1994.

[69] B. Maddison. Scour failure of bridges. In *Proceedings of the ICE - Forensic Engineering, Volume 165, Issue 1*, 2012.

[70] O. Madsen and W. Grant. *Sediment transport in the coastal environment.* R (Massachusetts Institute of Technology. Dept. of Civil Engineering). Ralph M. Parsons Laboratory for Water Resources and Hydrodynamics, Dept. of Civil Engineering, Massachusetts Institute of Technology, 1976.

[71] S. Malavasi, A. Radice, and B. F. Study of sediment motion in a local scour hole through an image processing technique. In *River Flow 2004, II International Conference on Fluvial Hydraulics*, 2004.

[72] M. Marek and A. Dittrich. 3d numerical calculations of the flow in an open channel consisting of an expansion and a contraction. In *Proc., 6th Int. Conf. on Hydro-Science and -Engineering (CD-ROM)*, 2004.

[73] F. R. Menter. Two-equation eddy-viscosity turbulence models for engineering applications. *AIAA Journal*, 32(8):1598–1605, 1993.

[74] E. Meyer-Peter and R. Muller. Formulas for bed-load transport. In *Proceedings of the 2nd Meeting of the International Association for Hydraulic Structures Research .pp. 39âĂŞ64*, 1948.

[75] A. Molinas, K. Kheireldin, and B. Wu. Shear stress around vertical wall abutments. *Journal of Hydraulic Engineering*, 124(8):822–830, 1998.

[76] A. J. Odgaard and M. A. Bergs. Flow processes in a curved alluvial channel. *Water Resources Research*, 24(1):45–56, 1988.

[77] N. R. B. Olsen and H. M. Kjellesvig. Three-dimensional numerical flow modelling for estimation of maximum local scour depth. *IAHR Journal of Hydraulic Research*, 36(4):579–590, 1998.

[78] N. R. B. Olsen and M. C. Melaaen. Three-dimensional calculation of scour around cylinders. *Journal of Hydraulic Engineering*, 119(9):1048–1054, 1993.

[79] M. C. Ong, D. Myrhaug, and P. Hesten. Scour around vertical piles due to long-crested and short-crested nonlinear random waves plus a current. *Coastal Engineering*, 73(0):106 – 114, 2013.

[80] S. Osher and J. A. Sethian. Fronts propagating with curvature- dependent speed: Algorithms based on hamilton-jacobi formulations. *Journal of Computational Physics*, 79:12–49, 1988.

[81] H. Palmer. Pro. civil engr. in the ocean ii, miami beach, p. 703- 716. In *Wave-Induced Scour on the Sea Floor*, 1969.

[82] S. V. Patankar and D. B. Spalding. A calculation procedure for heat, mass and momentum transfer in three-dimensional parabolic flows. *International Journal Heat Mass Transfer*, 15:1787–1806, 1972.

[83] D. Peng, B. Merriman, S. Osher, H. Zhao, and M. Kang. A PDE-based fast local level set method. *Journal of Computational Physics*, 155:410–438, 1999.

[84] M. Peric and J. Ferziger. *Computational Methods for Fluid Dynamics*. Springer, 2001.

[85] S. B. Pope. *Turbulent Flows*. Cambridge University Press, 2000, 2000.

[86] N. Rajaratnam and B. Nwachukwu. Flow near groinâĂŘlike structures. *Journal of Hydraulic Engineering*, 109(3):463–480, 1983.

[87] L. F. Richardson. The approximate arithmetical solution by finite differences of physical problems involving differential equations, with an application to the stresses in a masonry dam. *Philosophical Transactions of the Royal Society of London. Series A, Containing Papers of a Mathematical or Physical Character*, 210:pp. 307–357, 1911.

[88] A. Roulund, B. M. Sumer, J. Fredsøe, and J. Michelsen. Numerical and experimental investigation of flow and scour around a circular pier. *Journal of Fluid Mechanics*, 534:351–401, 2005.

[89] H. Rouse. *Criteria for Similarity in the Transportation of Sediment.* Scientific Book Company, 1939.

[90] E. Saito, S. Sato, and T. Shibayama. Local scour around a large circular cylinder due to wave action. *Coastal Engineering Proceedings*, 1(22), 2011.

[91] H. Schlichting. *Boundary layer theory.* McGraw-Hill Book Company, 1979.

[92] G. Seminara, L. Solari, and G. Parker. Bed load at low shields stress on arbitrarily sloping beds: Failure of the bagnold hypothesis. *Water Resources Research*, 38(31):1–16, 2002.

[93] A. Shields. Anwendungen der Ähnlichkeitsmechanik und der turbulenzforschung auf die geschiebebewegung, 1936.

[94] C. W. Shu and S. Gottlieb. Total variation diminishing runge-kutta schemes. *Mathematics of Computation*, 67:73–85, 1998.

[95] T. J. Smith and B. A. O'Connor. A two-dimensional model for suspended sediment transport. *IAHR-congress, Baden-Baden, West Germany*, 1977.

[96] R. L. Soulsby and K. R. Dyer. The form of the near-bed velocity profile in a tidally accelerating flow. *Journal of Geophysical Research: Oceans*, 86(C9):8067–8074, 1981.

[97] K. R. Stapleton and D. A. Huntley. Seabed stress determinations using the inertial dissipation method and the turbulent kinetic energy method. *Earth Surface Processes and Landforms*, 20(9):807–815, 1995.

[98] B. Sumer, N. Christiansen, and J. FredsÃÿe. Influence of cross section on wave scour around piles. *Journal of Waterway, Port, Coastal, and Ocean Engineering*, 119(5):477–495, 1993.

[99] B. Sumer and J. Fredsøe. Wave scour around a large vertical circular cylinder. *Journal of Waterway, Port, Coastal, and Ocean Engineering*, 127(3):125–134, 2001.

[100] B. Sumer and J. Fredsøe. *The Mechanics of Scour in the Marine Environment.* World Scientific, 2002.

[101] B. Sumer, J. FredsÃ¥e, and N. Christiansen. Scour around vertical pile in waves. *Journal of Waterway, Port, Coastal, and Ocean Engineering*, 118(1):15–31, 1992.

[102] M. Sussman, P. Smereka, and S. Osher. A level set approach for computing solutions to incompressible two-phase flow. *Journal of Computational Physics*, 114:146–159, 1994.

[103] T. Toue, H. Katsui, and K. Nadaoka. Mechanism of sediment transport around a large circular cylinder. *Coastal Engineering Proceedings*, 1(23), 1992.

[104] van der Vorst H. BI-GStab: A fast and smoothly converging variant of BI-CG for the solution of nonsymmetric linear systems. *SIAM J. Sci. Stat. Comput.*, 13:631–644, 1992.

[105] van Leer B. Towards the ultimate conservative difference scheme V. A second order sequel to Godunovs method. *Journal of Computational Physics*, 32:101–136, 1979.

[106] L. C. van Rijn. Sediment transport, part i: Bed load transport. *Journal of Hydraulic Engineering*, 110(10):1431–1457, 1984a.

[107] L. C. van Rijn. Sediment transport, part ii: Suspended load transport. *Journal of Hydraulic Engineering*, 110(11):1613–1641, 1984b.

[108] L. C. van Rijn. The state of the art in sediment transport modeling, in sediment transport modeling. *American Society of Civil Engineers, New York*, 1989.

[109] S. Wallin and A. V. Johansson. An explicit algebraic reynolds stress model for incompressible and compressible turbulent flows. *Journal of Fluid Mechanics*, 403:89–132, 2000.

[110] R. Wang and J. Herbich. *Combined Current and Wave-produced Scour Around a Single Pile.* COE report. Texas Engineering Experiment Station, 1983.

[111] S. Weise. Verifikation eines zweidimensionalen feststofftransportmodells anhand von hydraulischen versuchen. Master's thesis, Hochschule fuÌĹr Technik, Wirtschaft und Kultur Leipzig (FH), 2002.

[112] R. Whitehouse. *Scour at marine structures: a manual for practical applications.* Thomas Telford, 1998.

[113] J. Wiberg, Patricia L.; Dungan Smith. Model for calculating bed load transport of sediment. *Journal of Hydraulic Engineering*, 115:101, 1989.

[114] P. R. Wilcock. Estimating local bed shear stress from velocity observations. *Water Resources Research*, 32(11):3361–3366, 1996.

[115] D. C. Wilcox. *Turbulence Modeling for CFD.* DCW Industries Inc., La Canada, California., 1994.

[116] W. Wu, W. Rodi, and T. Wenka. 3d numerical modeling of flow and sediment transport in open channels. *Journal of Hydraulic Engineering*, 126(1):4–15, 2000.

[117] W. Wu and S. Wang. Depth-averaged 2d calculation of flow and sediment transport in curved channels. *Journal of Sediment Research*, 19(4):241–257, 2004.

[118] C. Yen and K. Lee. Bed topography and sediment sorting in channel bend with unsteady flow. *Journal of Hydraulic Engineering*, 121(8):591–599, 1995.

[119] J. Zeng, G. Constantinescu, and L. Weber. A fully 3d non- hydrostatic model for prediction of flow, sediment transport and bed morphology in open channels. In *n Proceedings of the 31st IAHR Congress, pages 1327âĂŞ1338*, 2005.